RELATIONSHIP BETWEEN INPUT AND OUTPUT: A SYSTEMATIC STUDY OF THE STABILITY OF HIGHLY FRACTURED ROCK SLOPES USING THE HOEK-BROWN STRENGTH CRITERION

by

Qian Qian

A thesis submitted for the degree of

Masters of Engineering Science

The University of Adelaide

School of Civil, Environmental and Mining Engineering

December 2012

ABSTRACT

Rock slope stability is a particularly important topic in rock engineering. The circular failure of highly fractured rock slopes is a critical failure mode that can cause severe damage. Over the past decades, significant research has been devoted to soil slopes and failure modes of rock slopes controlled by discontinuities. However, there have been few attempts to systematically study the circular failure mode of rock slopes.

Circular failure is controlled by the strength of the rock mass. While the strength of a rock mass is difficult to measure directly, the Hoek-Brown (HB) strength criterion has proved effective and convenient for its estimation.

This research presents a systematic study of the stability of highly fractured rock slopes using the HB strength criterion. Both deterministic analyses and probabilistic analyses are included. The relationship between the input (GSI, m_i, σ_{ci}, and their variability) and the output, Factor of Safety (FS) and Probability of Failure (PF), is investigated. *Slide6.0* and a limit equilibrium model programmed in *Matlab* are used for FS calculations; Monte Carlo simulations are applied for PF calculations.

The deterministic analysis aims to characterise the sensitivity of FS to the changes in HB parameters (FS sensitivity). A sensitivity graph analysis and an equation fitting analysis are developed. The sensitivity graph analysis displays the relationship between HB parameters and FS directly. The equation fitting analysis fits a large amount of data generated by *Slide6.0* with an equation connecting HB parameters and FS, and then determines FS sensitivity from the derivatives of this equation with respect to HB parameters. It is found

that slopes with the same geometry and the same FS (but different combinations of HB parameters) can have quite different sensitivity and GSI is the most critical parameter in this respect. With the increase in GSI, FS becomes increasingly sensitive to the change in GSI and that in σ_{ci}.

The probabilistic analysis investigates the relationship between the variability of HB parameters (quantified by the coefficient of variation COV and scale of fluctuation θ) and PF. Its effectiveness in assessing the impact of FS sensitivity on slope stability is also studied. A series of parametric studies are implemented. It is found that there is a strong relationship between FS sensitivity and PF: for slope cases with identical FS and the same COV of input HB parameters, a slope of higher FS sensitivity has a higher PF, indicating a higher risk. The relative contributions of the variability of HB parameters to PF are also compared. It is found that when the COV of GSI, m_i, and σ_{ci} are identical, the variability of GSI makes the largest contribution; however, when these COV are set to their upper-limit values observed in engineering practice, the high variability of σ_{ci} makes the largest contribution. Finally, the investigation demonstrates that spatial variability of HB parameters (applicable to m_i and σ_{ci} in this study) has significant influences on slope stability. For a slope with FS > 1, the PF increases as the scale of fluctuation θ of HB parameters increases. Also, larger θ makes the effect of FS sensitivity on slope stability more significant.

STATEMENT OF ORIGINALITY

I certify that this work contains no material which has been accepted for the award of any other degree or diploma in any university or other tertiary institution and, to the best of my knowledge and belief, contains no material previously published or written by another person, except where due reference has been made in the text. In addition, I certify that no part of this work will, in the future, be used in a submission for any other degree or diploma in any university or other tertiary institution without the prior approval of the University of Adelaide and where applicable, any partner institution responsible for the joint-award of this degree.

I give consent to this copy of my thesis, when deposited in the University Library, being made available for loan and photocopying, subject to the provisions of the Copyright Act 1968.

I also give permission for the digital version of my thesis to be made available on the web, via the University's digital research repository, the Library catalogue and also through web search engines, unless permission has been granted by the University to restrict access for a period of time.

Signed: …….. Date: ……..

ACKNOWLEDGEMENTS

I would like to express my sincere thanks to my principal supervisor, Associate Professor Chaoshui Xu, of the School of Civil, Environmental and Mining Engineering at the University of Adelaide. A/Prof Xu introduced me to the study and research opportunities available at the University of Adelaide and has provided me with extensive guidance since then. His support for my application to study here, guidance throughout the program, and help in editing this thesis are all gratefully acknowledged.

I also wish to thank Dr. Murat Karakus, of the School of Civil, Environmental and Mining Engineering. Dr. Karakus has been my co-supervisor since early 2011. He has provided considerable assistance to this research project, which is also much appreciated.

I would like to express my deep gratitude to Associate Professor Mark B. Jaksa, of the School of Civil, Environmental and Mining Engineering. A/Prof Jaksa became my co-supervisor in 2011. He has provided me with invaluable assistance in various aspects, including research guidance, emotional support, and the first tutoring opportunities which helped me in developing self-confidence. His warm personality towards every ordinary person will always serve as a role model to me in my future endeavours.

I would also like to extend my deep appreciation to my friend Dr. Alan F. Reid, AM, former Director of the CSIRO Institute of Minerals, Energy and Construction. Dr. Reid has assisted me significantly in the editing of this thesis (in accordance with Standards D and E of Australian Standards for Editing Practice) and has provided me with valuable help in practising English writing and speaking as well as in many other aspects of life for the past

two years. His kind nature, modesty, constant enthusiasm to help, and a deep sense of responsibility to society, will always be a source of inspiration to me.

I am deeply indebted to the School of Civil, Environmental and Mining Engineering and the University of Adelaide, who have provided me with a scholarship and many useful services and training opportunities throughout the program. My study and research here would not have been possible without the support of the scholarship. In addition, since recently commencing work as an engineer, I have more realised how valuable the research experience that I had here is. Sincere thanks are therefore given to School of Civil, Environmental and Mining Engineering and the University of Adelaide.

During my studies, considerable assistance has also been provided by my fellow postgraduate students. Among them, I particularly wish to thank Dr. Liang Huang, Mr. Jiayi Shen, and Miss Sarah Jewell. I wish every postgraduate student in our school a bright future and hope that our friendships will never fade.

Lastly, I would like to thank my parents and step parents, including Peidong, Pengyuan, Kemin, and Peter. Only after I have grown up did I realise how much I am like you. Thank you for bringing me into this world and the love ever since.

TABLE OF CONTENTS

LIST OF FIGURES

LIST OF TABLES

NOTATION (OTHER THAN DEFINED LOCALLY WITHIN EQUATIONS)

a	range of influence
$a_1, \ldots, a_9$	coefficients for the equation fitting
$\boldsymbol{a}$	coefficient matrix for the equation fitting
$\boldsymbol{A}$	HB parameter matrix for the equation fitting
ARD	absolute relative difference
b	width of a slice
c	cohesion
$\mathbf{C}$	covariance matrix
C_0	nugget variance
C	a parameter, when added to C_0, represents the *sill* of a variogram
COV	coefficient of variation
CSS	critical slip surface
$C(\tau)$	covariance between the data of two points separated by distance τ
D	rock mass disturbance factor
DF	driving force
$E_L; E_R; X_L; X_R$	normal and shear forces acting on both sides of a slice
FORM	first order reliability method
FOSM	first order second moment method
FS	factor of safety
GSI	Geological Strength Index
h_r	height of a slice
h_w	height of the water table

H	height of the slope
HB	Hoek-Brown
i	increment factor for HB parameters in sensitivity graphs
Is_{50}	point load index
LEM	limit equilibrium method
m_b; s; a	Hoek-Brown constants for the rock mass
m_i	Hoek-Brown constant for the intact rock
M	number of times that the system fails in a Monte Carlo simulation
MC	Mohr-Coulomb
MCS	Monte Carlo simulation
MPa	Mega-Pascal
N; N'	normal and effective normal forces acting on the base of a slice
N	total number of iterations in a Monte Carlo simulation
PDF	probability density function
PEM	point estimate method
PF	probability of failure
PF-GSI	probability of failure when only GSI is modelled as a random variable
PF-m_i	probability of failure when only m_i is modelled as a random variable
PF-σ_{ci}	probability of failure when only σ_{ci} is modelled as a random variable
PSSA	probabilistic slope stability analysis
r_r	unit weight of the soil/rock material
r_w	unit weight of water
RD	relative difference
RFEM	random finite element method
RF	resisting force
r_s	Spearman correlation coefficient

t	location in a random field
T	local averaging distance
u	water pressure along the slip surface
UCS	uniaxial compressive strength (= σ_{ci})
W	weight of a slice
x	an arbitrary parameter or a random variable (often serves as input)
x_1; x_2; x_3	GSI, m_i, and σ_{ci} representations in the equation fitting
y	an arbitrary parameter or a random variable (often serves as output)
$\boldsymbol{y}$	FS matrix for the equation fitting
α	base angle of a slice
β	slope face angle
β_r	reliability index
β_{HL}	Hansfor and Lind's reliability index
θ	scale of fluctuation
γ_h	variogram (semivariogram)
γ_h^*	experimental variogram
$\gamma(T)$	variance function
λ	parameter for demonstrating the concept of spatial variability
μ	mean
σ	standard deviation
σ_1	major principal stress
σ_3	minor principal stress
σ^2	variance
σ'	effective normal stress acting on the base of a slice
σ_{ci}	uniaxial compressive strength (= UCS)
σ_n	normal stress

τ	shear stress
τ_f	shear strength
σ_t	tensile strength of the intact rock
σ^2_{T}	variance of the locally averaged random field (over distance T)
$\rho(\tau)$	correlation function
φ	angle of friction

Chapter 1

INTRODUCTION

1.1 Introduction

Rock excavations are required in numerous engineering activities. These include highways, dams, urban or industrial constructions, and open pit mining. In the history of rock engineering, the slope stability problem has attracted more attention than any other topics and is still one of the most important issues in this discipline (Hudson and Harrison 2000).

Failures of rock slopes, varying from rock falls to global slope instability, apart from production losses and delays, can have severe social and economic consequences. Around 2500 people in the Italian town Longarone were killed when a wave produced by a landslide overtopped the Vajont dam, in October 1963 (Hoek 2007). This is one of the many examples that demonstrates the importance of preserving and predicting slope stability.

There are four basic failure modes for rock slopes, namely circular, plane, wedge, and toppling (further introduced in Section 2.2.1). Among these failure modes, the occurrences of the latter three are dominated by the existence and strength of discontinuities. On the other hand, circular failures occur in highly fractured rock slopes and are dominated by the overall strength of rock masses (a rock mass is the integration of intact rock and discontinuities). Although any of these failure modes can cause severe damage, most of the research effort in rock slope stability analysis has been devoted to discontinuity controlled failure modes and the circular failure mode has been relatively much less investigated.

The stability of many rock engineering projects, including highly fractured rock slopes, is controlled by the strength of the rock mass. Since rock mass strength is difficult to measure directly, its estimation has become a critical topic. A rock strength criterion, which is a principle or statement defining the condition under which the rock or rock mass reaches its maximum strength, serves this purpose. Among the rock strength criteria in use, Hoek-Brown (HB) is the one that has been widely recognised and adopted by the rock engineering community. The HB strength criterion links the descriptive rock mass appearance, two basic intact rock parameters, and the blasting or stress incurred damage with the overall strength of the rock or rock mass, which provides great convenience for rock engineering practitioners. Moreover, it is also one of the non-linear criteria, which allows more realistic estimates of the strength of a rock or rock mass than the traditional linear Mohr-Coulomb criterion.

The HB strength criterion can be used effectively to study the circular failure of highly fractured rock slopes. However, although several decades have passed since its first application, there have been few attempts to systematically investigate the stability of highly fractured rock slopes by using the HB strength criterion. The present study seeks to address this issue.

Another critical topic in rock engineering, or more broadly geotechnical engineering, is to deal with uncertainty. Geotechnical engineering is a subject particularly dominated by uncertainty, mainly due to the highly variable properties of earth or rock materials. Traditional deterministic analysis for slopes is unable to explicitly incorporate and evaluate the impact of input uncertainty on slope stability, since it is based on purely deterministic constitutive relationships. Probabilistic analysis, which employs various probabilistic

concepts and techniques that allow uncertainty to be quantified and incorporated in one way or another, has advanced significantly over the past 30 years.

A major source of uncertainty in geotechnical engineering is spatial variability, which simply speaking, refers to the differences between values of a parameter at different locations. In the early development of probabilistic analysis, spatial variability was generally not considered, mainly due to the limitations of computation and simulation techniques. However, it has been shown that the risk of having a slope failure can be either substantially overestimated (when the FS for the slope is more than 1) or underestimated (when the FS for the slope is less than 1) if spatial variability is not considered (Griffiths et al. 2009; Cho 2010). Hence, based on the rapid development of computation and simulation techniques, great efforts have been devoted to investigate the influence of spatial variability on slope stability in the past 10 years. Nevertheless, most of the attention has been paid to soil slopes rather than rock slopes.

1.2 Scope of the Study

The present research aims to systematically investigate the stability of highly fractured rock slopes using the HB strength criterion. The investigation is carried out under the framework of first deterministic analyses, then simplified probabilistic analyses without considering the spatial variability, and finally spatial probabilistic analyses that explicitly incorporate spatial variability.

Four parameters, namely the Geological Strength Index GSI, the HB intact rock constant m_i, the uniaxial compressive strength of intact rock σ_{ci}, and the blasting or stress disturbance factor D, are used as input when the HB strength criterion is applied to

estimate the strength of a rock mass. This study focuses on GSI, m_i, and σ_{ci}, since they are considered as intrinsic parameters of a rock mass.

Specific objectives of the present research are summarised in Chapter 3 after a review of the relevant literature in Chapter 2.

1.3 Layout of the Thesis

In Chapter 2, important publications that are relevant to this study are reviewed. Four parts are included: an overview of slope stability analysis, the HB strength criterion, the Limit equilibrium method (LEM), and probabilistic slope stability analysis (PSSA). The aims of the literature review are to provide necessary background knowledge and to identify specific research gaps for this study.

In Chapter 3, specific research gaps forming objectives of this study are identified based on the literature review in Chapter 2. Subsequently, the methodology for the current study is specified. The models involved in the study are also introduced and validated.

In Chapter 4, fractured rock slope stability is analysed within the framework of deterministic analyses. In Chapter 5, fractured rock slope stability is analysed within the framework of probabilistic analyses.

Finally, in Chapter 6, a summary and the conclusions of this study are presented, and recommendations for further research are given.

Chapter 2

LITERATURE REVIEW

2.1 Introduction

This literature review aims to provide background knowledge for the later chapters and identify specific research gaps. Six sections are included: firstly, an overview of slope stability analysis is given, where basic information about slope scale, failure modes, rock mass strength, and common approaches for slope stability analysis are discussed. Secondly, the Hoek-Brown (HB) strength criterion is introduced in terms of the criterion, input parameters, and their conversion to the equivalent Mohr-Coulomb (MC) parameters. Thirdly, the limit equilibrium method (LEM), which is adopted in the present study for FS calculations, is introduced in detail. Probabilistic slope stability analysis (PSSA) is then discussed in terms of input, methodology, and output. Following that, previous studies in PSSA are reviewed, major research directions are classified, and research gaps for the present research are identified. Finally, a summary is presented.

2.2 Overview of Slope Stability Analysis

2.2.1 Slope Scale and Slope Failure

Most of the rock slopes exist in open pits and the scale of such rock slopes is generally much larger than that of soil slopes. Based on the data given by Wyllie and Mah (2004), the height of most open pit rock slopes is between 100m and 300m.

Collapse/slide, lateral cracking, and large displacement of the rock material that constitutes the slope body, can all be viewed as slope failures (Chen 1995). On the other hand, depending on the scale of the failures relative to the slope size, slope failures include local inter-ramp failures as well as overall failures. Generally, collapse/slide of the overall slope is most critical and is the definition of slope failure in the present study.

There are four basic failure modes for rock slopes, namely circular, plane, wedge, and toppling (Hoek 2009). Illustrations of these failure modes are shown in Figure 2.1. Circular failures occur in heavily jointed rock masses where slope stability is controlled by the shear strength of the rock masses. Plane, wedge, and toppling failures occur in rock masses where dominant discontinuities exist and slope stability is controlled by the existence and the shear strength of the discontinuities. Most of the research effort in rock slopes has been devoted to discontinuity controlled failures because of their common occurrences; examples include: constitutive analysis (Low and Einstein 1992; Chen 2004), discontinuity network modelling (Dowd et al. 2007; Grenon and Hadjigeorgiou 2008; Xu and Dowd 2010), and probabilistic analysis (Park and West 2001; Park et al. 2005; Low 2008; Duzgun and Bhasin 2009; Park et al. 2011). On the other hand, although the rock mass controlled circular failure is also a critical mode of failure, it has been much less studied.

Figure 2.1 Four basic failure modes for rock slopes (reproduced from Hoek 2009)

2.2.2 Rock Mass Strength

Rock mass refers to the integration of intact rock and discontinuities. The strength of a rock mass is often necessary for carrying out stability analysis in rock engineering. However, rock mass strength is difficult to measure directly because of the problems associated with obtaining undisturbed samples and samples at the same scale as the failure (Read and Stacey 2009). A widely used alternative is to use the Hoek-Brown strength criterion to estimate rock mass strength (Cai et al. 2004; Priest 2005; Read and Stacey 2009).

2.2.3 Limit Equilibrium Method and Numerical Method

The limit equilibrium method (LEM) and the numerical method are two basic techniques for slope stability analysis. A brief introduction to these techniques is given below:

LEM treats the sliding part of a slope as a rigid body. It computes the driving force (DF) and resisting force (RF) of the sliding body along the slip surface, and slope stability is quantified by the factor of safety (FS), which equals RF/DF. The driving force is mostly contributed by the weight of the sliding body and water pressure, while the resisting force is contributed by the cohesive and frictional forces along the slip surface. Most LEM divide the sliding body into slices, based on which the analysis is carried out. This evaluation technique is termed the method of slices.

LEM produces reasonably accurate results and has the advantage of being relatively fast and simple to use. It has been widely applied for several decades and remains an effective type of slope stability analysis method. Its major disadvantages include that the slip surface is pre-determined and the sliding body is assumed to be rigid. LEM is therefore unable to

analyse the deformation and displacement of a rock mass. In addition, various assumptions are made for different types of LEM, which may cause inaccuracy in some situations.

The numerical method, on the other hand, divides the entire slope into elements. Elements are modelled with stress-strain relationships and deformation properties that define how the material behaves. After the stress states and boundary conditions are specified, the numerical method is able to compute the deformation and displacement of a rock mass. It can also compute the FS of a rock mass by applying the shear strength reduction technique (Read and Stacey 2009). Reviews of the numerical method for rock mass were given by Jing and Hudson (2002) and Jing (2003).

The numerical method has two major advantages. Firstly, it is capable of computing the deformation and displacement of a rock mass. Secondly, its process of analysis is more rigorous than that of LEM (e.g. the failure surface is sought out during the analysis instead of being pre-assumed and FS is calculated by the shear strength reduction technique). On the other hand, the numerical method is slow compared with LEM, making it unsuitable for certain types of analysis (such as sensitivity analysis or probabilistic analysis) where stability analysis needs to be repeated many times.

2.2.4 Deterministic Analysis and Probabilistic Analysis

Slope stability analysis can be classified into deterministic analysis or probabilistic analysis depending on how uncertainty is incorporated and evaluated. These two types of analysis are briefly introduced below.

The input for a deterministic analysis is a set of parameters of fixed values (usually at the mean values of the data obtained from site investigations). The process of a deterministic

analysis is one-off and is implemented by either LEM or the numerical method. The output from a deterministic analysis is mostly FS.

In contrast, the input for a probabilistic analysis consists of parameters that are modelled as random variables. Different types of uncertainty of the input, including spatial variability, statistical uncertainty and systematic uncertainty, can be considered. In a probabilistic analysis, slope stability is still analysed by LEM or the numerical method. However, probabilistic analysis techniques, common ones include first order second moment method (FOSM), first order reliability method (FORM), point estimate method (PEM), and Monte Carlo simulation (MCS), are used to evaluate the influence of input uncertainty on slope stability. The output from a probabilistic analysis is mostly the probability of failure PF or the reliability index β_r.

Deterministic analysis enjoys a long history of development and acceptable levels of FS for various conditions are well established. It has been taken as a routine step for slope stability analysis. However, deterministic analysis uses fixed input parameters and can only cope with the risk of uncertainty by requiring a large FS value. Thus the uncertainty is not explicitly considered. Probabilistic analysis, on the other hand, uses random variables as input and considers uncertainty in a more explicit way. However, the acceptable levels of PF for various conditions are not as well established as those for FS. Finally, neither FS nor PF can be obtained with high precision.

Based on these circumstances, it is recognised that deterministic analysis with FS as the output should remain a routine step for slope stability analysis, while probabilistic analysis with PF as the output is viewed as an important development that supplements deterministic analysis (Christian et al. 1994; Duncan 2000).

2.2.5 Sensitivity Analysis and Parametric Study

Sensitivity analysis and parametric study are two commonly used techniques to assess the influence of the variation or variability of input parameters on the output. The most common and simple form of a sensitivity analysis is one-way sensitivity analysis. One-way sensitivity analysis and parametric study are similar in process: one parameter is changed systematically within its range with other parameters fixed, and the variation of the corresponding output is evaluated. Sensitivity analyses are mostly associated with physical parameters, such as material strength, water pressure or, different courses of action. Parametric studies are mostly associated with statistical parameters, such as the coefficient of variation (COV), scale of fluctuation, and correlation coefficient. Sensitivity analysis and parametric study are useful as they can help find the parameter or the particular ranges of parameters that have the most critical influence on slope stability.

2.3 Hoek-Brown (HB) Strength Criterion

This section consists of four parts: firstly, the latest version of the HB strength criterion is introduced; secondly, input parameters involved in the HB strength criterion are discussed, particularly in terms of their variability; thirdly, methods for converting HB parameters to equivalent Mohr-Coulomb (MC) parameters, which are essential for using the HB strength criterion in conjunction with the LEM, are introduced; and lastly, the application of the HB strength criterion is briefly discussed.

2.3.1 HB Strength Criterion

The HB strength criterion was originally proposed in the 1980s (Hoek and Brown 1980) to provide input data for the analysis of underground excavations. It has been continually

reviewed and developed over the past three decades (primarily in 1983, 1988, 1992, 1995, 1997, and 2002) and has now become a widely used criterion for estimating the strength of either an intact rock or a rock mass (Cai et al. 2004; Priest 2005; Read and Stacey 2009). A comprehensive review of the development of the HB strength criterion was given by Hoek and Marinos (2007).

The latest version of the HB strength criterion (Hoek et al. 2002) is expressed as

$$\sigma_1 = \sigma_3 + \sigma_c \left\{ \left(\frac{m_b \sigma_3}{\sigma_{ci}} \right) + s \right\}^a \tag{2.1}$$

where σ_1 is the major principal stress at failure, σ_3 is the minor principal stress at failure, σ_{ci} is the uniaxial compressive strength of the intact rock material, and m_b, s, and a are constants for the rock mass that can be calculated from the following equations (Hoek et al. 2002):

$$m_b = m_i e^{\left(\frac{GSI-100}{28-14D} \right)} \tag{2.2}$$

$$s = e^{\left(\frac{GSI-100}{9-3D} \right)} \tag{2.3}$$

$$a = 0.5 + \frac{e^{\left(\frac{-GSI}{15} \right)} - e^{\left(\frac{-20}{3} \right)}}{6} \tag{2.4}$$

where GSI is the Geological Strength Index, m_i is the Hoek-Brown constant for intact rock, and D is a rock mass disturbance factor depending on the blast damage or stress relaxation.

When the HB strength criterion is applied to a rock mass, the input parameters are GSI, m_i, σ_{ci}, and D. Among these parameters, GSI, m_i, and σ_{ci} are intrinsic parameters of a rock

mass and are introduced in details in Section 2.3.2. It should be noted that the HB strength criterion is only applicable to the rock mass that contains a sufficient number of randomly oriented discontinuities such that it can be treated as isotropic.

The HB strength criterion (Equation 2.1) is expressed in principal stress space (σ_1 and σ_3). However, slope stability analyses are usually carried out in normal and shear stress space (σ_n and τ). Therefore, it is necessary to employ certain techniques to transform the HB strength criterion from principal stress representation to normal and shear stress representation in slope stability analysis. The exact transformation can be achieved by Balmer's solution (Balmer 1952), which is a generic solution that can be applied to any non-linear strength criterion. Balmer's solution can be written in the form of the following equations (Hoek et al. 2002):

$$\sigma_n = \frac{\sigma_1 + \sigma_3}{2} - \frac{\sigma_1 - \sigma_3}{2} \cdot \frac{d\sigma_1 / d\sigma_3 - 1}{d\sigma_1 / d\sigma_3 + 1} \tag{2.5}$$

$$\tau = (\sigma_1 - \sigma_3) \cdot \frac{\sqrt{d\sigma_1 / d\sigma_3}}{d\sigma_1 / d\sigma_3 + 1} \tag{2.6}$$

$$d\sigma_1 / d\sigma_3 = 1 + a m_b (m_b \sigma_3 / \sigma_{ci} + s)^{a-1} \tag{2.7}$$

where σ_n and τ are the normal and shear stresses at failure.

A detailed discussion of Balmer's solution was given by Carranza-Torres (2004).

2.3.2 HB Input Parameters: GSI, m_i and σ_{ci}

Three intrinsic rock mass parameters in the HB strength criterion, i.e. GSI, m_i, and σ_{ci}, are discussed in this section.

2.3.2.1 Geological Strength Index (GSI)

GSI describes the blockiness and discontinuity weathering conditions of a rock mass. It is used in the HB strength criterion to scale down the strength and other deformation properties of the rock mass from intact rock. GSI emerged formally in 1995 (Hoek et al. 1995) and since then has undergone continuous development. Marinos et al. (2005) provided a comprehensive review of GSI. On the other hand, it should be noted that GSI is only applicable to the rock mass that contains a sufficient number of randomly oriented discontinuities such that it can be treated as isotropic (as stated earlier, this is also the prerequisite for applying the HB strength criterion to a rock mass).

The value of GSI extends from unity for an extremely fractured rock mass to 100 for an intact rock. It can be estimated from charts (Marinos et al. 2005) and Hoek (1998) stated that it is desirable to assign a range of values (e.g. in the form of a normal distribution) to GSI instead of a single value. In the early stage of the development, GSI can be estimated from adjusted RMR or Q (two popular rock mass classification systems) values (Hoek and Brown 1997). However, this procedure is no longer recommended, particularly for a weak rock mass (Marinos et al. 2005). Marinos and Hoek (2000) discussed the ranges of GSI for typical rock masses. Marinos et al. (2005) presented detailed instructions for using GSI, including its applicability and the influence of rock mass size, anisotropy, depth, ground water, aperture, infilling, weathering, and soft rocks on its value. There have been several attempts to quantify GSI directly based on common discontinuities parameters (Sonmez

and Ulusay 1999; Cai et al. 2004; Cai et al. 2007). However, as pointed out by Marinos et al. (2005), these GSI quantification methods should be used with caution when applied to certain types of rock mass.

GSI is deemed to be the most important parameter in the HB strength criterion (Marinos et al. 2005; Fisher and Eberhardt 2012; Mao et al. 2012). The variability of GSI is generally low and Table 2.1 summarises the statistics of GSI from existing publications. It is shown that the COV of GSI is between 0.035 and 0.15.

2.3.2.2 HB Constant: m_i

The HB constant m_i is one of the two parameters in the HB strength criterion that describes the characteristics of the intact rock (the other one is σ_{ci}). It is produced from curve fitting of triaxial test data and does not have any specific physical meaning. A recent review of m_i was given by Richards and Read (2011).

Ideally, m_i should be determined by regression analysis on triaxial test data and the corresponding procedures and specifications were given by Hoek and Brown (1997). Alternatively, m_i can be estimated from the lithology (Hoek 2007). However, Mostyn and Douglas (2000) stated that m_i is not highly correlated to rock lithology based on analyses of a large amount of data they have collected. Further analyses carried out by Richards and Read (2011) suggested that σ_{ci}/σ_t, which is the ratio of uniaxial compressive strength of intact rock to the tensile strength of intact rock, is a good indicator of the m_i value. The value of m_i ranges from 3 for slate to 35 for granite (Hoek 2007). However, based on the data from Mostyn and Douglas (2000), the value of m_i ranges from 1 to 40.

The parameter m_i is less important in the HB strength criterion as compared with GSI and σ_{ci} (Marinos et al. 2005; Fisher and Eberhardt 2012; Mao et al. 2012). The variability of m_i is medium. Table 2.2 summarises the statistics of m_i from existing publications. It is shown that the COV of m_i is between 0.039 and 0.25.

2.3.2.3 Uniaxial Compressive Strength (UCS): σ_{ci}

The parameter σ_{ci} (UCS) of a rock is the maximum axial stress that a specific sample of such rock can sustain under a uniaxial compressive loading. It is one of the most important rock parameters in rock engineering, as firstly it is a critical indicator for the intact rock strength and secondly it is an essential input for most rock strength criteria and many rock classification systems. In this section, σ_{ci} is discussed within the framework of the HB strength criterion.

Ideally, the value σ_{ci} should be obtained directly from laboratory test (Hudson and Harrison 2000). Alternatively, it can be determined from Schmitt rebound hammer reading (Hudson and Harrison 2000) or estimated from published data (Hoek and Brown 1997). The value of σ_{ci} ranges from 0.25MPa for some extremely soft rocks to 250MPa for some highly strong rocks such as the granite (Hoek and Brown 1997).

σ_{ci} is also an important parameter in the HB strength criterion (Marinos et al. 2005; Fisher and Eberhardt 2012; Mao et al. 2012). The variability of σ_{ci} is generally high. Table 2.3 summarises the statistics of σ_{ci} from previous publications. It is shown that the COV of σ_{ci} is between 0.1 and 0.4.

Table 2.1 Statistics of GSI based on published data

Source	Project	Mean GSI	COV	Distribution
Fisher and Eberhardt (2012)	A dip slope located in southern California	49	0.12	Lognormal
Lü and Low (2011)	A horse-shoe shaped highway tunnel in China	25	0.2	Normal
Idris et al. (2011)	A stope geometry in Canadian blast hole stoping operations	65	0.077	Truncated normal
Sari et al. (2010)	Estimating the rock mass properties of Ankara andesites	55.9 - 74.9	0.077 – 0.153	Truncated normal
Fu et al. (2009)	A cutting slope at the Laohuzui hydropower station in China	40	0.062	Truncated normal
Cai et al. (2004)	Kannagawa underground powerhouse cavern in Japan	54 - 74	0.035	/
Cai (2011) Cai et al. (2004)	Kazunogawa underground powerhouse cavern in Japan	46 - 60	0.035 – 0.042	Normal
Mao et al. (2012) Lü and Low (2011) Hoek (1998)	Hypothetical slope and tunnel cases	25	0.1	Normal

Table 2.2 Statistics of m_i based on published data

Source	Project	Mean m_i	COV	Distribution
Fisher and Eberhardt (2012)	A dip slope located in southern California	17	0.039	Normal
Lü and Low (2011)	A horse-shoe shaped highway tunnel in China	13	0.2	Normal
Idris et al. (2011)	A stope geometry in Canadian blast hole stoping operations	28	0.071	Truncated normal
Sari et al. (2010)	Estimating the rock mass properties of Ankara andesites	4.1-10.5	0.15-0.25	Normal
Fu et al. (2009)	A cutting slope at the Laohuzui hydropower station in China	19.04	0.159	Truncated normal
Cai et al. (2004)	Kannagawa underground powerhouse cavern in Japan	9 - 22	0.125	\
Cai (2011) Cai et al. (2004)	Kazunogawa underground powerhouse cavern in Japan	19	0.125	Normal
Mao et al. (2012) Lü and Low (2011) Hoek (1998)	Hypothetical slope and tunnel cases	8	0.125	Normal

Table 2.3 Statistics of σ_{ci} based on published data

Source	Project	Mean σ_{ci} (MPa)	COV	Distribution
Fisher and Eberhardt (2012)	A dip slope located in southern California	15	0.4	Normal
Lü and Low (2011)	A horse-shoe shaped highway tunnel in China	160	0.25	Normal
Idris et al. (2011)	A stope geometry in Canadian blast hole stoping operations	282	0.124	Truncated normal
Sari et al. (2010)	Estimating the rock mass properties of Ankara andesites	53-128	0.1-0.2	Truncated normal
Fu et al. (2009)	A cutting slope at the Laohuzui hydropower station in China	125	0.15	Truncated normal
Cai et al. (2004)	Kannagawa underground powerhouse cavern in Japan	48 -162	0.1-0.212	\
Cai (2011) Cai et al. (2004)	Kazunogawa underground powerhouse cavern in Japan	108	0.389	Truncated normal
Mao et al. (2012) Lü and Low (2011) Hoek (1998)	Hypothetical slope and tunnel cases	10	0.25	Normal

2.3.3 Converting HB Parameters to Equivalent MC Parameters

The Mohr-Coulomb (MC) strength criterion is a commonly used strength criterion for soil. The MC strength criterion can be expressed in the normal and shear stress space (σ_n and τ) as:

$$\tau_f = c + \sigma_n \tan\varphi \tag{2.8}$$

where c is the cohesion, φ is the angle of friction, σ_n is the normal stress, and τ_f is the shear strength (shear stress at failure).

Since, historically, rock mechanics was a branch of soil mechanics, the MC strength criterion is also widely applied in rock engineering. Many slope stability analysis methods (such as the LEM) and software are based on the MC strength criterion and use MC parameters, i.e. c and φ, as input. Therefore, to use the HB strength criterion in conjunction with the LEM, it is necessary to convert HB parameters to their equivalent MC parameters.

The principle of the conversion can be defined as *under a specified level of normal stress, find the equivalent MC parameters c and φ that would give the same shear strength based on the MC strength criterion as that based on the HB strength criterion*. The conversion is illustrated in Figure 2.2. The solid line represents the failure envelope of the HB strength criterion in normal and shear stress space (σ_n and τ) for a rock with the following HB parameters: GSI = 100, m_i = 10, and σ_{ci} = 30MPa. When the normal stress σ_n = 10MPa, the HB strength criterion computes the shear strength τ_f = 15.8MPa. The equivalent MC parameters under normal stress σ_n = 10MPa that also give a shear strength of 15.8MPa for this rock is found to be c = 7.3MPa and φ = 40.2˚, and the dashed line represents the corresponding MC failure envelope.

There are two types of solutions for the conversion, i.e. the accurate solution and the approximate solution. These two types of solutions are introduced in the following sections.

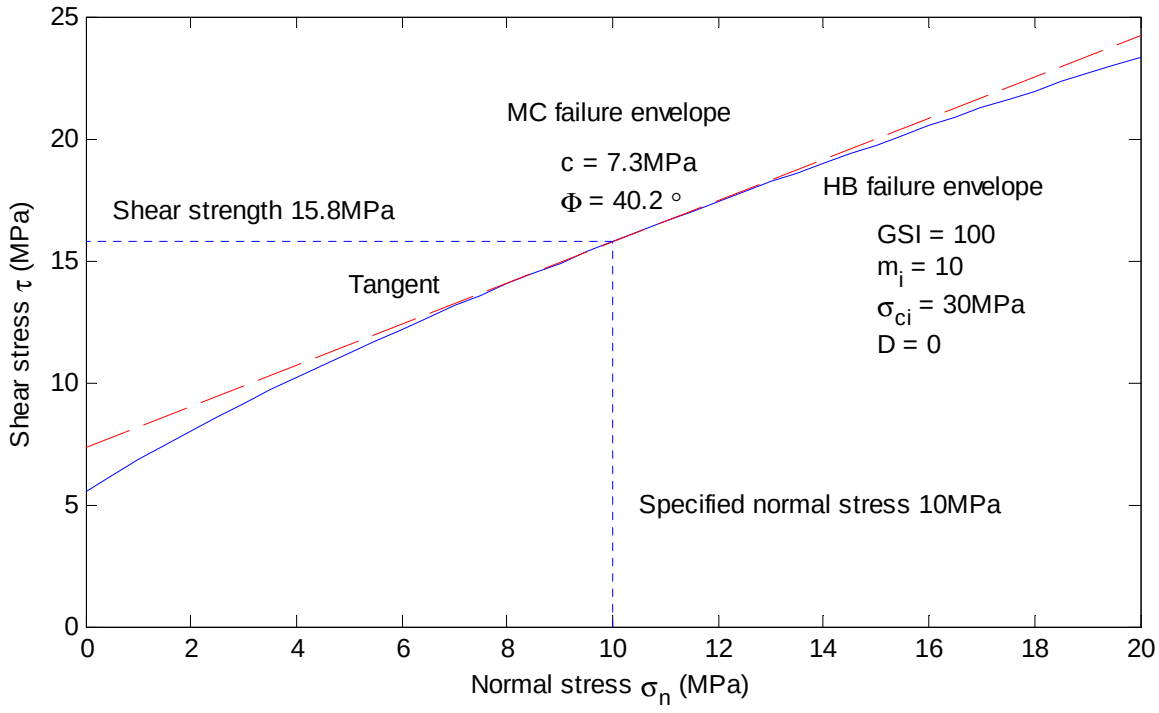

Figure 2.2 Conversion from HB parameters to MC parameters: a rock with GSI = 100, m_i = 10, and σ_{ci} = 30MPa under a normal stress σ_n = 10MPa

2.3.3.1 Accurate Solution

Accurate solutions, as implied by the name, compute *c* and φ that produce identical shear strength from the MC strength criterion as that from the HB strength criterion. This is achieved by determining the tangent line to the HB failure envelope at the failure point (Carranza-Torres 2004; Priest 2005). This tangent line is the equivalent MC failure envelope and the intercept and slope of this line are equal to *c* and tanφ respectively. Therefore, Figure 2.2 shows precisely the conversion strategy of accurate solutions. Note that the *c* and φ found by this method change instantaneously with the specified normal stress σ_n and therefore they are usually termed the instantaneous cohesion and angle of friction (Priest 2005).

Three accurate solutions are introduced in this section: they are Bray's solution for the intact rock, Kumar's solution, and Priest's solution.

Bray (reported by Hoek 1983) developed an accurate solution for the original HB strength criterion (Hoek and Brown 1980). The latest version of the HB strength criterion (Hoek et al. 2002) is only equivalent to the original HB strength criterion when GSI = 100 (which represents an intact rock). Therefore, for the latest version of the HB strength criterion, Bray's solution only produces accurate conversion when GSI = 100. For GSI of other values, the conversion error increases as GSI decreases (Kumar 1998).

Bray's solution consists only of analytical equations and does not need further numerical iterations. It is convenient to use and is still popular with research for the intact rock. Bray's solution is given in the following equations:

$$h = 1 + \frac{16\left(m_b\sigma_n + s\sigma_{ci}\right)}{3m_b^2\sigma_{ci}} \tag{2.9}$$

$$\theta = \frac{1}{3}\left(90 + \arctan\frac{1}{\sqrt{h^3 - 1}}\right) \tag{2.10}$$

$$\varphi = \arctan\frac{1}{\sqrt{4h\cos^2\theta - 1}} \tag{2.11}$$

$$\tau_f = \left(\cot\varphi - \cos\varphi\right)\frac{m_b\sigma_{ci}}{8} \tag{2.12}$$

$$c = \tau_f - \sigma_n \tan\varphi \tag{2.13}$$

where h and θ are intermediate parameters.

Kumar (1998) developed an accurate solution that is suitable for the latest HB strength criterion (although the latest HB strength criterion was developed in 2002, it has the same generic form as the 1997 version and therefore Kumar's solution can still be applied). Kumar's solution is given in the following equations:

$$\frac{2}{m_b a}(m_b \frac{\sigma_n}{\sigma_{ci}} + s)^{(1-a)} = \frac{(1-\sin\varphi)}{\sin\varphi}(1+\frac{\sin\varphi}{a})^{(1-a)} \tag{2.14}$$

$$\tau_f = \frac{\sigma_{ci}\cos\varphi}{2(1+\frac{\sin\varphi}{a})^a}(m_b \frac{\sigma_n}{\sigma_{ci}} + s)^a \tag{2.15}$$

$$c = \tau_f - \sigma_n \tan\varphi \tag{2.16}$$

Kumar's solution needs numerical iterations to calculate φ from Equation 2.15.

Priest (2005) developed another accurate solution for the latest HB strength criterion (Hoek et al. 2002). The strategy of Priest's solution is briefly introduced as follows. Firstly, Priest's solution introduces two normal stresses σ_n- and σ_n+ that are very slightly less and more than the specified normal stress σ_n. Secondly, the failure points on the HB failure envelope under σ_n- and σ_n+ are found by a series of equations. Afterwards, these two points are connected and the corresponding secant line is used to approximate the tangent line at the failure point of σ_n. Finally, c and φ are calculated from this secant line.

It should be noted that Priest's solution is not an exact accurate solution, as it uses a secant line to approximate the tangent line. However, the calculated c, φ, and shear strength τ_f are very close to those produced from the Kumar's solution. Priest's solution consists of a series of equations and needs the assistance of a few numerical routines (such as the Excel Solver). It is not further introduced here and interested readers are referred to Priest (2005).

Finding accurate shear strength for the failure surface is critical for slope stability analysis. The advantage of the accurate solution is that it provides accurate conversion from HB parameters to MC parameters. However, accurate solutions that are suitable for the latest HB strength criterion need to apply additional steps of numerical iterations, making the conversion slower than approximate solutions. This drawback is not evident for a single conversion but may cause significant delays when the solution is applied a large number of times, e.g. in a Monte Carlo simulation.

2.3.3.2 Approximate Solution

Approximate solutions are generally developed for efficiency purposes. In this section, two solutions that are specifically developed for the latest version of HB strength criterion are discussed. They are Hoek's solution and Shen's solution. On the other hand, Bray's solution can also be regarded as an approximate solution for the latest version of HB strength criterion when GSI < 100, as it does not produce accurate conversion unless GSI = 100.

Hoek's solution (Hoek et al. 2002) was developed in conjunction with the latest HB strength criterion. It is derived from curve fitting and is expressed in the following equations:

$$\varphi = \sin^{-1}\left[\frac{6am_b\left(s+m_b\sigma_{3n}\right)^{a-1}}{2(1+a)(2+a)+6am_b\left(s+m_b\sigma_{3n}\right)^{a-1}}\right] \tag{2.17}$$

$$c = \frac{\sigma_{ci}\left[(1+2a)s+(1-a)m_b\sigma_{3n}\right]\left(s+m_b\sigma_{3n}\right)^{a-1}}{(1+a)(2+a)\sqrt{1+\left(6am_b\left(s+m_b\sigma_{3n}\right)^{a-1}\right)\Big/\left((1+a)(2+a)\right)}} \tag{2.18}$$

$$\sigma_{3n} = \sigma_{3\max}/\sigma_{ci} \tag{2.19}$$

for tunnels $$\frac{\sigma_{3\max}}{\sigma_{cm}} = 0.47\left(\frac{\sigma_{cm}}{\gamma H}\right)^{-0.94} \tag{2.20}$$

where H is the depth of the tunnel below surface and γ is the unit weight of the rock material

for slopes $$\frac{\sigma_{3\max}}{\sigma_{cm}} = 0.72\left(\frac{\sigma_{cm}}{\gamma H}\right)^{-0.91} \tag{2.21}$$

where H is the height of the slope

and $$\sigma_{cm} = \sigma_{ci}\frac{\left(m_b + 4s - a\left(m_b - 8s\right)\right)\left(m_b/4 + s\right)^{a-1}}{2\left(1+a\right)\left(2+a\right)} \tag{2.22}$$

Shen et al. (2012) developed an approximate solution based on genetic programming. Shen's solution is expressed in the following equations:

$$\frac{\sigma_3}{\sigma_{ci}} = \frac{a\frac{\sigma_n}{\sigma_{ci}}}{\sqrt{a(1+\sqrt{m_b}) - \frac{\sigma_n}{\sigma_{ci}}}} \tag{2.23}$$

$$P = 2 + am_b(m_b\frac{\sigma_3}{\sigma_{ci}} + s)^{a-1} \tag{2.24}$$

$$\varphi = \arcsin(1 - \frac{2}{P}) \tag{2.25}$$

$$\tau_f = \sigma_{ci}\frac{\sqrt{P-1}}{P}\frac{(m_b\frac{\sigma_n}{\sigma_{ci}} + s)^a}{(\frac{Pa + P - 2}{aP})^a} \tag{2.26}$$

$$c = \tau_f - \sigma_n \tan\varphi \tag{2.27}$$

A simple numerical experiment was carried out to examine the accuracy of the above approximate solutions (including Bray's solution). Cases of rock masses with different combinations of blockiness (characterised by GSI), intact rock strength (characterised by m_i and σ_{ci}), and normal stress levels (σ_n) are designed. GSI values are selected to be 100, 70, and 30, which represent intact, fractured, and highly fractured rock mass respectively. Intact rock parameters (m_i/σ_{ci}) are selected to be 32/175MPa and 10/30MPa, which represent strong and soft rock respectively. Lastly, the normal stress level σ_n is selected to be 10MPa and 0.5MPa, which represent high and low normal stress levels in slope stability analysis. Therefore, there are $3 \times 2 \times 2 = 12$ cases in total and they are shown in Table 2.4.

Kumar's solution, Bray's solution, Hoek's solution (using Equation 2.21 with the slope height H set to 100m), and Shen's solution are applied to these cases. The output from Kumar's solution is used as a judgement, since it is an accurate solution. The calculated shear strength τ_f from these solutions for all 12 cases is compared in Table 2.4, where RD represents the relative difference. In addition, the detailed output for Case 5 is demonstrated in Table 2.5.

Based on Table 2.4, the following conclusions are drawn. Firstly, when Bray's solution is applied to the latest HB strength criterion, it produces systematic error, which gradually increases with decreasing GSI; however, the error is generally not very large ($\leq$ 10%). Secondly, Hoek's solution produces the largest overall error; when GSI is less or equal to 70, the errors of τ_f are mostly too large to be acceptable. Lastly, Shen's solution produces medium errors for low normal stress circumstances (σ_n = 0.5MPa) and small errors for high normal stress circumstances (σ_n = 10MPa). It is therefore suitable for high normal stress conditions.

Table 2.4 Comparison of three approximate solutions for converting HB parameters to equivalent MC parameters

Case	GSI	m_i	σ_{ci} (MPa)	σ_n (MPa)	Rock mass and normal stress level	Kumar τ_f (MPa)	Bray RD of τ_f (%)	Hoek RD of τ_f (%)	Shen RD of τ_f (%)
1	100	32	175	10	Intact/ strong rock/ high σ_n	40.62	0.00	-0.08	9.16
2	100	10	30	10	Intact/ soft rock/ high σ_n	15.77	0.00	6.07	3.15
3	100	32	175	0.5	Intact/ strong rock/ low σ_n	20.11	0.00	-3.30	25.63
4	100	10	30	0.5	Intact/ soft rock/ low σ_n	6.22	0.00	-3.67	18.30
5	70	32	175	10	Fractured/ strong rock/ high σ_n	23.05	0.10	8.81	0.52
6	70	10	30	10	Fractured / soft rock/ high σ_n	9.60	0.05	20.58	0.29
7	70	32	175	0.5	Fractured / strong rock/ low σ_n	4.25	0.26	8.24	17.80
8	70	10	30	0.5	Fractured / soft rock/ low σ_n	1.60	0.25	5.71	11.63
9	30	32	175	10	Highly fractured/ strong rock/ high σ_n	14.38	3.66	15.07	1.56
10	30	10	30	10	Highly fractured / soft rock/ high σ_n	5.55	3.06	34.01	0.56
11	30	32	175	0.5	Highly fractured / strong rock/ low σ_n	1.63	7.06	20.78	6.23
12	30	10	30	0.5	Highly fractured / soft rock/ low σ_n	0.73	6.90	8.38	4.57

Table 2.5 Detailed conversion output for Case 5 (in Table 2.4)

Case 5		Kumar	Bray	Hoek	Shen
GSI: 70	c (MPa)	7.13	7.15	3.52	7.35
m_i: 32	φ (degree)	57.86	57.87	65.12	57.70
σ_{ci}: 175MPa	τ_f (MPa)	23.05	23.07	25.08	23.17
σ_n: 10MPa	RD of τ_f (%)	0.00	0.10	8.81	0.52

2.3.4 Application of the HB Strength Criterion

The HB strength criterion and the corresponding GSI system provide a simple and effective solution for rock slope stability analysis (Pantelidis 2009). Examples of practical engineering application of the HB strength criterion include Hormazabal et al. (2009) and Sjöberg (1997). Examples of probabilistic slope stability analysis that employ the HB strength criterion include Fu et al. (2009) and Priest and Brown (1983). There are also attempts to develop stability charts for rock slopes based on the HB strength criterion (Li et al. 2008; Li et al. 2011); however, the reliability of these stability charts needs further confirmation.

2.4 Limit Equilibrium Method (LEM)

2.4.1 Overview of LEM

In the limit equilibrium method (LEM), analysis is carried out based on a slip surface, which can be either circular or non-circular. The FS for this slip surface is defined as

$$\text{FS} = \text{RF}/\text{DF} \tag{2.28}$$

where RF is the resisting force (available shear strength) and DF is the driving force (equilibrium shear stress).

For a given slope, there are theoretically an infinite number of possible slip surfaces. Among these slip surfaces, the one with the lowest FS is termed the critical slip surface (CSS). The CSS is considered to be the most likely surface along which the failure will occur and is the one to be examined in most LEM (Duncan and Wright 2005). Although in reality there are also other slip surfaces of concern, in the present study, the CSS is the focus.

The CSS is usually found by computer programs. For LEM that considers only circular slip surfaces, the CSS can be found by systematically searching through various centres and radii of slip circles. For LEM that considers non-circular slip surfaces, the CSS can be found by searching techniques that involve optimisation schemes (e.g. Baker 1980) or random process schemes (e.g. Boutrup and Lovell 1980).

There are three static equilibrium conditions to be satisfied for LEM: (1) force equilibrium in the vertical direction, (2) force equilibrium in the horizontal direction, and (3) moment equilibrium about any point. Some LEM implementations satisfy all the three equilibrium conditions; others satisfy only some of them. However, in all circumstances, there are always more unknown variables than the number of equilibrium equations, which makes the problem statically indeterminate. Therefore, assumptions must be made for LEM to balance the unknown variables with the equilibrium equations.

There are two broad types of LEM. One is based on the entire slipping soil or rock mass body and the other divides the slipping soil or rock mass body into slices. The first type of LEM can only be applied to slopes with certain geometry (e.g. infinite slope method,

Duncan and Wright 2005) or with a specific shape of slip surface (e.g. logarithmic spiral method, Frohlich 1953). This type of LEM will not be further discussed here, as it is beyond the scope of this thesis. The latter type of LEM is termed the method of slices and it is discussed in the following section.

2.4.2 Method of Slices

The method of slices divides the slipping soil/rock mass body into slices, based on which the analysis is carried out. Depending on the shape of the slip surface, there are methods that can only be applied to circular slip surfaces and others that can be applied to arbitrary (non-circular) slip surfaces. Table 2.6 (based on Duncan and Wright 2005) summarises commonly used method of slices and the static equilibrium conditions that they satisfy.

In terms of simplicity and accuracy of various methods listed in Table 2.6, methods that can be carried out by hand calculations are considered to be “simple”; otherwise they are “complicated”. Methods that satisfy all three equilibrium conditions (e.g. Method 6, 7, and 8) are generally considered to be accurate (Fredlund and Krahn 1977).

Methods that assume circular slip surfaces are generally simple. Among all method of slices, Method 1, the Ordinary method of slices, is the most straightforward and is the only one that does not need iterative calculations. However, it is less accurate, particularly when water pressure is involved in the calculation. Method 2, Bishop’s simplified method of slices (Bishop 1955), is simple and accurate (Wright et al. 1973; Fredlund and Krahn 1977). Its only limitation lies in the assumed circular slip surface. Among methods that assume arbitrary slip surfaces, Methods 3, 4, and 5 are simple but their accuracy is sensitive to their corresponding assumptions (Duncan and Wright 2005). Methods 6, 7, 8, and 9 satisfy all three equilibrium conditions and are robust and accurate (Fredlund and Krahn 1977;

Duncan and Wright 2005). However, they are more complicated and have higher computing cost compared with Methods 1 – 5.

Table 2.6 Static equilibrium conditions that commonly used method of slices satisfy (summarised based on Duncan and Wright 2005)

Shape of slip surface	Method of slices	Force equilibrium		Moment equilibrium
		Vertical	Horizontal	
circular	(1) Ordinary	×	×	√
	(2) Bishop's simplified	√	×	√
arbitrary (non-circular)	(3) Lowe & Karafiath	√	√	×
	(4) U.S. Army Corps of Engineers	√	√	×
	(5) Janbu's simplified	√	√	×
	(6) Spencer	√	√	√
	(7) Morgenstern and Price	√	√	√
	(8) Chen and Morgenstern	√	√	√
	(9) Sarma	√	√	√

For probabilistic slope stability analysis that involves MCS, Bishop's simplified method of slices is often used (unless the slip surface is not likely to be circular) for its simplicity and accuracy (El-Ramly et al. 2002; El-Ramly et al. 2003; El-Ramly et al. 2005; Wang et al. 2010). Bishop's method of slices is further discussed in detail in a later section. Meanwhile, as the Ordinary method of slices provides a simple solution for estimating the effective normal stress along the slip surface (which is necessary for converting HB parameters to MC parameters, as described in Section 2.3.3), it is also introduced here.

2.4.2.1 Ordinary Method of Slices

Figure 2.3 depicts a typical slice in the method of slices, including its geometry and all forces acting on it.

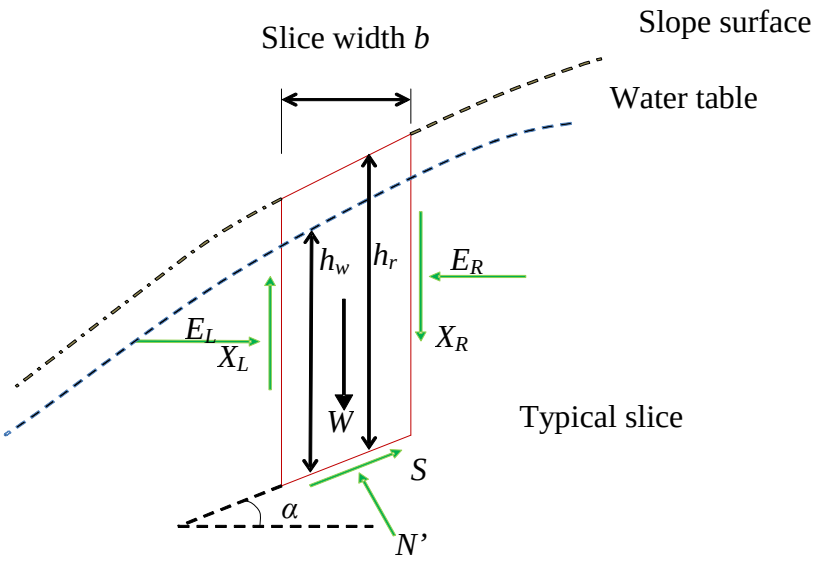

Figure 2.3 A typical slice in method of slices with forces acting on it

The Ordinary method of slices only satisfies the moment equilibrium condition. It assumes that the normal and shear forces acting on both sides of the slice, including E_L, X_L, E_R, and X_R (as shown in Figure 2.3), are equal to 0. Based on this assumption, the effective normal force N' acting on the base of the slice can be expressed as

$$N' = W\cos\alpha - \frac{ub}{\cos\alpha} \tag{2.29}$$

where W is the weight of the slice, α is the base angle, u is the water pressure along the slip surface, and b is the width of the slice. W and u can be calculated from the following equations

$$W = h_r b r_r \tag{2.30}$$

$$u = h_w r_w \tag{2.31}$$

where h_r is the height of the slice, r_r is the unit weight of soil/rock material, h_w is the height of the water table, and r_w is the unit weight of water.

Based on Equation 2.29, the effective normal stress σ' acting on the base of the slice is expressed as

$$\sigma' = \frac{W\cos^2\alpha}{b} - u \tag{2.32}$$

Equation 2.32 is the original expression of the effective normal force σ' for the Ordinary method of slices. However, this equation may lead to unrealistic low and even negative values of σ'. A more reasonable expression of the effective normal force N' is proposed by Turnbull and Hvorslev (1967) as

$$N' = (W - ub)\cos\alpha \tag{2.33}$$

the updated effective normal stress σ' is then expressed as

$$\sigma' = (\frac{W}{b} - u)\cos^2\alpha \tag{2.34}$$

Based on Equation 2.34, the MC strength criterion (Equation 2.8), and moment equilibrium about the centre of rotation, the FS for the ordinary method of slices is given by

$$FS = \frac{\sum (c + \sigma'\tan\varphi)b/\cos\alpha}{\sum W\sin\alpha} \tag{2.35}$$

where c and φ are cohesion and angle of friction along the slip surface.

2.4.2.2 Bishop's Simplified Method of Slices

In this section, Figure 2.3 is still used as the representation of a typical slice.

Bishop's simplified method of slices satisfies vertical force equilibrium and moment equilibrium conditions. It assumes that the horizontal forces acting on both sides of the slice, including X_L and X_R, are equal to 0.

The normal force N acting on the base of the slice for Bishop's simplified method of slices is expressed as

$$N = \frac{W - (1/FS)(cb - ub\tan\varphi)\tan\alpha}{\cos\alpha + (\sin\alpha\tan\varphi)/FS} \tag{2.36}$$

where W is the weight of the slice and can be calculated by Equation 2.30, FS is the factor of safety, c and φ are cohesion and angle of friction along the slip surface, and u is the water pressure along the slip surface and can be calculated by Equation 2.31.

Based on Equation 2.36, the effective normal stress σ' acting on the base of the slice is given by

$$\sigma' = \frac{N\cos\alpha}{b} - u \tag{2.37}$$

Based on Equation 2.37, the MC strength criterion (Equation 2.8), and moment equilibrium about the centre of rotation, Bishop's simplified method of slices calculates the FS by

$$FS = \frac{\sum\left[\dfrac{cb + (W - ub)\tan\varphi}{\cos\alpha + (\sin\alpha\tan\varphi)/FS}\right]}{\sum W\sin\alpha} \tag{2.38}$$

Since FS occurs at both sides of the above equation, an iterative process is necessary to compute the value of FS.

2.5 Probabilistic Slope Stability Analysis

Probabilistic Slope Stability Analysis (PSSA) is introduced in this section in terms of its input, methodology and output. Firstly, the input, including geotechnical variability and its characterisation, are discussed. Secondly, commonly used probabilistic analysis techniques, including first order second moment method (FOSM), first order reliability method (FORM), point estimate method (PEM), Monte Carlo simulation (MCS), and associated measures to incorporate and evaluate spatial variability, are introduced. Lastly, the output assessment for PSSA is briefly discussed.

2.5.1 Overview of Geotechnical Variability

The inherent variability of geotechnical parameters is a major source of uncertainty in geotechnical engineering (Baecher and Christian 2003; Duzgun et al. 2003; Christian 2004). Effective investigation and characterisation of the variability of geotechnical parameters can significantly improve the quality of analysis and design (Jaksa et al. 2005).

The variability of a geotechnical parameter is often simply quantified by the coefficient of variation (COV), which is given by the following equation

$$\mathrm{COV} = \frac{\sigma}{\mu} \tag{2.39}$$

where σ is the standard deviation and μ is the mean.

On the other hand, although the COV is useful, it is not able to characterise the important spatial variability of geotechnical parameters. For example, two soil or rock profiles can have similar μ and COV but exhibiting significant differences. Figure 2.4 illustrates such an example, where two profiles of a chosen parameter λ have similar μ and COV values but are very different in appearance.

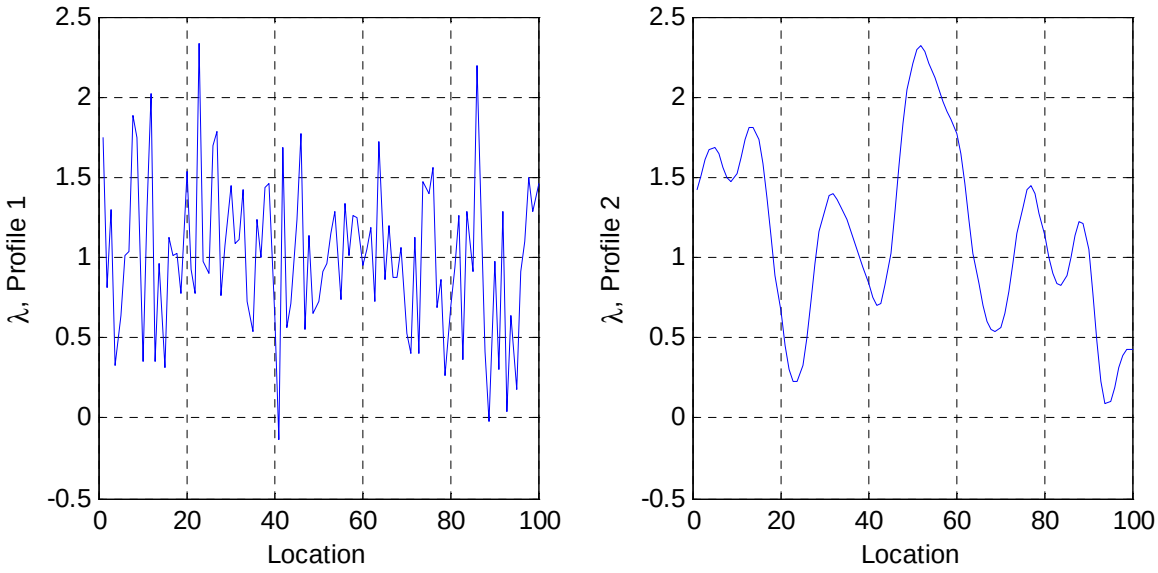

Figure 2.4 Example of two profiles of a chosen parameter λ with similar mean and COV values but exhibiting great differences

The two profiles have similar statistical parameters (for profile 1, μ = 1.02 and COV = 0.47; for profile 2, μ = 1.16 and COV = 0.48), but it is apparent from Figure 2.4 that the two profiles are very different. This is caused by the different spatial variability of these two profiles. Spatial variability refers to the differences between values of a variable at different locations. These values tend to be more similar when the distances between the locations are smaller. Spatial variability of the earth material has significant influences on slope stability. Without proper considerations of spatial variability, the risk of having a

slope failure can be either overestimated (when the FS for the slope is more than 1) or underestimated (when the FS for the slope is less than 1) (Griffiths et al. 2009; Cho 2010).

Spatial variability can be characterised by the scale of fluctuation θ. Larger θ represents low spatial variability and results in a less variable profile (such as that in Figure 2.4b) and smaller θ represents high spatial variability and results in a more variable profile (such as that in Figure 2.4a). The equivalent measure of spatial variability in geostatistics is the range α. Both these measures will be discussed in more detail.

The variability of geotechnical parameters has been investigated and summarised by several researchers (Jaksa 1995; Phoon and Kulhawy 1999; Duncan 2000; El-Ramly et al. 2003). However, most of the work has focused on soil. From the published work, the COV of soil parameters show large variations in terms of different materials, testing methods, and locations. The scale of fluctuation for many soil parameters were found to be similar and within the range of 40-60m in the horizontal direction and 2-6m in the vertical direction.

For the present study, Tables 2.1, 2.2, and 2.3 in Section 2.3.2 summarise the COV of HB parameters from the literature. However, for the scale of fluctuation, only studies on σ_{ci} were found. Wang et al. (2000) investigated the spatial variability of the point load index Is_{50} of sandstone and claystone for an open-pit coal mine slope project. The scale of fluctuation of Is_{50} for the sandstone and clay stone along the strike of slope (horizontal direction) is found to be within 3-6m.

2.5.2 Explicit Characterisation of Geotechnical Variability

Random field theory and geostatistics are two commonly used techniques for the explicit characterisation of geotechnical variability. They are introduced in the following sections.

2.5.2.1 Random Field Theory

Random field theory was systematically established by Vanmarcke (1983). Being restricted by the computation capability, the potential of random field theory has not been fully exploited until the most recent decade. Fenton and Griffiths (2008) re-elaborated random field theory with some of its latest applications. The above two publications form the basis of our discussion in this section. Also, the discussion is mostly restricted to one-dimensional stationary Gaussian random field.

(1) Basic Concepts and Common Assumptions

In random field theory, the point variability at any location t is characterised by a random variable *X(t)* with the probability density function (PDF) $f_X(x)$, and the entire random field is characterised by the joint PDF $f_{x_1 x_2 \ldots}(x_1, x_2, \ldots.)$ of all the random variables. Theoretically, the PDF of the point variability can evolve with location and it can take any form. However, this would make the resultant random field impractical to use.

To simplify the problem, three assumptions, including Gaussian process, stationarity, and isotropy, are usually made. Gaussian process means that the joint PDF of the random field is a normally distributed random process. Such joint PDF is expressed as

$$f_{X_1 X_2 \ldots X_K}(x_1, x_2, \ldots, x_k) = \frac{1}{(2\pi)^{k/2}} \frac{1}{|\mathbf{C}|^{1/2}} \exp\left\{-\frac{1}{2}(X-u)^T \mathbf{C}^{-1}(X-u)\right\} \qquad (2.40)$$

where X is the input vector, μ is the mean vector, $\mathbf{C}$ is the covariance matrix, and $|\mathbf{C}|$ is the determinant of $\mathbf{C}$. Under the assumption of Gaussian process, a random variable at any point of the random field follows a normal distribution.

Stationarity means that the joint PDF of the random field depends only on the relative distances between the points rather than on their absolute positions. Under this assumption, covariance and other higher order moments of the random field are constant in space.

Isotropy indicates that for a random field of higher dimensions ($\geq$ 2D), the joint PDF of the random field is invariant with rotation.

Stationary Gaussian random field is the most widely used random field in practice. Fenton and Griffiths (2008) stated that since there was great uncertainty involved in the most basic statistical parameters, it is "of little point in adopting other joint distributions".

(2) Characterisation of Random Fields

A random field can be fully characterised by the field mean μ and the covariance function $C(\tau)$, where $C(\tau)$ represents the covariance between two points separated by distance τ. $C(\tau)$ can be normalised into the correlation function $\rho(\tau)$ by the following equation (Fenton and Griffiths 2008)

$$\rho(\tau) = \frac{C(\tau)}{\sigma^2} \tag{2.41}$$

where σ^2 is the field variance.

Under the assumption of stationarity, μ and σ^2 of a random field are invariant in space and the covariance function and correlation function depend only on the relative distance τ between points.

A simple measurement of the spatial variability of a random field is the scale of fluctuation θ, which is mathematically defined as (Vanmarcke 1983)

$$\theta = 2\int_0^{\infty} \rho(\tau) d\tau \tag{2.42}$$

As explained in Section 2.5.1, larger θ represents a less variable (i.e. highly correlated) random field.

(3) Spatial Averaging and Variance Reduction

Fenton and Griffiths (2008) stated that all engineering properties are virtually properties of local average to a certain degree. For instance, the σ_{ci} of a rock is measured at the scale of the specimen rather than at the scale of rock particles.

The local average of a one dimensional random field being averaged over a window of width T centred at location t is expressed as (Fenton and Griffiths 2008)

$$X_T(t) = \frac{1}{T}\int_{t-T/2}^{t+T/2} X(\xi) d\xi \tag{2.43}$$

where $X_T(t)$ is the local average over width T of the point properties $X(t)$.

For a stationary random field, the locally averaged field preserves the mean of the original field but significantly reduces the variance. To illustrate, Figures 2.5(a) and 2.5(b) demonstrate the random field in Figure 2.4(a) being averaged over width 10 and 20

respectively. It is apparent that the field mean is largely unaffected whereas the variance is significantly reduced.

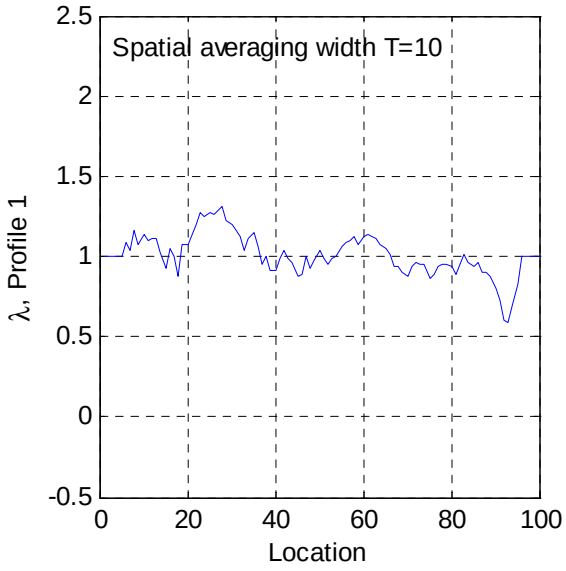

Figure 2.5 (a) The random field shown in Figure 2.4 (a) being locally averaged over width T = 10

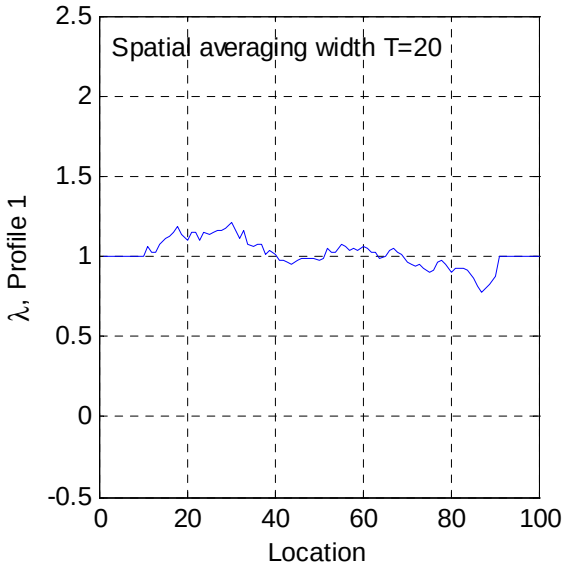

Figure 2.5 (b) The random field shown in Figure 2.4 (a) being locally averaged over width T = 20

The variance reduction caused by local averaging over width T is quantified by the variance function γ(T) so that

$$\sigma_T^2 = \sigma^2 \gamma(T) \tag{2.44}$$

where σ^2_{T} is the variance of the locally averaged field and σ^2 is the variance of the original field. For a one-dimensional stationary random field, the variance function γ(T) is expressed as (Fenton and Griffiths 2008)

$$\gamma(T) = \frac{2}{T^2}\int_0^T (T-\tau)\rho_X(\tau)d\tau \tag{2.45}$$

where $\rho_X(\tau)$ is the correlation function of the original random field.

Furthermore, Vanmarcke (1983) suggested that for simplicity, the variance function can be approximated by the following equation

$$\gamma(T)=\begin{cases}1 & \text{if } \theta \le T\\ \dfrac{\theta}{T} & \text{if } \theta > T\end{cases} \tag{2.46}$$

(4) Some Commonly Used Correlation Function Models

Three commonly used correlation function models, including their corresponding variance functions, are presented in Table 2.7.

Table 2.7 Three correlation function models and the corresponding variance functions

Model	Correlation function / Variance function	
Triangular	Correlation function	$\rho(\tau)=\begin{cases}1-\lvert\tau\rvert & \text{if } \lvert\tau\rvert \le \theta\\ 0 & \text{if } \lvert\tau\rvert > \theta\end{cases}$
	Variance function	$\gamma(T)=\begin{cases}1-\dfrac{T}{3\theta} & \text{if } T \le \theta\\ \dfrac{\theta}{T}\left[1-\dfrac{\theta}{3T}\right] & \text{if } \lvert\tau\rvert > \theta\end{cases}$
Markov	Correlation function	$\rho(\tau)=\exp\left\{-\dfrac{2\lvert\tau\rvert}{\theta}\right\}$
	Variance function	$\gamma(T)=\dfrac{\theta^2}{2T^2}\left[\dfrac{2\lvert T\rvert}{\theta}+\exp\left\{-\dfrac{2\lvert T\rvert}{\theta}\right\}-1\right]$
Gaussian	Correlation function	$\rho(\tau)=\exp\left\{-\pi(\dfrac{\tau}{\theta})^2\right\}$
	Variance function	$\gamma(T)=\dfrac{\theta^2}{\pi T^2}\left[\dfrac{\pi\lvert T\rvert}{\theta}\operatorname{erf}\left\{-\dfrac{\sqrt{\pi}\lvert T\rvert}{\theta}\right\}+\exp\left\{-\dfrac{2T^2}{\theta^2}\right\}-1\right]$

where θ is the scale of fluctuation.

The correlation functions in Table 2.7 for θ = 1 are plotted in Figure 2.6. It is shown that the correlations between points decrease as the distance τ increases.

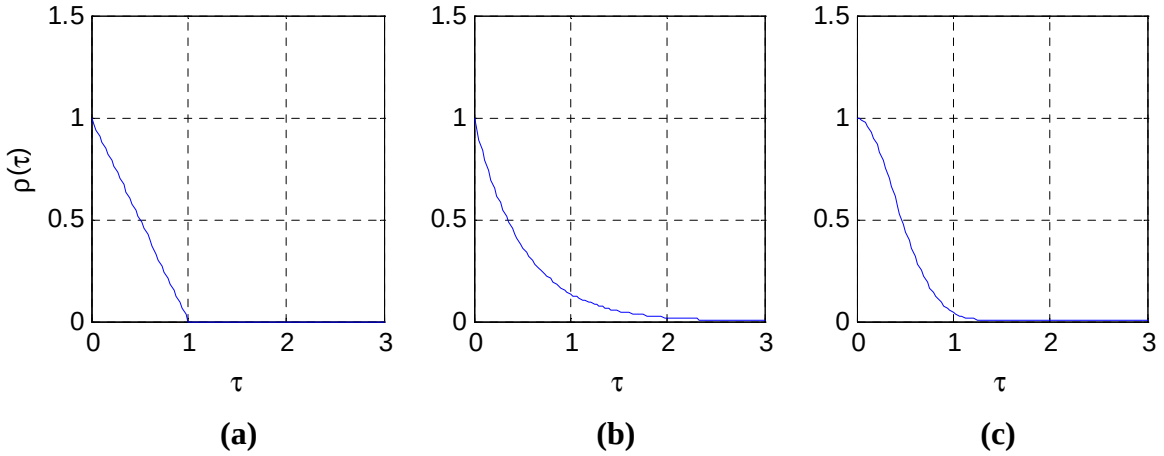

Figure 2.6 Correlation functions of Triangular, Markov and Gaussian models for θ = 1

2.5.2.2 Geostatistics

Geostatistics was originally developed for the purpose of mineral resource estimation (Journel and Huijbregts 1978). It has later been applied to various disciplines including geotechnical engineering, water engineering, and earthquake engineering (Wang et al. 2000; Webster and Oliver 2007). The discussion of geostatistics in this section is mostly restricted to the variogram and its estimation.

(1) Variogram

In geostatistics, the variogram (semivariogram) is used to measure the auto-correlation between points along a specific direction. The variogram γ_h is expressed as (Dowd 2006)

$$\gamma_h = \frac{1}{2} E\left[\left(X_{i+h} - X_i \right)^2 \right] \tag{2.47}$$

where X_i is the value of the point at location i, X_{i+h} is the value of the point at location i+h, and h is the distance between the two points.

In reality, it is impossible to obtain the values of all points to determine the expectation by Equation 2.47 and the variogram is usually estimated from available data by the experimental variogram γ_h^*. The experimental variogram is determined by

$$\gamma_h^* = \frac{1}{2N_s}\sum_{i=1}^{N}\left[\left(X_{i+h} - X_i\right)^2\right] \tag{2.48}$$

where N_s is the number of data pairs that are separated by distance h.

(2) Some Commonly Used Variogram Models

Experimental variograms are usually fitted with different models. Three commonly used variogram models are presented in Table 2.8.

Table 2.8 Three commonly used variogram models

Model	Mathematical expression
Spherical	$\gamma_h = C(\frac{3h}{2a} - \frac{h^3}{2a^3}) + C_0$ when $h \le a$ $\gamma_h = C + C_0$ when $h \ge a$
Exponential	$\gamma_h = C(1 - e^{-h/a}) + C_0$
Gaussian	$\gamma_h = C(1 - e^{-h^2/a^2}) + C_0$

The parameters involved in the above models are explained below.

C_0 is the nugget variance. It represents the variance that arises within the distance that is shorter than the sampling interval and is caused by variations of micro-structures within

the material, statistical errors, and measurement errors (Jaksa 1995). Nugget variance causes the variogram to go from zero to the level of C_0 when the distance h between two points becomes non-zero.

$C + C_0$ is the sill value. It measures half the maximum squared difference between point pairs and is equal to the variance of the sample data.

a is the range of influence or simply range, which is a simple measurement of spatial variability in geostatistics (equivalent to the scale of fluctuation in random field theory). For the spherical model, the variogram γ_h increases to the sill (which indicates that the auto-correlation between points diminishes to zero) when h reaches a. For exponential and Gaussian models, γ_h reaches $0.95C + C_0$ when h reaches $3a$ and $\sqrt{3}$.a respectively; thus $3a$ and $\sqrt{3}$.a are the effective ranges of the exponential and Gaussian models.

The variograms of the three models in Table 2.8 for $C_0 = 0$, $C = 1$, and $\alpha = 1$ are plotted in Figure 2.7.

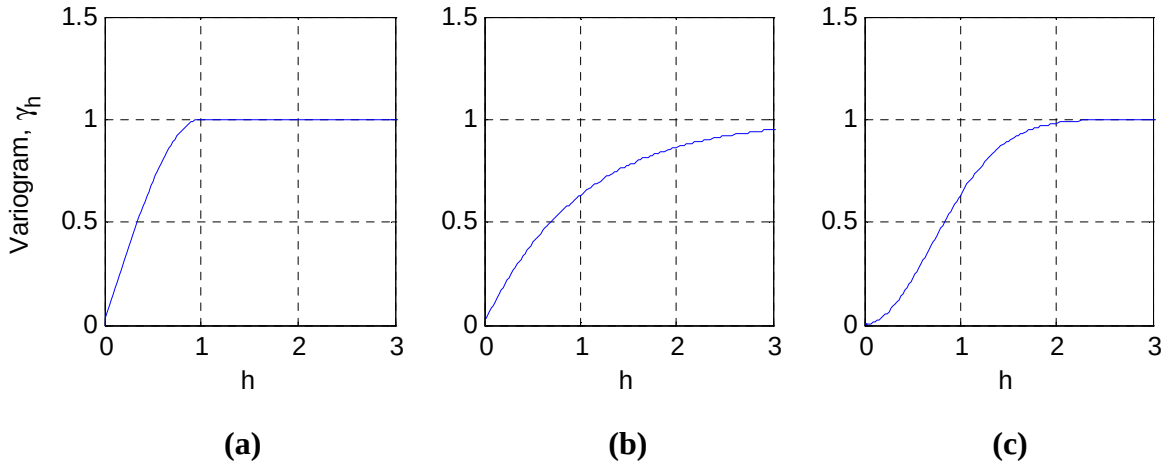

Figure 2.7 Variograms of Spherical, Exponential and Gaussian models for $C_0 = 0$, $C = 1$, and $a = 1$

As they are two explicit methods for characterising geotechnical variability, there are connections between random field theory and geostatistics. Specifically, many of the correlation function models used in random field theory have equivalent geostatistics variogram models. For instance, the Markov model (given in Table 2.7) in random field theory is equivalent to the exponential model (given in Table 2.8) in geostatistics: if the random field Markov model has a mean value of μ, a variance of σ^2, and scale of fluctuation of θ, the equivalent geostatistical exponential model would have the same mean value μ, a sill value $C + C_0 = \sigma^2$ (with $C_0 = 0$), and a range $a = ½\ \theta$. Similarly, the Gaussian model (given in Table 2.7) in random field theory is equivalent to the Gaussian model (given in Table 2.8) in geostatistics: if the random field Gaussian model has a mean value of μ, a variance of σ^2, and scale of fluctuation of θ, the equivalent geostatistical Gaussian model would have the same mean value μ, a sill value $C + C_0 = \sigma^2$ (with $C_0 = 0$), and a range $a = (1/\sqrt{\pi})\ \theta$.

2.5.3 Probabilistic Analysis Techniques

After the variability of input parameters being characterised, the next step is to incorporate and evaluate its influence on slope stability. In a probabilistic analysis, slope stability is primarily quantified by the probability of failure (PF) or the reliability index β_r.

Suppose that the FS of a slope is a performance function with n input parameters $x_1, x_2, \ldots, x_n$ such that $FS = f(x_1, x_2, \ldots, x_n)$, PF is then defined as

$$PF = Probability\{FS < 1\} \tag{2.49}$$

and β_r is defined as

$$\beta_r = \frac{\mu_{FS} - 1}{\sigma_{FS}} \tag{2.50}$$

where μ_{FS} is the mean of FS and σ_{FS} is the standard deviation of FS.

Common probabilistic techniques to compute PF or β_r include first order second moment method (FOSM), first order reliability method (FORM), point estimate method (PEM), and Monte Carlo simulation (MCS). These techniques are introduced in the following sections.

2.5.3.1 First Order Second Moment Method

The basic concept of FOSM is that from the first and second moments (i.e. mean and variance) of the input variables, the first and second moments of FS can be estimated using the first order items of the Taylor series expansion (Baecher and Christian 2003), i.e.

$$\mu_{FS} = f(\mu_{x_1}, \mu_{x_2}, ..., \mu_{x_n}) \tag{2.51}$$

$$\sigma_{FS}^2 = \sum_{i=1}^{n} \frac{\partial FS^2}{\partial x_i} \sigma_{x_i}^2 \tag{2.52}$$

where x_i is the input variable.

PF can then be estimated from μ_{FS}, σ^2_{FS}, and the assumed distribution of FS (a normal or lognormal distribution is commonly adopted). β_r can be calculated by Equation 2.50.

Due to the complexity of slope problems, it is often difficult to evaluate the partial derivatives of FS with respect to input variables directly as required in Equation 2.52. Under such circumstances, a finite difference approach is commonly adopted to approximate the partial derivative.

FOSM has the advantage of being efficient. It enables sensitivity analysis to be easily carried out since the variance of FS is the sum of contributions from the variances of the input variables, as shown in Equation 2.52. However, FOSM has several drawbacks, major ones including: firstly, its results can be inaccurate if the performance function cannot be well approximated by the first order items of the Taylor series expansion; secondly, only mean and variance of FS are estimated and other higher order moments are unknown; and lastly, the calculated PF is sensitive to the assumed distribution of FS.

2.5.3.2 First Order Reliability Method

Another problem associated with FOSM is that it produces inconsistent PF for the same problem stated in equivalent performance functions but of different forms. This is because FOSM essentially calculates the distance from the mean point to the failure surface in a certain direction (the direction of the gradient) instead of finding out the global minimum distance (from the mean point to the failure surface). Hasofer and Lind (1974) proposed the First Order Reliability Method (FORM) as an improvement of FOSM to address this problem.

The Hansfor and Lind's reliability index β_{HL} is defined as (Low 2003)

$$\beta_{HL} = \min_{\mathbf{x} \in \Psi} \sqrt{\left[\frac{x_i - m_i}{\sigma_i}\right]^T [\mathbf{C}]^{-1} \left[\frac{x_i - m_i}{\sigma_i}\right]} \tag{2.53}$$

where x_i is the input variable, $\mathbf{x}$ is the vector of input variables, m_i is the mean of the input variables, $\mathbf{C}$ is the covariance matrix, and Ψ is the failure domain. FORM computes the global minimum distance from the mean point to the failure surface. Such process needs to use an optimisation algorithm.

FORM is more accurate than FOSM. However, the requirement of optimisation algorithms reduces its efficiency. In addition, FORM is based on normally distributed input variables and modifications are necessary for it to incorporate variables of other distributions.

2.5.3.3 Point Estimate Method

Point estimate method (PEM) is a simple probabilistic technique proposed by Rosenblueth (1975; 1981) to estimate the mean, variance or any higher moments of a function. Christian and Baecher (1999) presented a detailed explanation of PEM and demonstration of its applications in geotechnical engineering.

PEM evaluates the values of the performance function at a number of discrete points and then uses these values to estimate the desired moments of FS. In practice, if there are n input variables, then the performance function is evaluated at 2^n points, which include all possible combinations of variables at one standard deviation above and below their means.

Christian and Baecher (1999) concluded that PEM is easy to use and is generally more accurate than methods that are based on Taylor series expansion (FOSM and FORM). Its limitation lies in the significant increment of computation cost when the number of input variables is large.

2.5.3.4 Monte Carlo Simulation

Monte Carlo simulation (MCS) establishes the distribution of FS from a large number of random experiments in the form of numerical simulations. The PF and statistical properties of FS can be obtained from the distribution of FS. MCS has a long history of application and is discussed in detail by Baecher and Christian (2003).

The procedures of a MCS include four steps. Firstly, the probability density function (PDF) of each input variable is determined. Secondly, random values of the input variables are generated based on their PDF. Thirdly, the system performance (such as FS) is evaluated. Finally, Steps 2 and 3 are repeated N times and PF is calculated from the following equation

$$P_f = \frac{M}{N} \tag{2.54}$$

where M is the number of times that the system fails (in our case, FS < 1).

The advantages of MCS include the clear concept, simple process, and robust results. In addition, MCS is the only probabilistic method that can explicitly incorporate random fields, which are necessary for the explicit characterisation of spatial variability. The disadvantage of MCS is its high computation cost. This problem, however, can be effectively improved by various variance reduction techniques[1] (Baecher and Christian 2003).

2.5.3.5 Incorporating Spatial Variability in Probabilistic Analysis

Suchomel and Mašín (2010) concluded that there are two types of method to incorporate spatial variability in probabilistic analysis: hybrid method and explicit method.

The hybrid method is adopted when FOSM, FORM, or PEM is applied. It incorporates spatial variability indirectly by reducing the variance of input by Equation 2.44 or by modelling the material by more than one random variables and changing the correlation matrix (**C** in Equation 2.53) of these random variables. The explicit method can only be

[1] Variance reduction here refers to the technique in MCS to reduce iteration numbers. It is different from the variance reduction in random field theory.

adopted when MCS is applied. It incorporates spatial variability directly by modelling input variables as random fields. Two most rigorous explicit methods are the random finite element method (RFEM) developed by Griffiths and Fenton (2004) and Random LEM developed by Cho (2010).

The explicit method is expected to produce the most accurate results (Suchomel and Mašín 2010). However, the implementation of MCS together with random field generations is very time consuming. On the other hand, the hybrid method indirectly takes into account spatial variability and produces results of reasonable accuracy. It is viewed as an effective substitute for the explicit method when the computation requirement is unachievable (El-Ramly et al. 2002; Suchomel and Mašín 2010).

2.5.4 Output Assessment

PF or β_r is the final output from a probabilistic analysis. Several acceptance criteria have been developed for PF, including ones proposed by Priest and Brown (1983), SRK consulting (Read and Stacey 2009), and Sullivan (Read and Stacey 2009). On the other hand, Christian (2004) stated that it is often more useful to examine the comparative PF values from various alternative courses of action instead of relying on the absolute PF values.

Apart from PF and β_r, a probabilistic analysis yields the mean and variance of FS. When MCS is adopted, the distribution of FS can also be obtained. The distribution of FS is useful as it enables a detailed statistical analysis on FS.

2.6 Previous Studies on Probabilistic Slope Stability Analysis

Probabilistic Slope Stability Analysis (PSSA) has been a primary area of research in slopes for the past three decades. This section presents a review of previous studies in PSSA, with the aim of identifying specific research directions and research gaps for the present study.

A selection of literature on PSSA is presented in chronological order in Table 2.9. The information regarding these studies is divided into six components. Firstly, the type of project is either “Slope” or “Others” (such as tunnel or foundation). Most of the investigations focus on slopes (29/33); others are selected because methodologies similar to PSSA were used. Secondly, the type of the material is either “Soil” or “Rock”. The focus of the research in the present thesis is highly fractured rock slopes, whose failures are similar to those of soil slopes. Therefore, much of the research reviewed is in soil slopes. Thirdly, the applied strength criterion is MC, HB, or others. Fourthly, the analysis method (for FS calculations) is LEM or the numerical method. Fifthly, the probabilistic analysis technique is FOSM, FORM, PEM, MCS, or others. “Others” here include those less commonly used techniques, such as the second order second moment method (SOSM). Lastly, research is also tagged with None (which means spatial variability is not considered), Hybrid method, or Explicit method, depending on how spatial variability of input parameters is quantified and evaluated.

Table 2.9 Selected previous studies on probabilistic slope stability analysis: scope

ID	Year	Reference	Project	
			Slope	Others
1	2012	(Fisher and Eberhardt 2012)	√	
2	2012	(Mao et al. 2012)		√
3	2011	(Idris et al. 2011)		√
4	2011	(Cai 2011)		√
5	2011	(Wang et al. 2011)	√	
6	2011	(Lü and Low 2011)		√
7	2010	(Suchomel and Mašín 2010)	√	
8	2010	(Cho 2010)	√	
9	2009	(Fu et al. 2009)	√	
10	2009	(Griffiths et al. 2009)	√	
11	2008	(Hong and Roh 2008)	√	
12	2007	(Cho 2007)	√	
13	2007	(Low 2007)	√	
14	2006	(Hsu and Nelson 2006)	√	
15	2006	(El-Ramly et al. 2006)	√	
16	2005	(El-Ramly et al. 2005)	√	
17	2004	(Griffiths and Fenton 2004)	√	
18	2004	(Babu and Mukesh 2004)	√	
19	2003	(Low 2003)	√	
20	2003	(El-Ramly et al. 2003)	√	
21	2002	(El-Ramly et al. 2002)	√	
22	2000	(Duncan 2000)	√	√
23	2000	(Wang et al. 2000)	√	
24	1999	(Hassan and Wolff 1999)	√	
25	1998	(Hoek 1998)	√	√
26	1997	(Low and Tang 1997a)	√	
27	1997	(Low and Tang 1997b)	√	
28	1995	(Chowdhury and Xu 1995)	√	
29	1994	(Christian et al. 1994)		√
30	1992	(Chowdhury and Xu 1992)	√	
31	1987	(Li and Lumb 1987)	√	
32	1984	(Whitman 1984)	√	√
33	1983	(Priest and Brown 1983)	√	

Table 2.9 *Continued*

ID	Material		Strength criterion			Analysis method	
	Soil	Rock	MC	HB	Others	LEM	Numerical
1		√	√	√		√	
2		√		√		√	
3		√		√			√
4		√		√			√
5	√				√	√	
6		√	√	√	√	√	√
7	√		√			√	√
8	√		√		√	√	
9		√	√	√			√
10	√		√		√		√
11	√		√			√	
12	√		√			√	
13	√		√			√	
14		√	√				√
15	√		√			√	
16	√		√			√	
17	√				√		√
18	√		√			√	
19	√		√			√	
20	√		√			√	
21	√		√			√	
22	√				√	√	
23		√	√				√
24	√		√			√	
25		√	√	√		√	
26	√		√			√	
27	√		√			√	
28	√		√			√	
29	√		√			√	
30	√		√			√	
31	√		√			√	
32	√		√			√	
33		√		√		√	

Table 2.9 *Continued*

ID	Probabilistic analysis technique					Spatial variability		
	FOSM	FORM	PEM	MCS	Others	None	Hybrid	Explicit
1				√		√		
2				√		√		
3				√		√		
4			√	√		√		
5	√	√		√				√
6		√		√	√	√		
7	√			√		√	√	√
8				√				√
9			√			√		
10		√		√				√
11		√					√	
12		√		√				√
13		√		√			√	
14				√				√
15				√				√
16				√				√
17				√				√
18	√						√	
19		√		√			√	
20				√				√
21	√			√			√	√
22	√					√		
23				√			√	
24		√				√		
25			√	√		√		
26		√					√	
27		√				√		
28	√	√				√		
29	√						√	
30	√	√				√		
31		√					√	
32	√				√	√		
33				√		√		

Some trends are evident from Table 2.9. For instance, it is apparent that with the advance in computer technology over the years, the numerical method, MCS, and explicit ways to incorporate spatial variability have gained increasing popularity in PSSA. However, in cases where the HB strength criterion is applied (highlighted), none has yet taken into account spatial variability.

Further analysis was taken to identify specific research directions arising from the selected PSSA literature (Table 2.9). While it is impossible to exhaust all directions, six major emphases have been identified, as shown in Table 2.10. These include firstly, input parameters, which means that the research has focused on site investigations, studies of the variability of geotechnical parameters, or data analyses; secondly, improvement of methodology, which means that the research has focused on improving the accuracy (e.g. in identifying failure surfaces, incorporating spatial variability, or computing PF), efficiency, or user-friendliness; thirdly, comparison of methodology, which means that the research has focused on comparing the accuracy or efficiency of different probabilistic techniques or different ways to incorporate spatial variability; fourthly, acceptance criterion, which means that the research has focused on the definition or acceptable values of PF or β_r; fifthly, engineering application of PSSA, which means that the research has focused on demonstrating and promoting the ideas and techniques of PSSA; and lastly, input and output studies, where the research has focused on systematic studies of the relationship between the input parameters and the output for specific cases, mainly by sensitivity analysis and parametric study.

Among these research directions, outcomes from the first five are largely universal, meaning that the conclusion from one case is applicable to other cases. On the other hand,

the outcome from the sixth research direction is case dependent, particularly on different types of slopes and strength criteria.

The sixth research direction, i.e. the relationship between input and output, can be further divided into seven sub-areas, i.e. 1) COV (single-parameter), where the research aims to investigate the relative contribution of the variability of each input parameter to PF; 2) COV (multi-parameter), where the research aims to investigate the influence of changes in the variability (usually quantified by the COV) of input parameters on PF; 3) Distribution, where the research aims to investigate the influence of distributions of input parameters on PF; 4) Cross-correlation, where the research aims to investigate the influence of cross-correlations between input parameters on PF; 5) Spatial variability, where the research aims to investigate the influence of spatial variability of input parameters on PF; 6) Anisotropy, where the research aims to investigate the influence of anisotropy of input parameters on PF and 7) Courses of action, where the research aims to investigate the influences of various design decisions, such as different slope geometry and supports, on PF.

The selected literature in Table 2.9 is classified into the above summarised research directions and shown in Table 2.10, with research that employs the HB strength criterion being highlighted.

Table 2.10 shows that all six major research directions have been intensively investigated for soil slopes, where the MC strength criterion is mainly applied. However for fractured rock slopes, where the HB strength criterion is employed, there has been little research in terms of the sixth research direction, i.e. the relationship between input parameters and output.

Table 2.10 Selected previous studies on probabilistic slope stability analysis: major research directions

ID	Major research directions (1-5)				
	Input parameters	Improvement of methodology	Comparison of methodology	Acceptance criterion	Engineering application
1					
2		√			
3					√
4	√				√
5		√	√		
6		√	√		
7			√		
8		√			
9					√
10		√	√		
11					
12		√			
13		√	√	√	
14	√				
15	√				√
16	√			√	
17		√			
18					
19		√	√		
20	√			√	√
21	√	√	√	√	√
22	√				√
23					√
24		√			
25					√
26		√			
27		√			
28		√		√	
29	√			√	√
30			√		
31		√			
32	√			√	√
33				√	√

Table 2.10 *Continued*

ID	Major research directions (6th) Input and output studies: sensitivity analysis or parametric study						
	COV single-parameter	COV multi-parameter	Distribution	Cross-correlation	Spatial variability	Anisotropy	Courses of action
1	√						
2	√	√	√	√			√
3							√
4							
5					√		
6			√	√			√
7		√			√		
8				√		√	
9							
10	√	√		√	√		√
11		√	√		√		
12	√				√	√	
13					√		
14							
15					√		√
16					√		√
17		√			√		
18					√	√	√
19			√				
20	√				√		
21	√						
22	√	√					
23							
24							
25							
26							
27							√
28							
29							√
30		√		√			
31		√			√		√
32		√					
33							√

2.7 Summary

In this chapter, slope stability analysis, the Hoek-Brown (HB) strength criterion, the Limit Equilibrium Method (LEM), and Probabilistic Slope Stability Analysis (PSSA) as well as its applications, have been reviewed. The HB strength criterion is demonstrated to be an effective tool for rock slope stability analysis. However, even though the relationship between input and output has been an important research area for the last three decades, there has been little research into the relationship between the input (HB parameters and their variability) and the output (FS and PF) for highly fractured rock slopes.

Chapter 3

RESEARCH OBJECTIVES AND METHODOLOGY

3.1 Research Objectives

Based on the literature review in Chapter 2, it was decided that the focus of the present study would be to investigate the stability of highly fractured rock slopes in terms of the relationship between the input, Hoek-Brown (HB) parameters and their variability, and the output, Factor of Safety (FS) and Probability of Failure (PF). Five specific research objectives are identified and given below:

1) to study the sensitivity of FS to the changes in HB parameters

Given the complexity of the slope problem, it is likely that the sensitivity of FS to the changes in HB parameters (abbreviated as "FS sensitivity") is non-linear. Therefore, the first objective is to find out whether there are any particular ranges of HB parameters that cause high FS sensitivity and whether such ranges are affected by different combinations of HB parameters.

Additionally, for efficiency purposes, it is important to determine whether such FS sensitivity is affected by slope geometry. If it is not, then the present research can be carried out on a representative slope case and the corresponding conclusions should be reasonably general.

2) to investigate the influence of changes in the variability of HB parameters (quantified by the COV) on PF

This objective corresponds to the "COV multi-parameter" research area in Table 2.10.

3) to evaluate the relative contribution of the variability of each HB parameter (quantified by the COV) to PF

This objective corresponds to the "COV single-parameter" research area in Table 2.10 and aims to identify the HB parameter whose variability makes the largest contribution to PF.

4) to investigate the influence of the spatial variability of HB parameters (quantified by the scale of fluctuation θ) on PF

This objective corresponds to the "Spatial variability" research area in Table 2.10.

5) to explore the relationship between FS sensitivity and PF

Since PF is the probability of FS being less than 1, there should be a connection between FS sensitivity and the value of PF. For a slope with specific geometry, there are many possible cases where different combinations of HB parameters (GSI, m_i, and σ_{ci}) can give the same FS. A specific question to answer is that for these cases with the same FS values, if the variability of HB parameters (quantified by the COV) is also identical, what will be the corresponding PF values?

Among the five objectives, the first four are selected with the aim to provide a better understanding about the input and output relationship in the stability analysis of highly fractured rock slopes. The results should help to identify the most critical input parameters or most critical ranges of input parameters so that relevant precautions can be taken for

slope designs and site investigations. The last objective aims to compare the effectiveness of PF as a safety index with that of FS. On the other hand, other research directions, including “Input distribution” and “Cross correlation” (as discussed in Section 2.6), are not included here since there have been few distributions other than normal that have been adopted for HB parameters and there have been few proofs of cross correlations between HB parameters.

Two major chapters are devoted to the study of the above five objectives. The first objective, which focuses on FS sensitivity, is investigated in Chapter 4. Since FS is the output of a deterministic analysis, Chapter 4 is entitled “deterministic analysis”. The remaining objectives are investigated in Chapter 5, which is entitled “probabilistic analysis”. The methodologies for the deterministic analysis and probabilistic analysis are introduced in the following sections.

3.2 Methodology for the Deterministic Analysis

3.2.1 Outline of the Methodology

In the deterministic analysis, FS sensitivity is examined as well as the influence of slope geometry. A sensitivity graph analysis and an equation fitting analysis are developed here. The software involved in the deterministic analysis includes *Slide6.0* (Rocscience 2011) which is a limit equilibrium slope stability analysis software and *Matlab.*

For the sensitivity graph analysis, the relationship between FS and HB parameters is plotted in a series of figures. These figures are used to determine whether FS sensitivity is affected by slope geometry and to provide some initial insights into FS sensitivity. For the equation fitting analysis, *Slide6.0* is used to create large sets of data between HB

parameters and FS based on wide combinations of HB parameters. This data is then fitted with a suitable equation (as FS = f (GSI, m_i, σ_{ci})), and FS sensitivity is analysed by taking derivatives (rates of change) of this equation with respect to HB parameters. Lastly, sensitivity graphs are again used to provide a visual verification of the final conclusions.

The proposed methodology for the deterministic analysis has the advantages of being straightforward and precise, as both qualitative and quantitative approaches are applied.

In the following sections, the Limit Equilibrium Method (LEM) model used in the deterministic analysis, *Slide6.0*, is firstly introduced. The sensitivity graph analysis and the equation fitting analysis are then discussed.

3.2.2 LEM Model (*Slide6.0*)

The LEM software *Slide6.0* is adopted for the deterministic analysis. There are several LEM models incorporated in *Slide6.0*. Among them, Bishop's simplified method of slices is chosen for the present study. Bishop's model produces reasonably accurate results and is relatively simple. While some other LEM models, such as the Spencer (Duncan and Wright 2005) and Morgenstern-Price (Duncan and Wright 2005), have the advantages of satisfying complete equilibrium (i.e. both force and moment equilibrium) and being able to model irregular failure surfaces, they are complicated and time-consuming, which are significant drawbacks for the present study (especially for the later probabilistic analysis, where Monte Carlo simulation, MCS, is applied).

The settings in the LEM model are given here. The slip surface is set to be "Circular" and is found by the "Grid search" method. "General Hoek-Brown" is selected as the "Strength type" in "Material property" and the "Number of slices" is set at 30.

3.2.2.1 Number of Slices

Duncan and Wright (2005) stated that the change in number of slices does not have a strong impact on FS when the slope geometry and material below the slope surface have been confirmed. In the present study, five cases with identical slope geometry and material properties but different number of slices are examined to find out the sufficient number of slices. The slope geometry and material properties are shown in Figure 3.1 and the results are presented in Table 3.1.

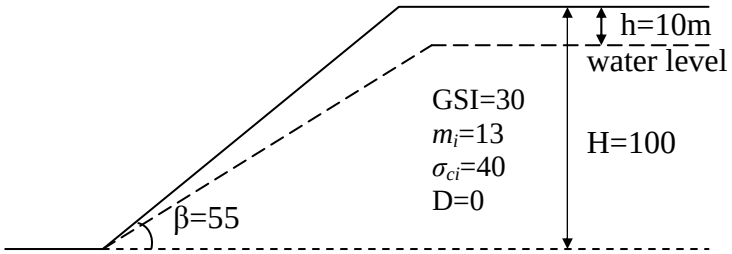

Figure 3.1 Slope geometry and rock mass properties for examining the effect of changes in number of slices on FS

Table 3.1 Effect of changes in number of slices on FS

Case	1	2	3	4	5
Number of slices	20	30	40	60	100
FS	1.289	1.284	1.282	1.282	1.282

The results in Table 3.1 confirm that when the number of slices is ≥ 30, its change has little influence on the computed FS. Since a fewer number of slices requires less computation effort, 30 slices is selected for the present study.

3.2.3 Sensitivity Graph Analysis

The sensitivity graph analysis presents the relationship between FS and HB parameters in a qualitative graphical form. The employment of this analysis serves three purposes:

1. to examine whether FS sensitivity is affected by slope geometry

2. to provide some initial insights into FS sensitivity

3. to display and verify the final conclusions of the deterministic analysis

The process of this analysis is given below:

Firstly, for a particular slope, a set of GSI, m_i, and σ_{ci} values are specified and denoted as the "mean values". The corresponding slope model is built in *Slide6.0*.

Secondly, based on the mean values, a global minimum FS is calculated and this FS is denoted as the "mean FS".

Thirdly, for each of the input parameters, i.e. GSI, m_i, and σ_{ci}, a range is specified. Each parameter is then varied in uniform increments within its range (while all other parameters are held constant at their mean values), and the variations of FS are calculated. This step is implemented by the "sensitivity analysis" function in *Slide6.0*.

Finally, the resultant FS vs. the input HB parameters are plotted in *Matlab*, and the relationship between FS and HB parameters can be analysed.

The specified ranges of HB parameters are listed in Table 3.2. The changes of the parameters are based on an increment factor i, which extends from 0 to 1 in increments of 0.1.

For GSI and m_i, the ranges are selected based on their physical limits. For σ_{ci}, its value can be up to 200MPa; however, a range of 10 - 150MPa is reasonable for most types of rock.

Table 3.2 Ranges and the increment factor for HB parameters in sensitivity graphs

Parameter	Range	Increment factor i = 0 - 1
GSI	10 - 100	10 + 90i
m_i	5 - 40	5 + 35i
σ_{ci} (MPa)	10 - 150	10 + 140i

To illustrate, the sensitivity graph for the slope in Figure 3.1 is shown in Figure 3.2. The slope face angle β, slope height H, mean values of HB parameters, and the mean FS are given at the top of the figure (slope angle β and slope height H are given in this and all subsequent figures in the form of β-H, in this case 55-100). Each line represents the variation of FS corresponding to the change in one HB parameter, with others fixed at their mean values.

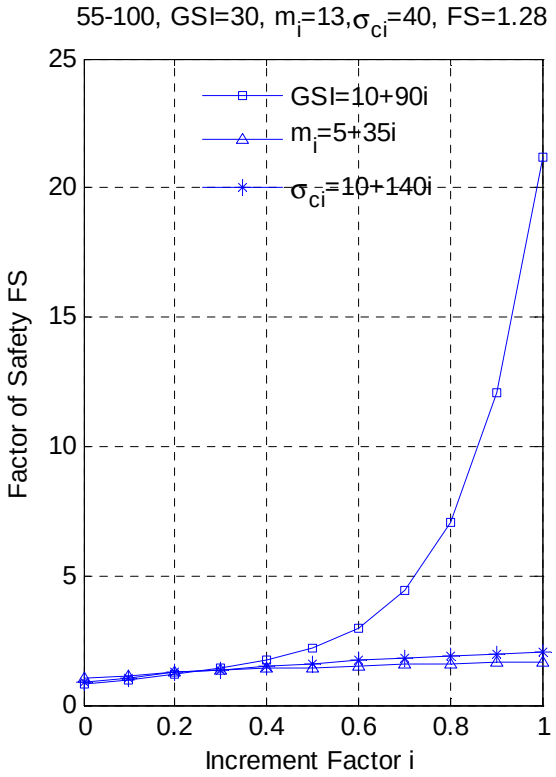

Figure 3.2 Sensitivity graph for the slope shown in Figure 3.1

To examine whether FS sensitivity is affected by the slope geometry, cases with the same HB parameters but different geometry are designed and sensitivity graphs are generated. The results are then compared to examine whether any general pattern exists.

The sensitivity graphs are also used to obtain preliminary information about FS sensitivity. However, given the complexity of slope stability problem, a quantitative approach is deemed necessary.

3.2.4 Equation Fitting Analysis

The equation fitting analysis is developed to supplement the sensitivity graph analysis. *Slide6.0* is used to generate a large number of data between FS and HB parameters and the data are fitted with a suitable equation (as FS = f (GSI, m_i, σ_{ci})). The sensitivity of FS is then analysed by taking the derivatives of FS with respect to HB parameters based on the fitted equation.

To implement this analysis, a large amount of data and an effective form of equation are required. Both of these requirements are discussed below.

3.2.4.1 Data

The data should consist of sets of mappings from GSI, m_i, and σ_{ci} to FS, covering a wide range of combinations between GSI, m_i, and σ_{ci}. For this purpose, data points that are uniformly distributed within the range of each HB parameter are selected. Taking n data points for GSI, m data points for m_i, and t data points for σ_{ci}, creates n × m × t combinations of GSI, m_i, and σ_{ci} and corresponding FS values for the equation fitting. The actual values of n, m, and t, are specified in Chapter 4. In addition, to make the derivatives

of FS to the HB parameters comparable with each other, all data for the equation fitting, including GSI, m_i, σ_{ci}, and FS, are normalised into the interval [0, 1].

3.2.4.2 Form of the Equation

The equation used in this case needs to obey two principles. Firstly, it should be easy to differentiate and the derivative of FS to each HB parameter should be simple. Secondly, it should satisfy the required precision. While equations with more complicated forms, such as exponentials, may be more precise, they do not conform to the first principle. A candidate equation is proposed as follows:

$$y = a_1x_1 + a_2x_2 + a_3x_3 + a_4x_1^2 + a_5x_2^2 + a_6x_3^2 + a_7x_1x_2 + a_8x_2x_3 + a_9x_1x_3 \quad (3.1)$$

where y represents FS, and x_1, x_2, x_3 represent GSI, m_i, σ_{ci} respectively.

The polynomial form is chosen as it is convenient to differentiate. It should also allow a high precision as three components are included: $a_1x_1 + a_2x_2 + a_3x_3$ is the linear component, $a_4x_1^2 + a_5x_2^2 + a_6x_3^2$ is the nonlinear component, and $a_7x_1x_2 + a_8x_2x_3 + a_9x_1x_3$ is the component representing mutual influences.

3.2.4.3 Sensitivity Analysis

Once the coefficients for Equation 3.1 have been determined and the precision has been validated, the sensitivity analysis can be carried out. For instance, the derivative of FS with respect to GSI is $\partial y/\partial x_1 = a_1 + 2a_4x_1 + a_7x_2 + a_9x_3$. The sensitivity of FS to GSI can then be measured by $\partial y/\partial x_1$ and it depends on two terms: one is $a_1 + 2a_4x_1$, which represents the

contribution from GSI itself, and the other is $a_7x_2 + a_9x_3$, which represents the contributions from other parameters and thus reflects the degree of mutual influences.

3.3 Methodology for the Probabilistic Analysis

3.3.1 Outline of the Methodology

The probabilistic analysis is carried out based on Monte Carlo simulation (MCS) using two probabilistic analysis models developed in *Matlab*. Furthermore, since *Slide6.0* is not able to incorporate spatial variability, a LEM model is developed in *Matlab* based on Bishop's simplified method of slices for the probabilistic analysis. The outline of the methodology for the probabilistic analysis is given below.

The first research objective in the probabilistic analysis is to examine the influence of changes in the variability of HB parameters on PF. The investigation is based on a parametric study where the COV of HB parameters vary systematically from 0.1 to 1. All three HB parameters are modelled as random variables simultaneously and for simplicity, their COV are assumed to be the same.

The second research objective in the probabilistic analysis is to evaluate the relative contribution of the variability of each HB parameter to PF. This is achieved through two approaches. The first employs a parametric study, where the COV of each HB parameter again varies systematically from 0.1 to 1. However, HB parameters are modelled as random variables separately (i.e. one of them is modelled as a random variable and others are fixed at their mean values). The relative contributions from the variability of HB parameters can then be related to the corresponding PF values. The second approach employs the Spearman correlation coefficient r_s, which measures the monotonic correlation

between two variables and has been used as an indicator of the contribution of the variability of an input variable to the output in several studies (El-Ramly et al. 2002; Fisher and Eberhardt 2012). In particular, a probabilistic analysis is implemented where all three HB parameters are modelled as random variables with their COV being set to the maximum values observed in engineering practice. The Spearman ranking correlation coefficients between the input HB parameters and the output FS are then measured and compared.

The third research objective in the probabilistic analysis is to examine the influence of the spatial variability of HB parameters on PF. This objective is achieved through another parametric study, where the scale of fluctuation θ of HB parameters varies from a small value to infinity. In the corresponding probabilistic analyses, HB parameters that are considered as spatial random variables are modelled as random fields (while other parameters are still modelled as random variables). It will be further discussed in Section 3.3.2.1 that which HB parameters will be considered as spatial variables.

The fourth research objective in the probabilistic analysis is to investigate the relationship between FS sensitivity and PF. This requires outcomes from the deterministic analysis and will be carried out in conjunction with investigations of the previous three research objectives.

In the present study, probabilistic analysis that does or does not consider spatial variability of input variables is termed “simplified probabilistic analysis” or “spatial probabilistic analysis” respectively.

The methodology of the Monte Carlo simulation (MCS) is discussed in Section 2.5.3.4 and our implementation is schematically illustrated in Figure 3.3. Codes of the developed *Matlab* probabilistic analysis models are provided in Appendix A.

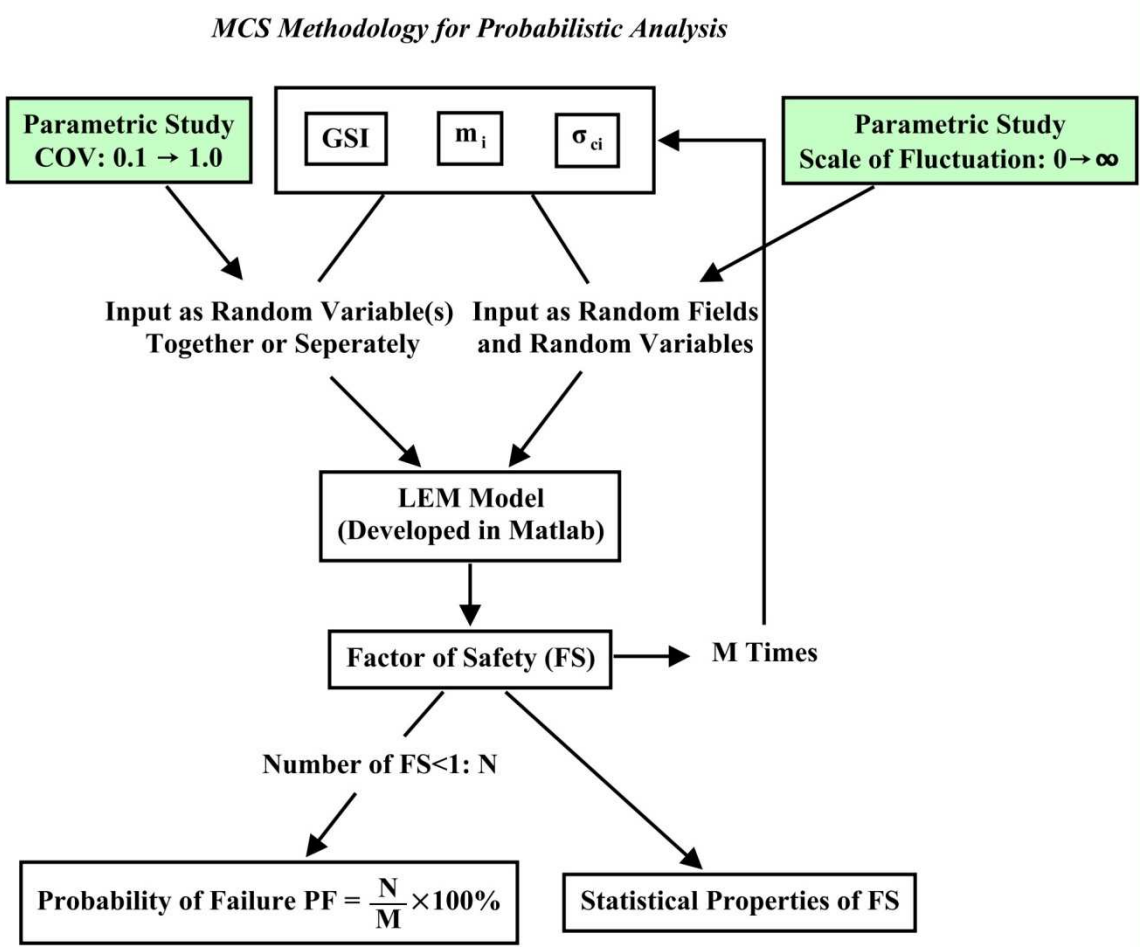

Figure 3.3 MCS methodology for the probabilistic analysis (codes of the probabilistic analysis models are provided in Appendix A)

3.3.2 Monte Carlo Simulation

3.3.2.1 Statistical Characteristics of HB Parameters

(1) Upper-Limit COV

In some of the probabilistic analyses, the COV of HB parameters are set to their observed upper limit values in engineering practice. For GSI, its variability is generally small compared with that of m_i and σ_{ci}. Based on the data in Section 2.3.2, 0.15 is selected as the upper-limit COV for GSI. Similarly, 0.2 is selected for m_i. The parameter σ_{ci} has the largest variability and in most circumstances its COV value lies between 0.1 – 0.25. However, Cai (2011) showed that the COV of σ_{ci} can be up to 0.39. Since the σ_{ci} data in Cai (2011) were obtained from measurement rather than estimation and are considered to be reliable. Marinos et al. (2005) also stated that there is a tendency to underestimate the importance of σ_{ci}. Based on these considerations, 0.4 is selected as the upper-limit COV value for σ_{ci}.

(2) Probability Distributions

Normal and lognormal distributions are the two most widely applied statistical distributions for geotechnical parameters. For traditionally used soil or rock strength parameters, such as c and φ (MC parameters), lognormal distributions are commonly assumed, due to the need to avoid negative values (Christian 2004; Fenton and Griffiths 2008). However, two of the HB parameters GSI and m_i not only have physical lower-limits as c and φ do, but also have physical upper-limits, which are 100 and 40 respectively. Truncated normal distributions are therefore considered to be more appropriate for them, and this is consistent with the literature. For σ_{ci}, test data shows that it also tends to follow

a normal distribution (Ruffolo and Shakoor 2009; Cai 2011). Consequently, truncated normal distributions are assumed for all three HB parameters in this study.

(3) Spatial Variability

The influence of the horizontal spatial variability of HB parameters along the slip surface on PF is investigated. The spatial variability is modelled by random fields, and is characterised by the scale of fluctuation θ. In the current study, only m_i and σ_{ci} are modelled as spatial variables, as they are intact rock parameters, whose spatial variability is considered to be theoretically sound and relatively easy to measure. In contrast, GSI is a measure for the blockiness of the entire rock mass. Thus it will not be modelled as a spatial variable but a random variable. For simplicity, the scale of fluctuation θ of m_i and σ_{ci} is assumed to be equal.

The random field along the slip surface is modelled based on the method of slices and each slice is a unit for the random field. Based on random field theory, the width of the slice should not exceed the scale of fluctuation, otherwise spatial averaging needs to be applied (Equation 2.46). Therefore, in the spatial probabilistic analysis, the number of slices for the LEM model is set to 100.

3.3.2.2 Issues in Simulation

(1) Number of Iterations

Number of iterations directly relates to the accuracy of a MCS. PF from a MCS only stabilises after a certain number of iterations has been reached and this number, M, is different from one case to another. Generally, the smaller the PF is, the higher number of

iterations is required. A practical approach to ensure that the required number of iterations has been reached is to plot M against PF and visually check the stabilisation. This approach is employed in the present study.

(2) Variance Reduction Technique

A major drawback of the MCS is the high computation cost required for the iterations. In the present research, MCS needs to be carried out for a large number of times in the parametric studies, which can result in extensive computation cost.

For efficiency purposes, a variance reduction technique is applied here. Such technique is commonly used in MCS to reduce the computation cost for a required level of accuracy, or equivalently, to increase the accuracy for the same number of iterations. Common variance reduction techniques include importance sampling, anthithetic sampling, correlated sampling, controlled variates, and Latin Hypercubic sampling (Baecher and Christian 2003). Most techniques mentioned above require that the analytical solution of the problem to be exact or can be approximated. However, neither of the two conditions applies to rock slope stability problems. Latin Hypercubic sampling does not have such restrictions and is used in the present study.

3.3.2.3 Analysis of the Output

For a MCS based probabilistic analysis, the output is a large number of FS. Probability of failure, PF, is the number of the FS less than 1 relative to the total number of iterations. In some situations where PF is expected be very small, the number of iterations required to stabilise PF can be too high to achieve (even if a variance reduction technique has been applied). In such situations, a simple approach given by Fenton and Griffiths (2008) is

applied to estimate the PF: firstly, as many iterations as possible are performed; afterwards, the best fit statistical distribution is found for the obtained large amount of FS; and finally, PF is estimated from the fitted distribution of FS.

After PF is obtained, its absolute value can be evaluated based on various acceptance criteria. However, in the present study, the "Comparative PF" (Christian 2004), such as the variation of PF corresponding to the changes in the COV of input parameters, is more of interest. Apart from PF, the distribution and statistical properties of FS, including the mean, standard deviation, and COV, will also be examined.

3.3.3 LEM model (Developed in *Matlab*)

A LEM model was programmed in *Matlab* for the probabilistic analysis. The codes of this model are given in Appendix A. In this section, theory and validation of this LEM model are presented.

3.3.3.1 Theory of the LEM Model

The LEM model developed here uses the slip surface imported from the program *Slide6.0* and calculates FS by Bishop's simplified method of slices. Bishop's simplified method of slices is based on the MC strength criterion and uses MC parameters as input. Therefore, to use the HB strength criterion in conjunction with Bishop's simplified method of slices, an additional step that converts HB parameters to equivalent MC parameters is necessary. For the present study, Kumar's solution (discussed in Section 2.3.3.1), which is an accurate converting solution, is applied.

The algorithm of the LEM model is described below and also shown in Figure 3.4.

1. Calculate m_b, s, and a from input HB parameters by Equations 2.2, 2.3, and 2.4 and then calculate the effective normal stresses on the slip surface by the updated Fellenius's solution (Equation 2.34).

2. Convert HB parameters to equivalent MC parameters by Kumar's solution (Equations 2.14, 2.15, and 2.16).

3. Give an initial input of FS (1 is selected for the present study).

4. Calculate the first FS by Equation 2.38.

5. Calculate a second FS based on the updated FS (from Step 4) by Equation 2.38.

6. If the difference between the first and second FS is more than a threshold value (0.001 is selected for the present study), return to Step 4 and use the second FS as input for the calculation. Repeat Steps 4 and 5 until the difference between the last two FS is less than the threshold value.

(End of the algorithm).

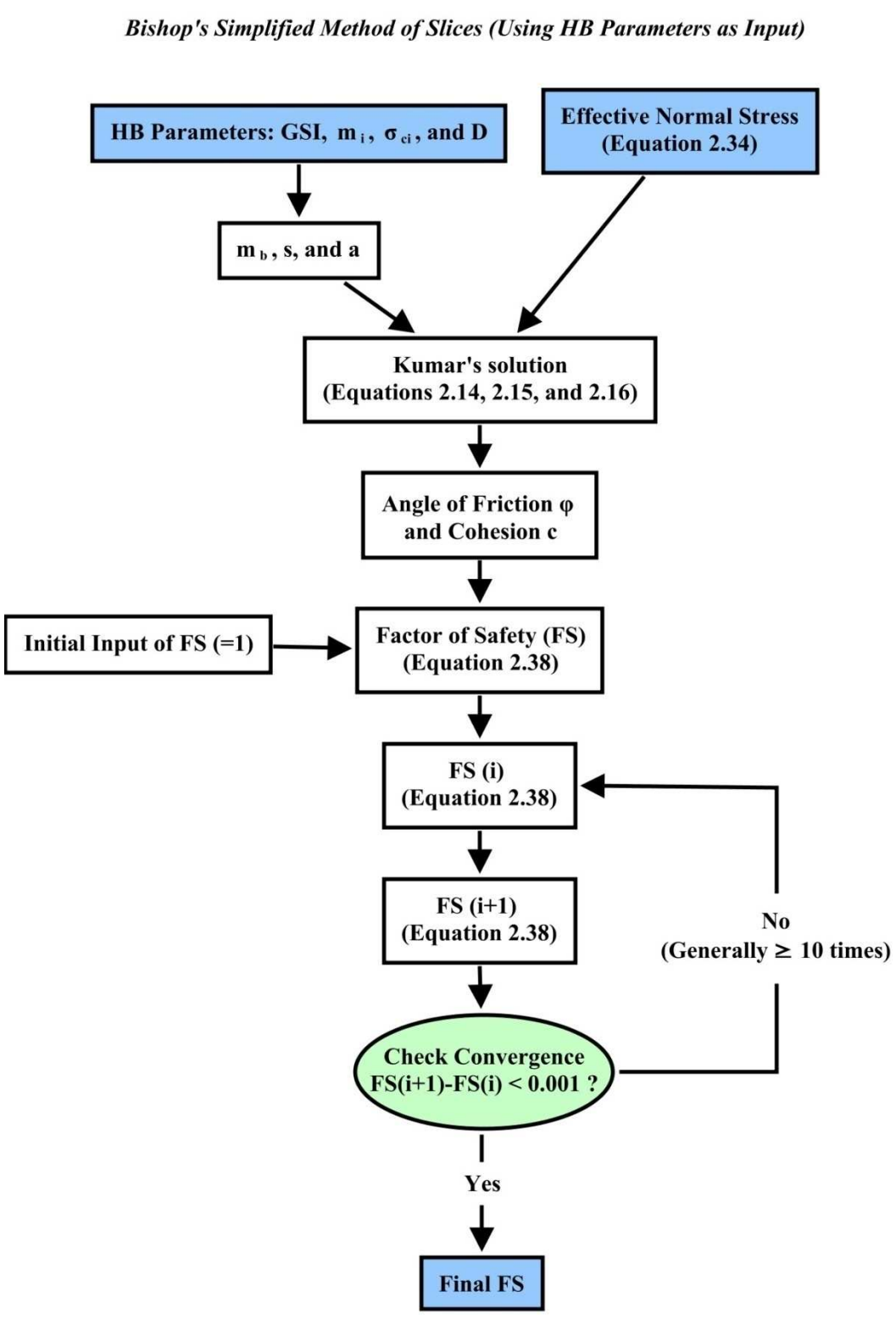

Figure 3.4 Algorithm of the LEM model developed in *Matlab* for the probabilistic analysis (codes given in Appendix A)

3.3.3.2 Validation of the LEM Model

The accuracy of the LEM model developed here using *Matlab* needs to be validated as it is the basis for the entire probabilistic analysis. The model is validated against *Slide6.0* by comparing the output for a wide range of cases, Table 3.3.

Seven combinations of arbitrarily selected HB parameters are applied to three slope cases with the same height but different slope face angles β (equal to 40, 55, and 70). Therefore, there are totally 21 cases, listed in Table 3.3. The slope geometry is shown in Figure 3.5.

Table 3.3 Cases for validation of the LEM model developed in *Matlab*

Case	GSI	m_i	σ_{ci} (MPa)	Slope angle β	FS *Slide6.0*	FS Developed model	RD (%)
1	10	5	10	40	0.58	0.58	0.08
2	30	13	40	40	1.96	1.96	0.14
3	50	21	70	40	3.69	3.70	0.25
4	75	30	100	40	8.91	8.92	0.12
5	100	40	150	40	37.22	37.22	0.01
6	100	5	10	40	6.89	6.89	0.06
7	10	40	150	40	2.39	2.39	-0.09
8	10	5	10	55	0.38	0.39	0.96
9	30	13	40	55	1.28	1.29	1.07
10	50	21	70	55	2.59	2.60	0.45
11	75	30	100	55	7.01	7.03	0.28
12	100	40	150	55	33.67	33.71	0.13
13	100	5	10	55	5.87	5.88	0.15
14	10	40	150	55	1.57	1.57	0.50
15	10	5	10	70	0.27	0.27	1.55
16	30	13	40	70	0.87	0.89	2.05
17	50	21	70	70	1.80	1.83	1.52
18	75	30	100	70	5.53	5.58	0.84
19	100	40	150	70	27.74	27.78	0.15
20	100	5	10	70	4.92	4.95	0.57
21	10	40	150	70	1.00	1.04	3.29

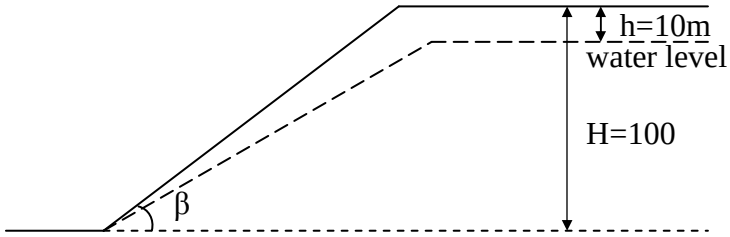

Figure 3.5 Slope geometry for validation of the LEM model developed in *Matlab*

The FS calculated by *Slide6.0* and by the developed LEM model are given in Table 3.3. The relative differences are given in the right column of Table 3.3 and plotted in Figure 3.6.

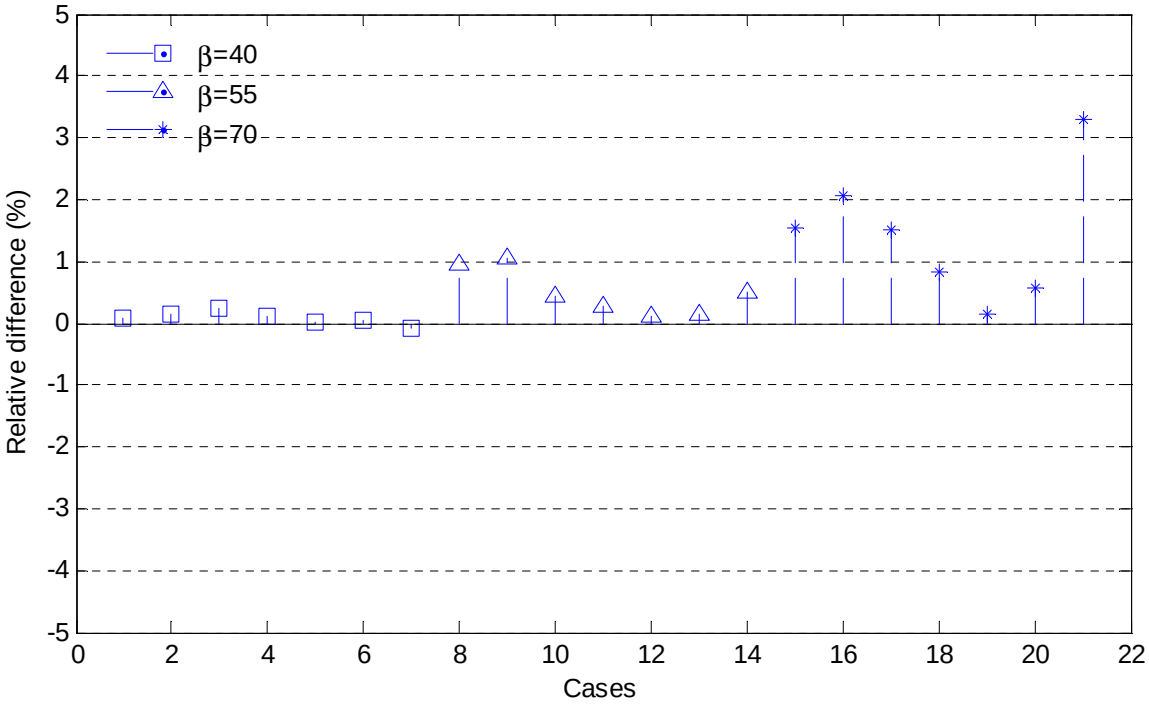

Figure 3.6 Relative differences between the FS calculated by *Slide6.0* and by the LEM model developed in *Matlab*

Figure 3.6 shows that the FS calculated by *Slide6.0* and by the developed LEM model are very similar, with relative differences mostly less than 2%. The developed LEM model can therefore be viewed as validated.

3.3.4 Validation of the Random Field Generator

3.3.4.1 Introduction

The random field generator used in the present study was developed by Constantine (2010). While this generator has the advantages of being simple and user-friendly, its accuracy has not been fully validated yet. In this section, a detailed validation of the random field generator is given.

The Constantine random field generator is based on the covariance matrix decomposition method (Davis 1987). Among the commonly used random field simulation methods, this one has the appeal of accuracy and simplicity (Fenton and Griffiths 2008) but has the drawbacks of being inefficient and difficult for generating large fields. However, these drawbacks are not an issue for the current research as the random fields required here are one dimensional and small in sizes. For the correlation structure of the generated random field, the Markov correlation function (Table 2.7) has been widely applied in geotechnical engineering and is adopted in the present study.

3.3.4.2 Validation

The validation of the random field generator focuses on the mean and covariance function, since together they are able to characterise a random field completely. Three sets of data, with the scale of fluctuation θ equal to 0 (or precisely, very close to 0), 10, and 40, are generated and used for the validation. In particular, each set of data includes 40 1×100 random fields. The means and variances of these random fields are set to 0 and 1 respectively.

(1) Mean

The mean values of the generated random fields are calculated and plotted. Figures 3.7(a), 3.8(a), and 3.9(a) show one of the 40 random fields in each set of data, and Figures 3.7(b), 3.8(b), and 3.9(b) show the mean values of the entire 40 random fields (i.e. the mean value of the random field in the left figure corresponds to one of the circles in the right figure).

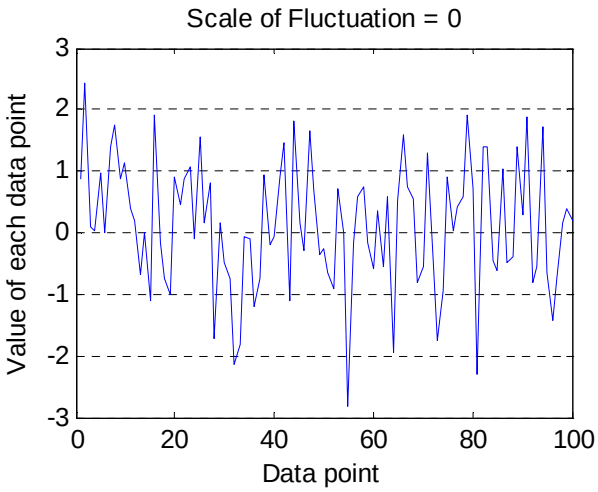

Figure 3.7 (a) Example of a random field with scale of fluctuation = 0

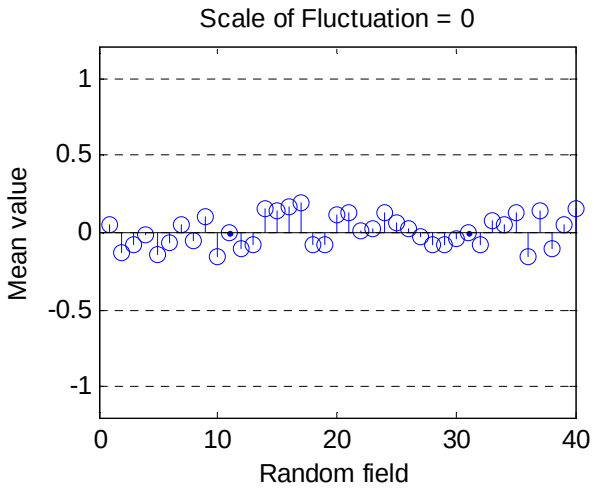

Figure 3.7 (b) Mean values of the 40 random fields with scale of fluctuation = 0

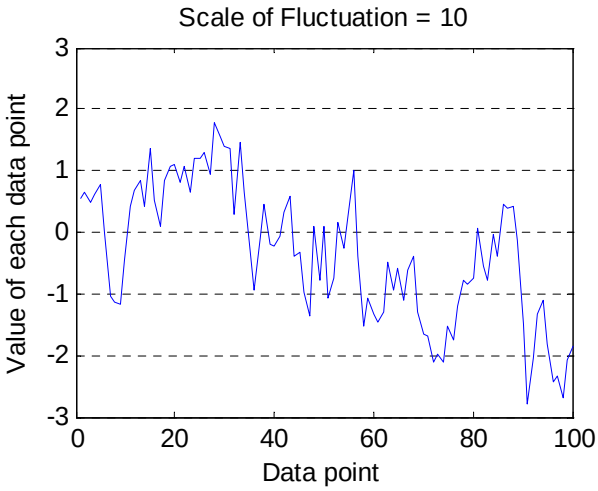

Figure 3.8 (a) Example of a random field with scale of fluctuation = 10

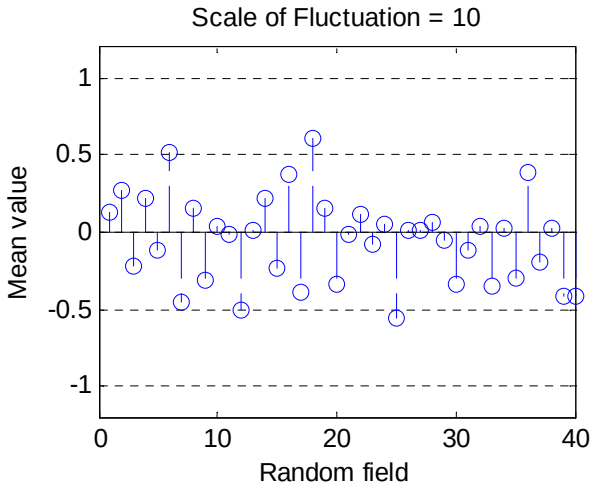

Figure 3.8 (b) Mean values of the 40 random fields with scale of fluctuation = 10

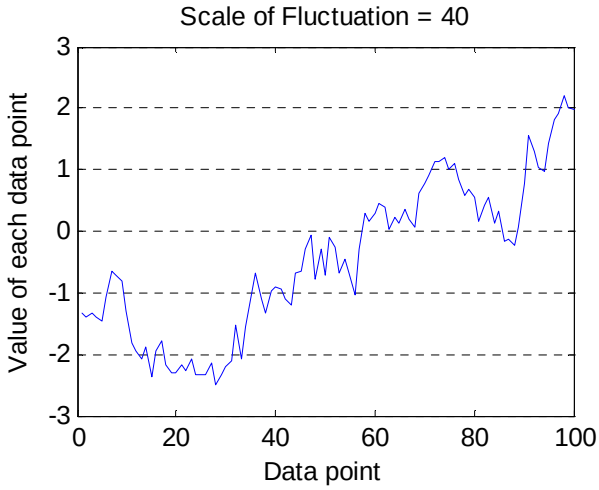

Figure 3.9 (a) Example of a random field with scale of fluctuation = 40

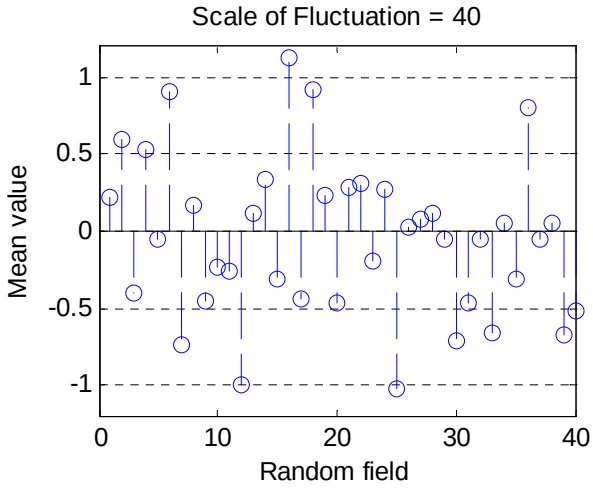

Figure 3.9 (b) Mean values of the 40 random fields with scale of fluctuation = 40

From Figures 3.7(a), 3.8(a) to 3.9(a), the random fields become more and more smooth, because as the scale of fluctuation increases, the data (in the random fields) become more correlated. On the other hand, the mean values of the random fields in Figures 3.7(b), 3.8(b), and 3.9(b) (represented by the circles) space evenly at both sides of the horizontal axes, suggesting that the mean values of the generated random fields are unbiased and equal to the theoretical value (0 in this case).

In addition, the circles in Figures 3.7(b), 3.8(b), and 3.9(b) become more spread out. This is also caused by the increase of the scale of fluctuation: when the scale of fluctuation is small, the data in the random field are less correlated and tend to self cancel each other around the mean (as in Figure 3.9a); when the scale of fluctuation becomes large, this effect is less significant and therefore the mean values tend to be more variable and spread out.

Based on the above discussions, we can conclude that the means of the random fields generated by the Constantine algorithm are unbiased and equal to the theoretical values.

(2) Covariance Function

The covariance functions of the generated random fields are tested by *GSwin* (Xu and Dowd 2005), which is a geostatistics modelling software. The Markov model (given in Table 2.7) in random field theory is equivalent to the exponential model (given in Table 2.8) in geostatistics. Specifically, if the random field Markov model has a variance of σ^2 and scale of fluctuation of θ, the equivalent geostatistical exponential model would have a sill value $C + C_0 = \sigma^2$ (with $C_0 = 0$) and a range $a = ½\ \theta$ (the effective range would be $3a$). In practice, the validation of the generated random fields is facilitated by comparing their experimental variograms with the corresponding theoretical variograms.

An example of the experimental variogram for a generated random field is plotted in Figure 3.10. The stars in the picture represent the experimental variogram values, while the solid line represents the theoretical variogram. The distance ranges from 1 to 99, as the dimension of the random field is 1×100.

The specific process of validation is given below. Firstly, each set of data, including 40 random fields, are imported into *GSwin* and their experimental variograms are calculated. Secondly, the experimental variogram values are exported into *Matlab* and arranged together (thus there will be 40 variogram values for a specific distance h). Thirdly, the maximum and minimum experimental variogram values for each specific distance h are truncated (2 out of 40) and the remaining experimental variogram values (95%) are plotted. Lastly, the envelopes and means of the experimental variograms are drawn against the theoretical variograms. In all, three figures are plotted for three sets of data, as shown in Figures 3.11, 3.12, and 3.13.

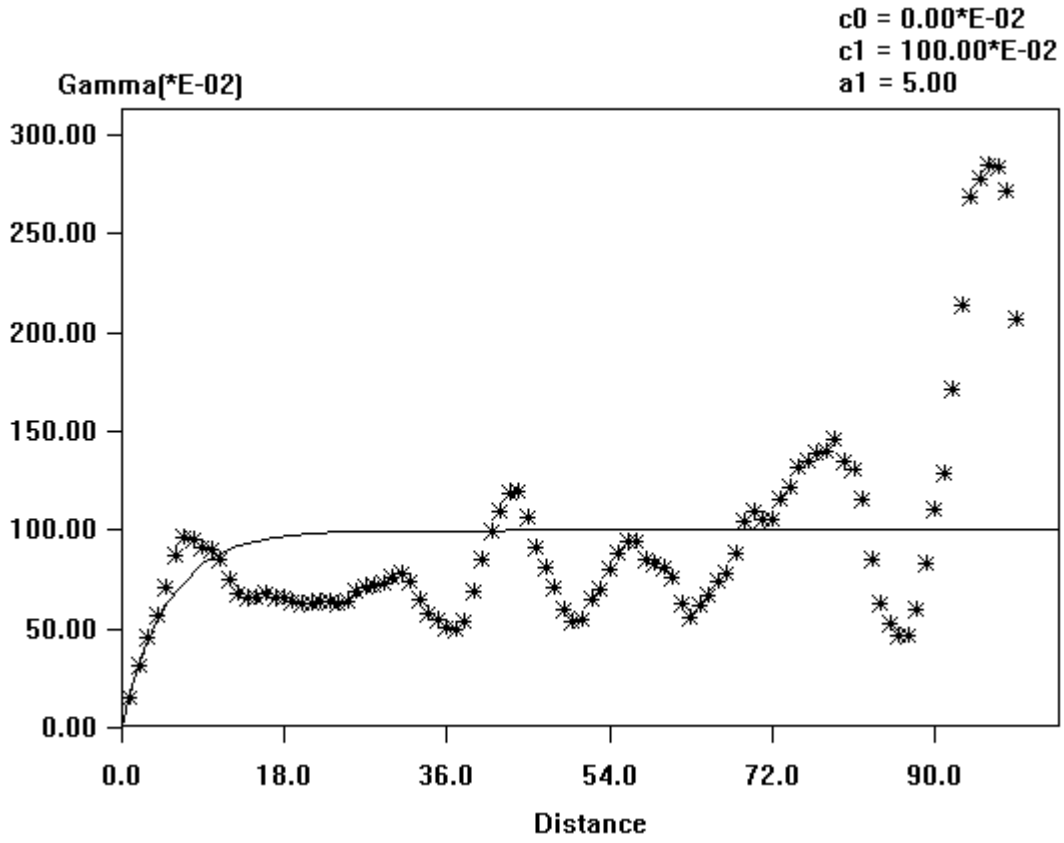

Figure 3.10 Experimental and theoretical variograms for a generated random field with scale of fluctuation = 10 (the stars represent experimental variogram values and the solid line represents the theoretical variogram, Gamma represents the variogram γ_h, and a1 is the range)

Based on Figures 3.11, 3.12, and 3.13, it is clear that the means of the experimental variograms (the red solid lines in the middle) correspond very well to the theoretical variograms (the green circled lines). This demonstrates that the covariance functions of the simulated random fields are accurate.

Based on the above results, the Constantine random field generator can be viewed as validated.

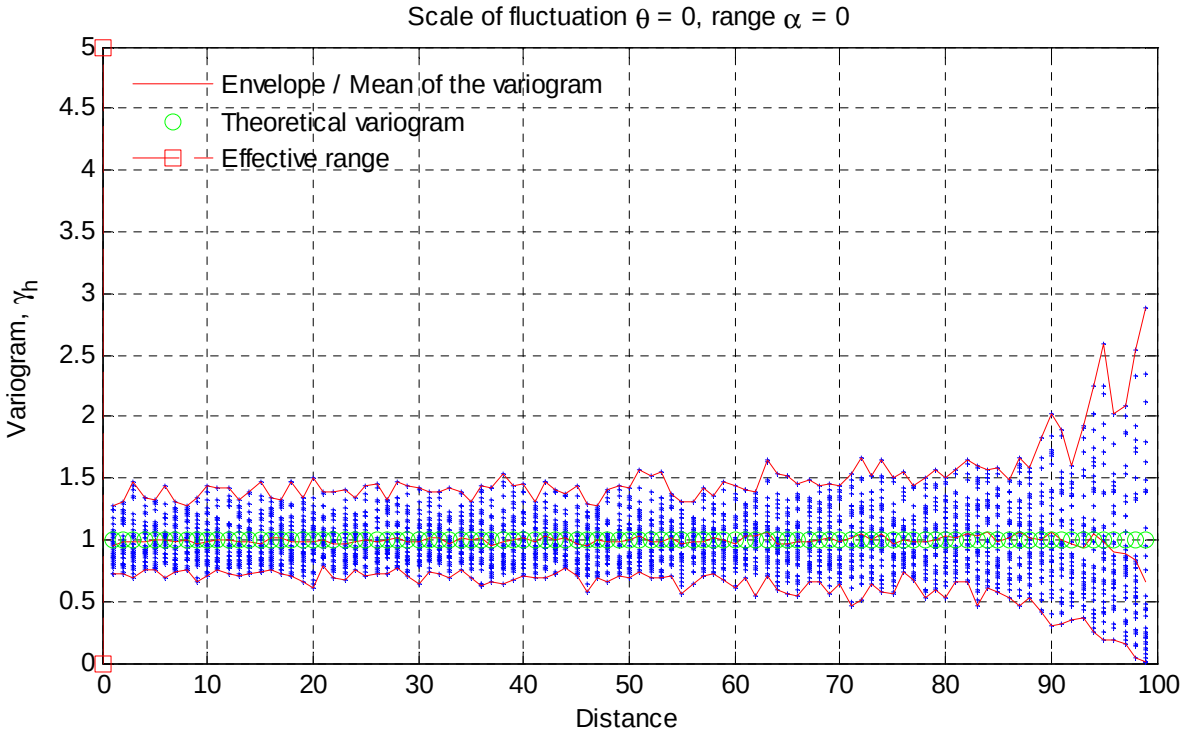

Figure 3.11 Experimental variogram values for data set 1 (40 random fields with scale of fluctuation = 0) vs. the theoretical variogram

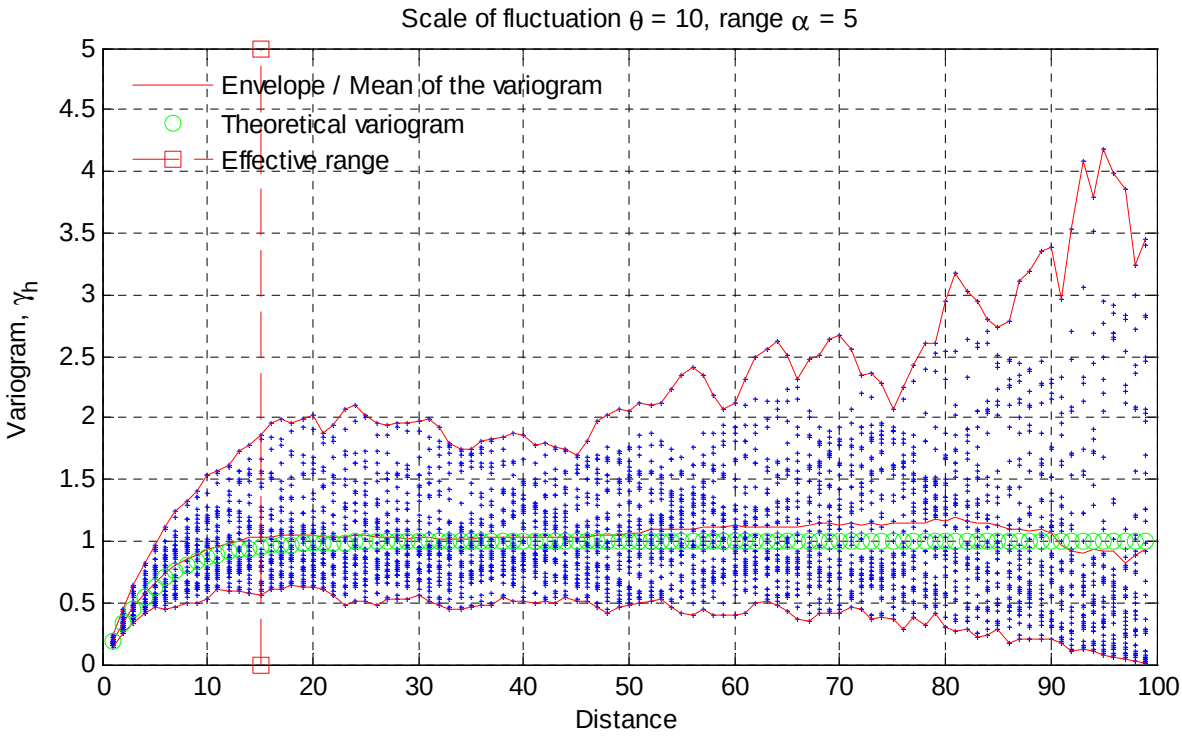

Figure 3.12 Experimental variogram values for data set 2 (40 random fields with scale of fluctuation = 10) vs. the theoretical variogram

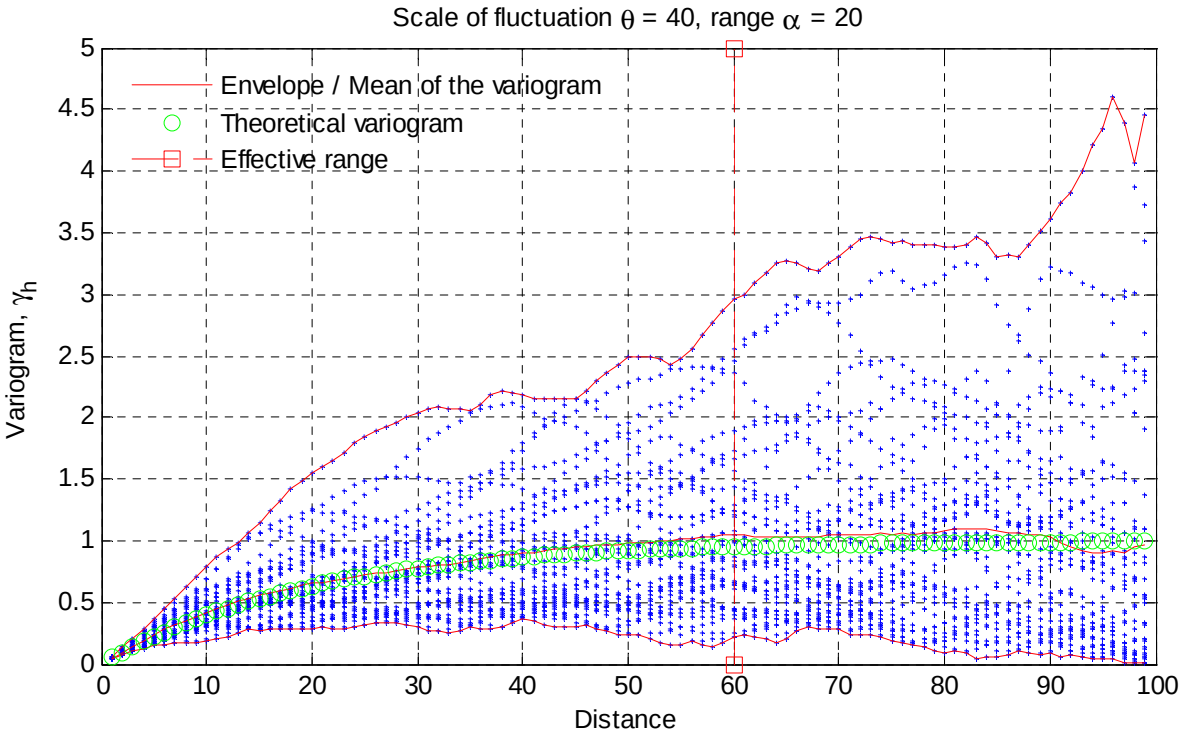

Figure 3.13 Experimental variogram values for data set 3 (40 random fields with scale of fluctuation = 40) vs. the theoretical variogram

3.4 Summary

In this chapter, specific research objectives of this thesis were proposed and methodologies to achieve these objectives were developed. It was decided that a deterministic analysis chapter and a probabilistic analysis chapter would be devoted to study the research objectives. For the deterministic analysis, the involved LEM software, *Slide6.0*, was firstly introduced. Afterwards, a sensitivity graph analysis and an equation fitting analysis were developed. For the probabilistic analysis, a series of parametric studies were firstly designed. The methodology of the Monte Carlo simulation (MCS) was then discussed in detail, in terms of the input, process, and output. Since *Slide6.0* is not able to incorporate spatial variability, a LEM model based on Bishop's simplified method of slices was developed in *Matlab* for the probabilistic analysis. The algorithm of the developed LEM

model was given and its accuracy was validated. Finally, the random field generator used for the probabilistic analysis was examined and proved to be valid.

Chapter 4

DETERMINISTIC ANALYSIS

In this chapter, the sensitivity of FS to the changes in HB parameters (FS sensitivity), and whether such sensitivity is affected by slope geometry, are studied. A sensitivity graph analysis and an equation fitting analysis are employed to achieve the research objectives.

4.1 Preliminary Analysis by Sensitivity Graphs

4.1.1 Influence of Slope Geometry

This section aims to determine whether FS sensitivity is affected by slope geometry. Sensitivity graphs are generated and compared for cases with the same HB parameters but different slope geometry.

Five cases with different combinations of slope face angle β and slope height H are designed and given in Table 4.1. The generic form of the slope geometry for these cases is shown in Figure 4.1. Two sets of HB parameters are used as mean values for the sensitivity analysis (as explained in Section 3.2.3) and they are given in Table 4.2. Thus there are 5 × 2 = 10 cases in total. The sensitivity graphs for these cases are shown in Figures 4.2 to 4.11.

There are three lines in every figure. Each line represents the variation of FS corresponding to the change in one HB parameter, with others fixed at their mean values.

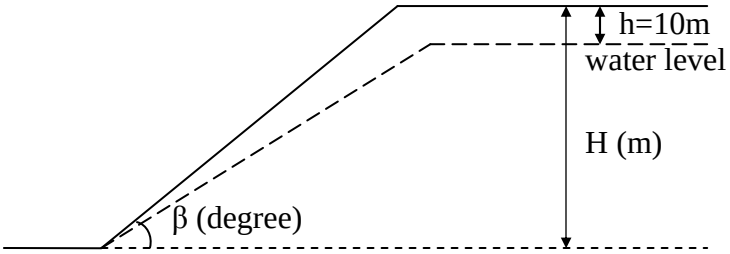

Figure 4.1 Generic form of the slope geometry for investigating the effect of varying slope geometry on FS sensitivity

Table 4.1 Cases for investigating the effect of varying slope geometry on FS sensitivity

β (degree) \ H (m)	50	100	150
40	/	Case 2	/
55	Case 1	Case 3	Case 5
70	/	Case 4	/

Table 4.2 Mean values of HB parameters for investigating the effect of varying slope geometry on FS sensitivity

Parameter	Set 1	Set 2
GSI	30	75
m_i	13	30
σ_{ci} (MPa)	40	100

Comparing the five sensitivity graphs for each set of HB parameters (i.e. comparing within Figures 4.2-4.6 and within Figures 4.7-4.11), we observe that although the sensitivity lines within each graph show high degrees of complexity, the relative positions of all three lines and the pattern for each individual line are similar between cases. The only difference lies in the scale of the vertical axes, which is caused by the influence of slope geometry on the absolute values of FS. These suggest that there is a general pattern of FS sensitivity exists, which is independent of slope geometry. Therefore, FS sensitivity can be studied using a representative slope case and Case 3 (β = 55, H = 100) in Table 4.1 is selected here.

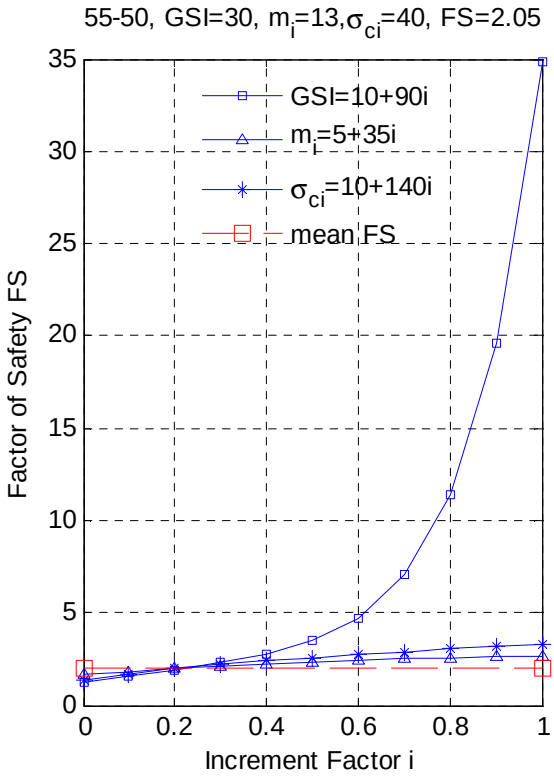

Figure 4.2 Sensitivity graph for slope case 1 with HB parameters set 1 as mean values

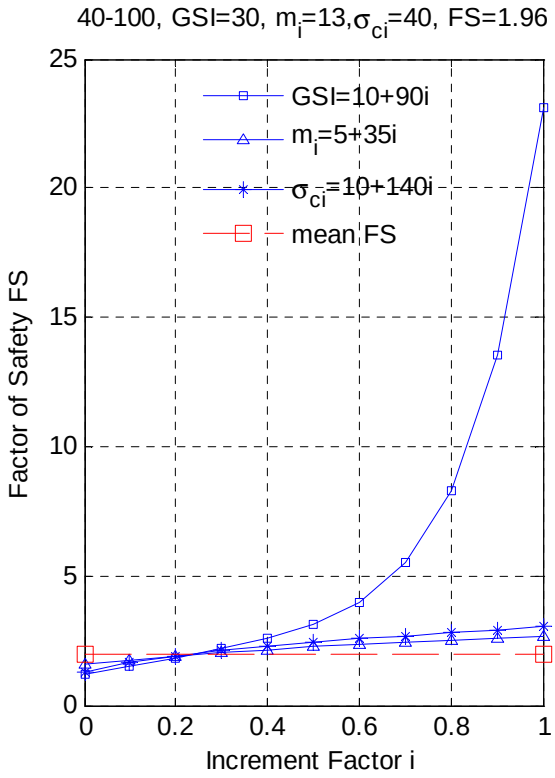

Figure 4.3 Sensitivity graph for slope case 2 with HB parameters set 1 as mean values

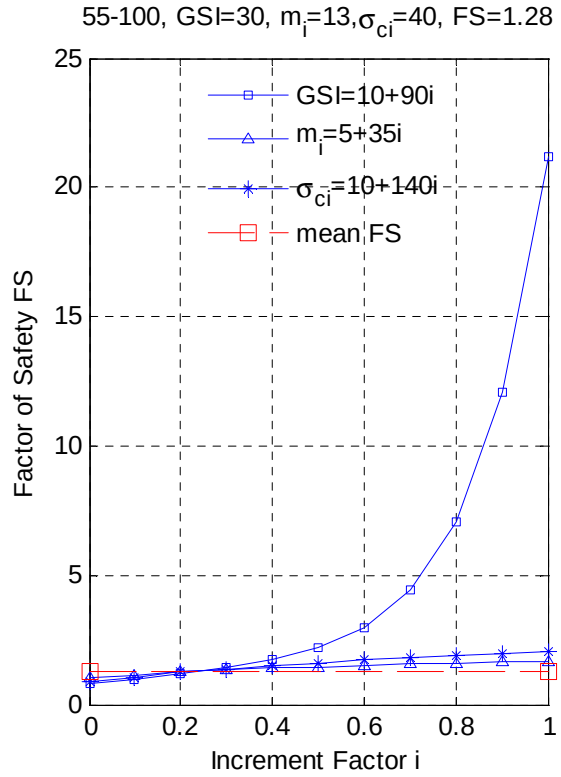

Figure 4.4 Sensitivity graph for slope case 3 with HB parameters set 1 as mean values

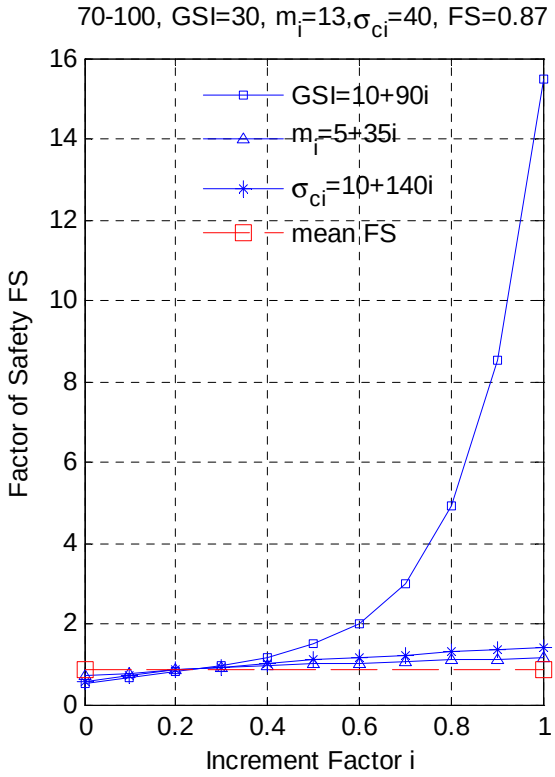

Figure 4.5 Sensitivity graph for slope case 4 with HB parameters set 1 as mean values

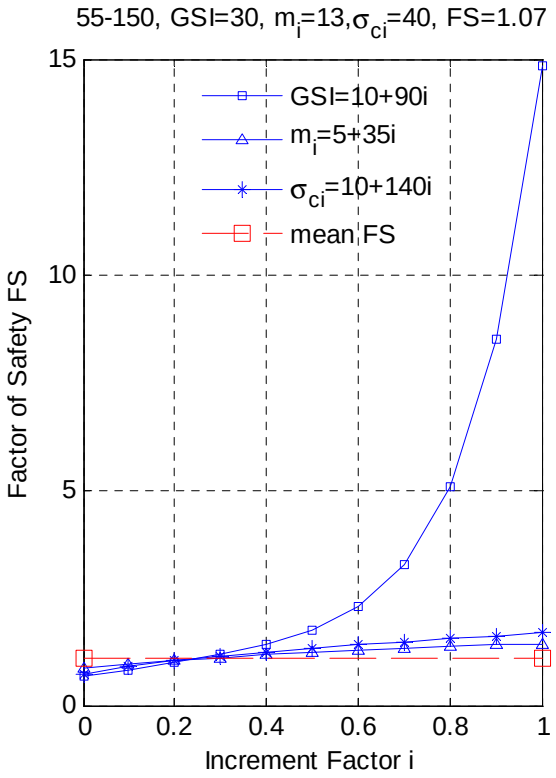

Figure 4.6 Sensitivity graph for slope case 5 with HB parameters set 1 as mean values

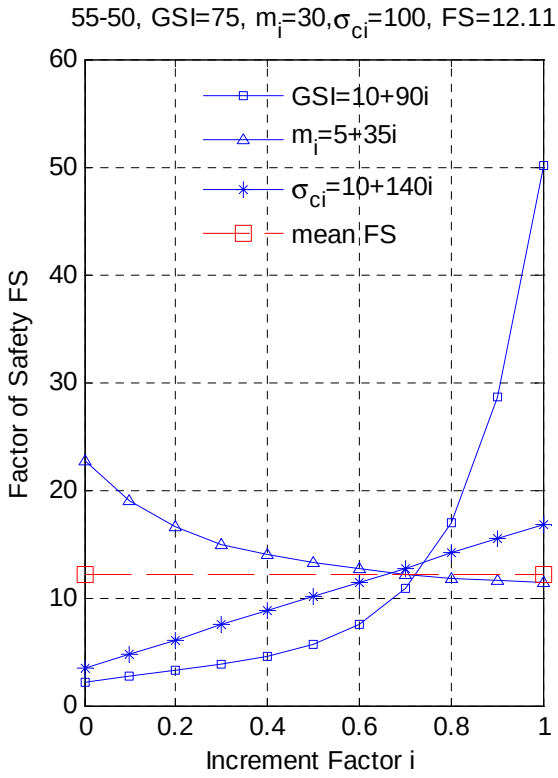

Figure 4.7 Sensitivity graph for slope case 1 with HB parameters set 2 as mean values

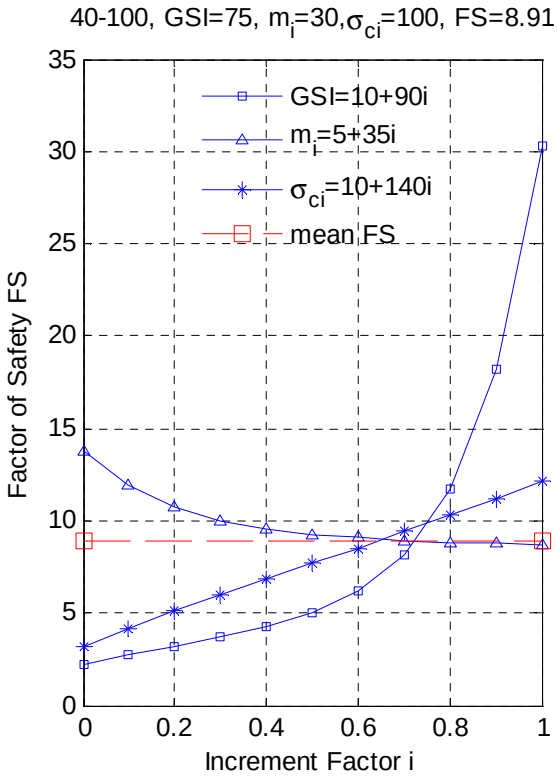

Figure 4.8 Sensitivity graph for slope case 2 with HB parameters set 2 as mean values

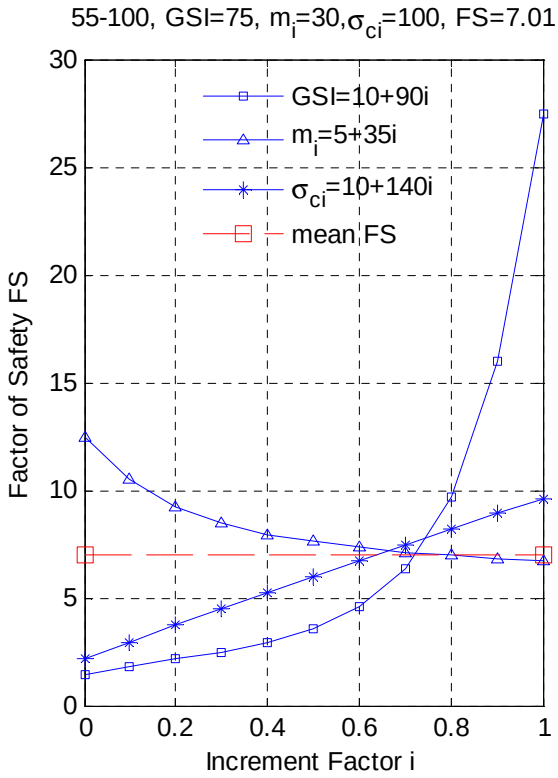

Figure 4.9 Sensitivity graph for slope case 3 with HB parameters set 2 as mean values

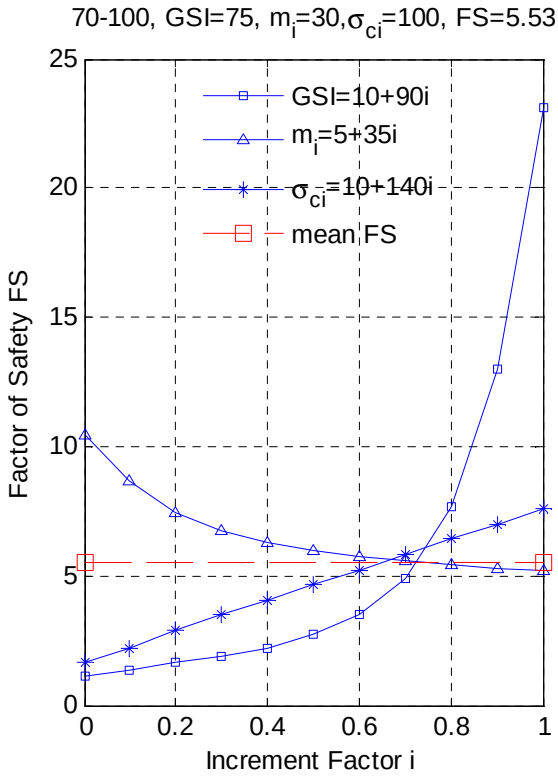

Figure 4.10 Sensitivity graph for slope case 4 with HB parameters set 2 as mean values

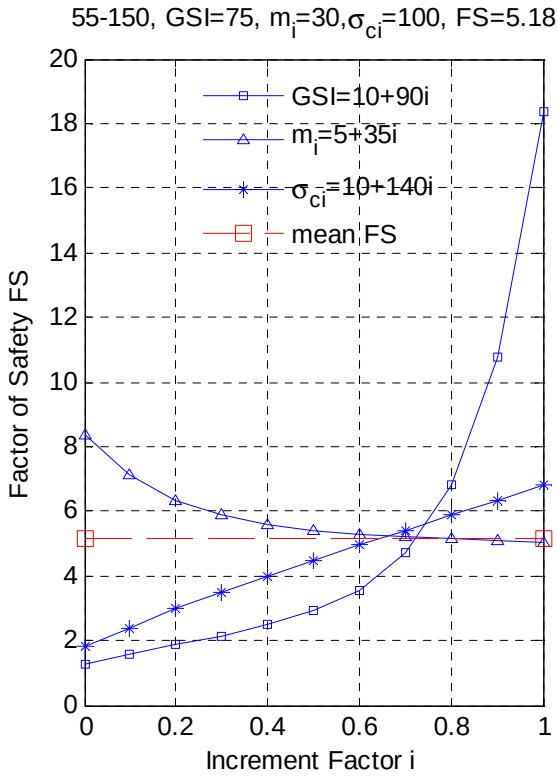

Figure 4.11 Sensitivity graph for slope case 5 with HB parameters set 2 as mean values

4.1.2 Initial Investigation of FS Sensitivity

This section aims to provide some initial insights into FS sensitivity by generating sensitivity graphs for the representative slope case (Case 3 in Table 4.1) with different combinations of HB parameters taken as mean values.

Four sets of mean values of HB parameters are chosen, as listed in Table 4.3. The sensitivity graphs for them are shown in Figures 4.12 to 4.15.

Table 4.3 Mean values of HB parameters for initial investigation of FS sensitivity

Parameter	Set 1	Set 2	Set 3	Set 4
GSI	30	50	75	100
m_i	13	21	30	40
σ_{ci} (MPa)	40	70	100	150

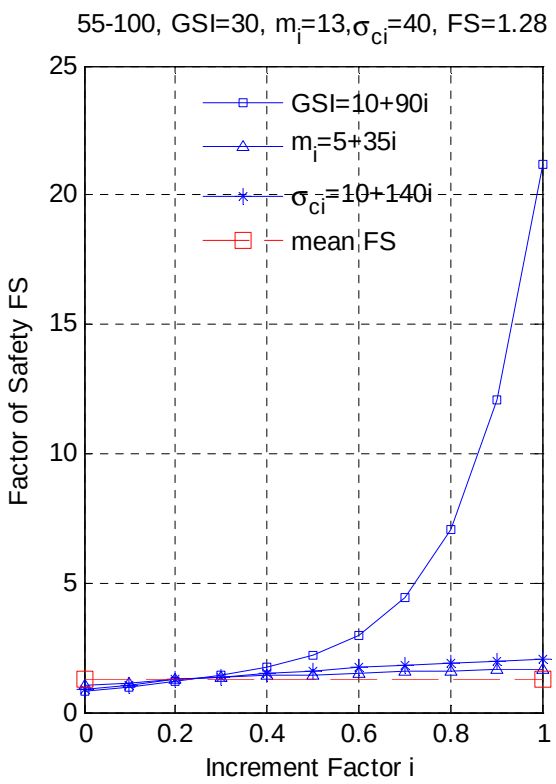

Figure 4.12 Sensitivity graph for using HB parameters set 1 as mean values

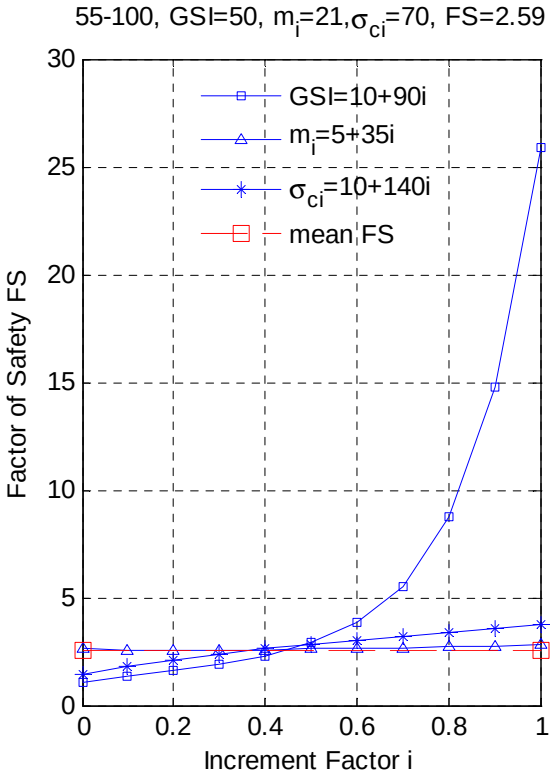

Figure 4.13 Sensitivity graph for using HB parameters set 2 as mean values

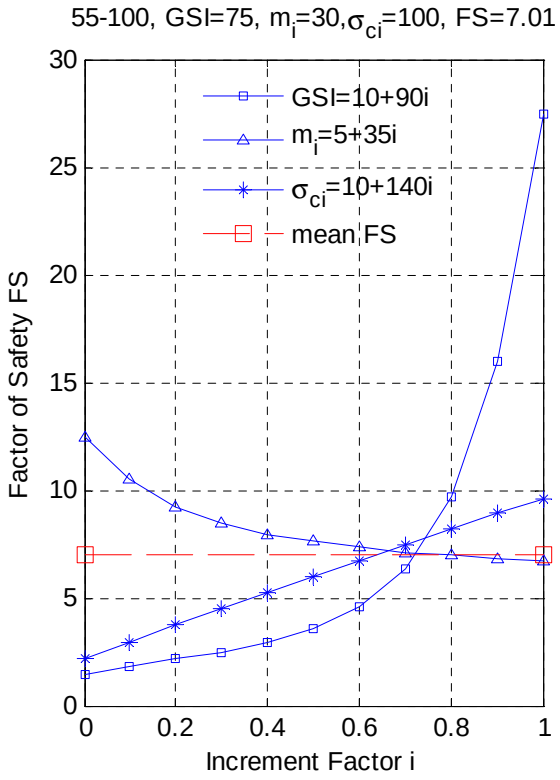

Figure 4.14 Sensitivity graph for using HB parameters set 3 as mean values

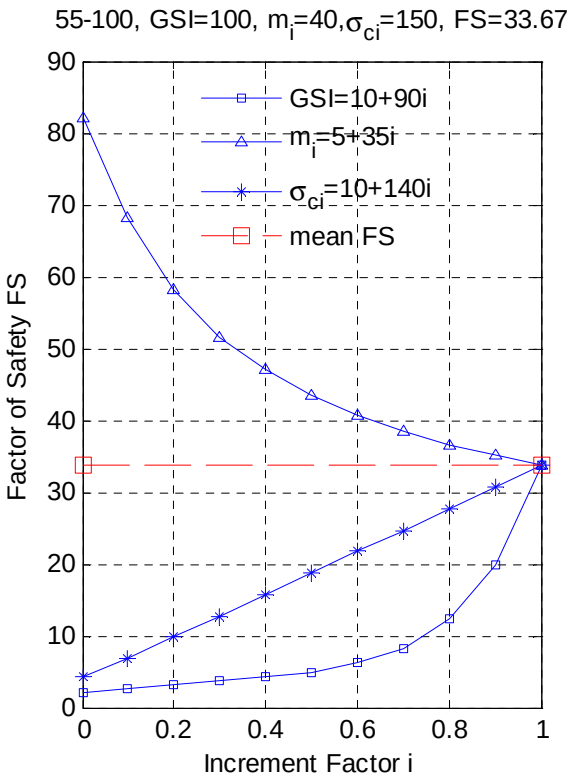

Figure 4.15 Sensitivity graph for using HB parameters set 4 as mean values

Discussions about these figures are given below. Firstly, the sensitivity lines for GSI are generally steep, which suggests that GSI has a large influence on FS. However, the lines also display large curvature, which suggests the relationship between FS and GSI is non-linear. Secondly, the influence of m_i on FS is small in Figures 4.12 and 4.13 but it becomes much larger in Figures 4.14 and 4.15. Also, its influence on FS is positive in the first two graphs and then becomes negative. These results suggest that the sensitivity of FS to the change in m_i is affected by the mean values of other parameters (i.e. GSI and σ_{ci}), since they are the only factors that have changed. Lastly, for σ_{ci}, the corresponding sensitivity lines are also much steeper in Figures 4.14 and 4.15 than those in Figures 4.12 and 4.13. In addition, the influence of σ_{ci} on FS is always positive.

The above results confirm that the sensitivity of FS to the change in HB parameters is non-linear and it is affected by different combinations of HB parameters. However, the sensitivity graphs alone are not sufficient to provide conclusions for FS sensitivity and a further analysis is necessary.

4.2 Sensitivity Analysis by Equation Fitting

This section aims to investigate FS sensitivity by the equation fitting analysis. The equation fitting, including the fitting data, results, and errors are firstly discussed. Sensitivity analysis is then conducted based on the fitted equation.

4.2.1 Equation Fitting

As discussed in Section 3.2.4.1, the data for the equation fitting are generated by *Slide6.0*. It consists of sets of mappings from GSI, m_i, and σ_{ci} to FS, covering a wide range of combinations between GSI, m_i, and σ_{ci}. Based on the conclusions from Section 4.1, GSI is the most influential parameter on FS, with σ_{ci} the second and m_i the last. Therefore, 7, 4, and 6 data points are chosen for GSI, m_i, and σ_{ci} respectively, as listed in Table 4.4. Thus there are 7 × 4 × 6 = 168 sets of data in total and the first 12 sets of them are shown in Table 4.5 (full sets of data are provided in Appendix B). After the data being generated, all parameters, including GSI, m_i, σ_{ci}, and FS, are normalised to the range of [0, 1]. The following polynomial form of equation (Equation 3.1) will be used for the fitting, as discussed in Section 3.2.4.2.

$$y = a_1x_1 + a_2x_2 + a_3x_3 + a_4x_1^2 + a_5x_2^2 + a_6x_3^2 + a_7x_1x_2 + a_8x_2x_3 + a_9x_1x_3 \qquad 3.1$$

where y represents FS, and x_1, x_2, x_3 represent GSI, m_i, σ_{ci} respectively.

Table 4.4 Values of the data points of HB parameters for the equation fitting

Parameter	Data point						
GSI	10	25	40	55	70	85	100
m_i	5	17	28	40			
σ_{ci} (MPa)	10	35	65	95	120	150	

The unknown items in Equation 3.1 are the 9 coefficients, i.e. a_1 to a_9. They can be represented by the 9×1 matrix in Equation 4.2. There are 168 sets of data, which can be represented by the HB parameter matrix $\boldsymbol{A}$ and FS matrix $\boldsymbol{y}$, as in Equation 4.1 and Equation 4.3. Therefore, the task is to solve the linear equation system in Equation 4.4.

Table 4.5 First twelve sets of data (out of 168) for the equation fitting (full sets of data are provided in Appendix B)

Data set	GSI	m_i	σ_{ci} (MPa)	FS
1	10	5	10	0.38
2	10	5	35	0.551
3	10	5	65	0.664
4	10	5	95	0.751
5	10	5	120	0.812
6	10	5	150	0.874
7	10	17	10	0.608
8	10	17	35	0.84
9	10	17	65	0.976
10	10	17	95	1.076
11	10	17	120	1.145
12	10	17	150	1.215
…	…	…	…	…

$$\vec{A} = [x_1 \quad x_2 \quad x_3 \quad x_1^2 \quad x_2^2 \quad x_3^2 \quad x_1x_2 \quad x_2x_3 \quad x_1x_3] \ (168\times 9) \tag{4.1}$$

$$\vec{a} = [a_1 \quad a_2 \quad a_3 \quad a_4 \quad a_5 \quad a_6 \quad a_7 \quad a_8 \quad a_9]' \ (9\times 1) \tag{4.2}$$

$$\vec{y} = [FS_1 \quad ... \quad FS_{168}]' \ (168\times 1) \tag{4.3}$$

$$\vec{A}\times\vec{a} = \vec{y} \tag{4.4}$$

The least square solution for the linear equation system in Equation 4.4 is presented in Table 4.6. To examine the accuracy of the fitted equation, the 168 sets of GSI, m_i, and σ_{ci} (original data for the equation fitting) are input into the fitted equation to recalculate the FS. These recalculated FS values are termed the fitted FS. The overall absolute relative difference (ARD) between the fitted FS and the true FS (original data) is then calculated by Equation 4.5.

Table 4.6 Least square solutions for a in the linear equation system in Equation 4.4

Coefficient	a_1	a_2	a_3	a_4	a_5	a_6	a_7	a_8	a_9
Value	-0.364	0.067	0.006	0.551	0.075	-0.021	-0.260	-0.134	0.447

$$ARD = \frac{\sum_{i=1}^{168} \left| \frac{FS_i(Fitted) - FS_i(True)}{FS_i(True)} \right|}{168} \tag{4.5}$$

In this case, the overall ARD is 200%. The comparison between the fitted FS and the true FS is shown in Figure 4.16 (please note that all FS values have been normalised into [0, 1]). In Figure 4.16, the horizontal axis corresponds to the 168 sets of data, which are arranged in the ascending order of GSI. The blue circle represents the true FS, which gradually increases with the growth of GSI (the abruptness is caused by the variations of m_i and σ_{ci}). The red triangle represents the fitted FS.

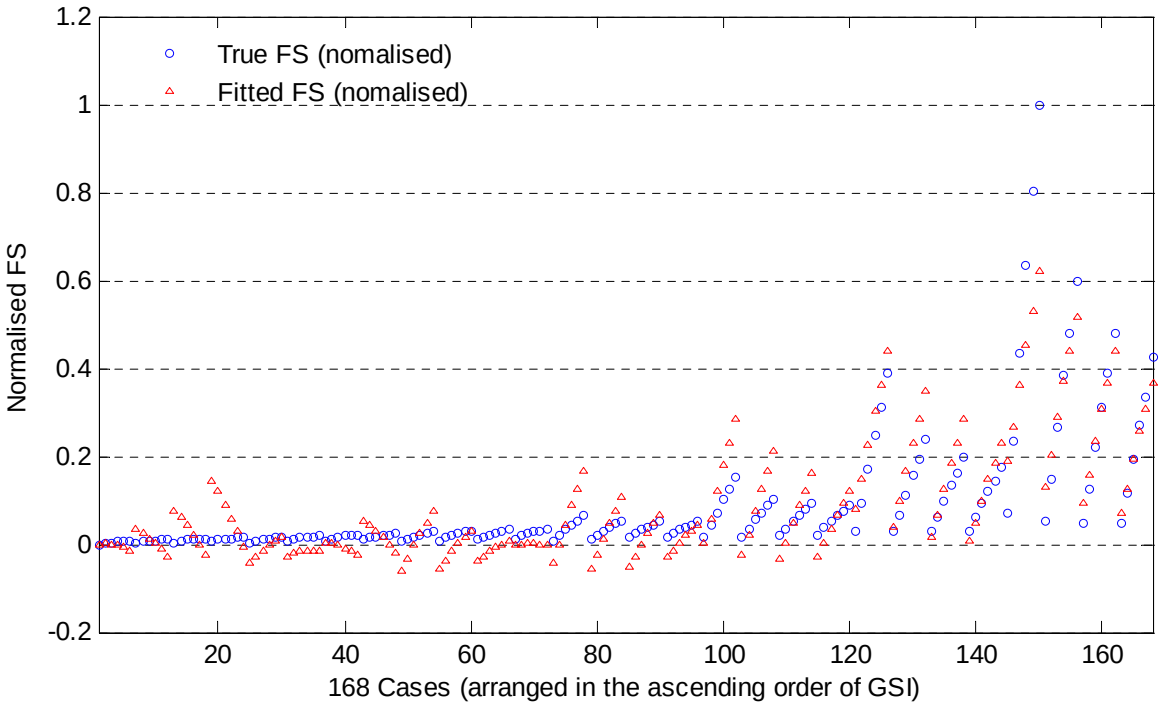

Figure 4.16 Comparison between the true FS values (original data) and the fitted FS values (calculated by the fitted equation with coefficients *a* in Table 4.6)

The ARD between the fitted FS and true FS is quite large, as reflected by the poor overlap between the circles and triangles shown in Figure 4.16. On the other hand, Figure 4.16 shows that in terms of FS (blue circles), there are considerable discrepancies between the first 120 sets of data (corresponding to GSI $\leq$ 70) and the next 48 sets of data (corresponding to GSI > 70). The large ARD is likely to be caused by attempting to fit data with such large differences into one equation.

A second version has been trialled, which fits 2 equations separately for the first 120 and the next 48 sets of data. Two sets of linear equation systems as shown in Equation 4.12 and Equation 4.13 are solved. The least square solutions for these fittings are given in Tables 4.7 and 4.8.

$$\vec{A}_1 = [x_1 \quad x_2 \quad x_3 \quad x_1^2 \quad x_2^2 \quad x_3^2 \quad x_1x_2 \quad x_2x_3 \quad x_1x_3] \quad (GSI \leq 70 \quad 120\times 9) \tag{4.6}$$

$$\vec{A}_2 = [x_1 \quad x_2 \quad x_3 \quad x_1^2 \quad x_2^2 \quad x_3^2 \quad x_1x_2 \quad x_2x_3 \quad x_1x_3] \quad (GSI > 70 \quad 48\times 9) \tag{4.7}$$

$$\vec{a}_1 = [a_1 \quad a_2 \quad a_3 \quad a_4 \quad a_5 \quad a_6 \quad a_7 \quad a_8 \quad a_9]' \quad (GSI \leq 70 \quad 9\times 1) \tag{4.8}$$

$$\vec{a}_2 = [a_1 \quad a_2 \quad a_3 \quad a_4 \quad a_5 \quad a_6 \quad a_7 \quad a_8 \quad a_9]' \quad (GSI > 70 \quad 9\times 1) \tag{4.9}$$

$$\vec{y}_1 = [FS_1 \quad ... \quad FS_{120}]' \quad (GSI \leq 70 \quad 120\times 1) \tag{4.10}$$

$$\vec{y}_2 = [FS_{121} \quad ... \quad FS_{168}]' \quad (GSI > 70 \quad 48\times 1) \tag{4.11}$$

$$\vec{A}_1 \times \vec{a}_1 = \vec{y}_1 \quad (GSI \leq 70) \tag{4.12}$$

$$\vec{A}_2 \times \vec{a}_2 = \vec{y}_2 \quad (GSI > 70) \tag{4.13}$$

Table 4.7 Least square solutions for a_1 in the linear equation system in Equation 4.12 (GSI ≤ 70)

Coefficient	a_1	a_2	a_3	a_4	a_5	a_6	a_7	a_8	a_9
Value	-0.043	0.013	0.015	0.134	0.010	-0.010	-0.048	-0.018	0.117

Table 4.8 Least square solutions for a_2 in the linear equation system in Equation 4.13 (GSI > 70)

Coefficient	a_1	a_2	a_3	a_4	a_5	a_6	a_7	a_8	a_9
Value	-0.545	0.754	-1.345	0.682	0.269	-0.003	-1.128	-0.371	2.104

The ARD between the new fitted FS and true FS is again calculated. For the first sets (Equation 4.12), the ARD is 29%, while for the second sets (Equation 4.13), the ARD is 25%. The comparison between the fitted FS and true FS is shown in Figure 4.17.

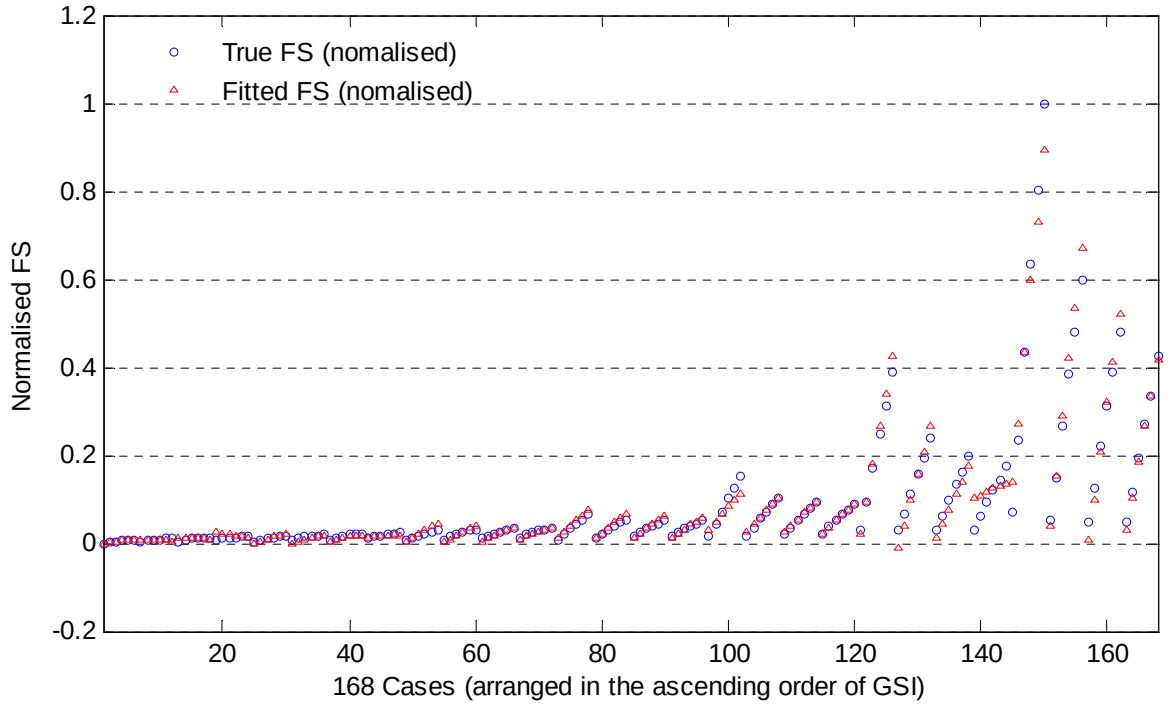

Figure 4.17 Comparison between the true FS values (original data) and the fitted FS values (calculated by the fitted equation with coefficients a_1 in Table 4.7 and coefficients a_2 in Table 4.8)

Apparently, the accuracy is greatly improved, which is reflected by the good overlap between the fitted FS and true FS in Figure 4.17. Given the complexity involved in slope stability analysis, such ARD is considered acceptable for sensitivity analysis purpose. In addition, several other forms of equations and data arrangements have been tried, but this one produced the best accuracy. Therefore, Equation 3.1 with the coefficients shown in Tables 4.7 and 4.8 are used for the sensitivity investigations.

4.2.2 Derivative Based Sensitivity Analysis

This section employs the equation fitted in the previous section to analyse FS sensitivity by taking the derivatives (rates of change) of FS with respect to HB parameters.

The derivatives of FS with respect to HB parameters are given in Equations 4.14 to 4.19 (both sides are multiplied by a factor of 100). There are two sets of derivative equations, which correspond to GSI ≤ 70 and GSI > 70 respectively.

$$100\frac{\partial FS}{\partial GSI} = -4.3 + 26.9GSI - 4.8m_i + 11.7\sigma_{ci} \quad (GSI \le 70) \tag{4.14}$$

$$100\frac{\partial FS}{\partial m_i} = 1.3 - 4.8GSI + 1.9m_i - 1.8\sigma_{ci} \quad (GSI \le 70) \tag{4.15}$$

$$100\frac{\partial FS}{\partial \sigma_{ci}} = 1.5 + 11.7GSI - 1.8m_i - 2.1\sigma_{ci} \quad (GSI \le 70) \tag{4.16}$$

$$100\frac{\partial FS}{\partial GSI} = -55 + 136GSI - 113m_i + 210\sigma_{ci} \quad (GSI > 70) \tag{4.17}$$

$$100\frac{\partial FS}{\partial m_i} = 75 - 113GSI + 54m_i - 37\sigma_{ci} \quad (GSI > 70) \tag{4.18}$$

$$100\frac{\partial FS}{\partial \sigma_{ci}} = -135 + 210GSI - 37m_i - 0.6\sigma_{ci} \quad (GSI > 70) \tag{4.19}$$

These equations show that the sensitivity of FS to each HB parameter (measured by the derivative) is contributed not only by that parameter itself but also by other parameters. Such contributions can be measured by the corresponding coefficients. A positive coefficient indicates that the corresponding parameter makes a positive contribution, and vice versa; while a large coefficient indicates a large contribution, and vice versa.

Table 4.9 summarises the contribution of each HB parameter to the derivatives. In particular, a plus sign represents a positive contribution from that parameter and a negative sign represents a negative contribution. Double underline means that parameter makes a large contribution. Single underline means a medium contribution and no underline means a small contribution. Lastly, if any coefficient is extremely small compared with others, the corresponding parameter is ignored in Table 4.9. The selection criteria for the weight of the contributions are given in Table 4.10.

Table 4.9 Contribution of each HB parameter to FS sensitivity (measured by the derivative)

Sensitivity	Weight of contribution (GSI ≤ 70)	Weight of contribution (GSI > 70)
∂FS/∂GSI	- Constant, + <u>GSI</u>, - m_i, + <u>σ_{ci}</u>	- Constant, + <u>GSI</u>, - <u>m_i</u>, + <u>σ_{ci}</u>
$\partial FS/\partial m_i$	+ Constant, - GSI, + m_i, - σ_{ci}	+ Constant, - <u>GSI</u>, + m_i, - σ_{ci}
$\partial FS/\partial \sigma_{ci}$	+ Constant, + <u>GSI</u>, - m_i, - σ_{ci}	- <u>Constant</u>, + <u>GSI</u>, - m_i

Table 4.10 Selection criteria for the weight of contribution of each HB parameter to FS sensitivity

Weight	Value of coefficient (GSI ≤ 70)	Value of coefficient (GSI > 70)	Weight sign
Large	≥ 20	≥ 200	double underline
Medium	10 ~ 20	100 ~ 200	single underline
Small	1~10	10~100	none
Ignored	≤ 1	≤ 10	Ignored

4.2.3 Discussions and Verifications

Discussions and verifications of the information in Table 4.10 are presented below.

For ∂FS/∂GSI (the derivative of FS with respect to GSI), GSI itself has a large (GSI ≤ 70) or a medium (GSI > 70) positive contribution, which suggests that FS will become sensitive to GSI when GSI itself is large. This is demonstrated by the sensitivity graphs in Section 4.1.2, i.e. Figures 4.12 to 4.15. In each of these figures, the ∂FS/∂GSI line (squared line) becomes steeper as GSI increases. On the other hand, m_i has a small (GSI ≤ 70) or medium (GSI > 70) negative contribution to ∂FS/∂GSI and σ_{ci} has a medium (GSI ≤ 70) or large (GSI > 70) positive contribution, which suggests that FS will become sensitive to GSI when m_i is small and σ_{ci} is large. To verify this, three cases with different combinations of m_i and σ_{ci} values are tested, as shown in Table 4.11. In these cases, GSI varies from 10 to 100 and the sensitivity lines for FS to the change in GSI are compared. Case 1 has a small m_i but a large σ_{ci}, which corresponds to the most sensitive situation; while Case 3 is the opposite and thus it should be the least sensitive. Case 2 is the medium sensitive case. The sensitivity graph for these cases is given in Figure 4.18. It is apparent that Case 1 is the most sensitive case (as the sensitivity line for Case 1 is the steepest) and Case 3 is the least sensitive case (as the sensitivity line for Case 3 is the flattest).

Table 4.11 Cases for verification of situations where FS is highly sensitive to GSI

Case	GSI	m_i	σ_{ci} (MPa)	Predicted sensitivity
1	10-100	5	150	High
2	10-100	40	150	Medium
3	10-100	40	10	Low

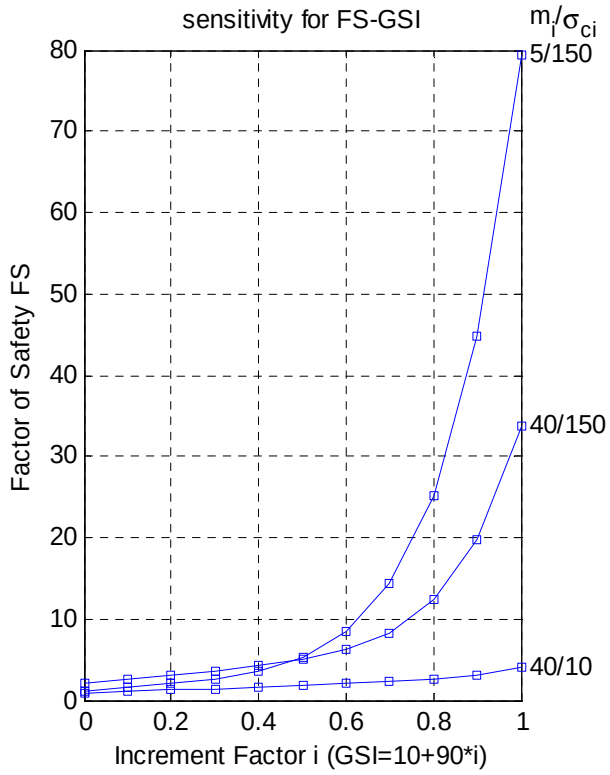

Figure 4.18 Verification of situations where FS is highly sensitive to the change in GSI

Based on these observations, it can be concluded that the association between FS and GSI is always positive (i.e. FS always increases as GSI increases). Three factors cause FS to be sensitive to the change in GSI: large GSI, small m_i, and large σ_{ci}. Among these factors, GSI and σ_{ci} are the most influential.

For $\partial FS/\partial m_i$ (the derivative of FS with respect to m_i), when GSI $\leq$ 70, both GSI and σ_{ci} have small negative contributions. The constant and m_i itself have small positive contributions. Thus, the contributions of these four items are all small and effectively

cancel each other. Therefore, FS should not be sensitive to m_i when GSI ≤ 70. This is supported by Figures 4.12 and 4.13 in Section 4.1.2 (in which the mean values of GSI are ≤ 70), where the $\partial FS/\partial m_i$ sensitivity lines (triangular lines) are flat, suggesting low sensitivity. On the other hand, when GSI > 70, GSI has a medium negative contribution to $\partial FS/\partial m_i$ and σ_{ci} has a small negative contribution. This suggests that when GSI and σ_{ci} are both large, FS will decrease as m_i increases and its sensitivity should be high. This is supported by Figures 4.14 and 4.15 in Section 4.1.2, in which both GSI and σ_{ci} are large. In these two figures, FS decreases with the increase of m_i. Also, $\partial FS/\partial m_i$ lines are steep, suggesting large sensitivity.

Based on these discussions, it can be conclude that the association between FS and m_i is positive (i.e. FS increases as m_i increases) and FS is not sensitive to the change in m_i when GSI ≤ 70. When GSI > 70 and σ_{ci} is large, the association between FS and m_i is negative (i.e. FS decreases as m_i decreases) and FS is sensitive to the change in m_i.

For $\partial FS/\partial \sigma_{ci}$ (the derivative of FS with respect to σ_{ci}), GSI has a medium or large positive contribution, suggesting that FS will become sensitive to the change in σ_{ci} when GSI is large. To prove this, several cases with different GSI mean values are tested, as given in Table 4.12. In these cases, σ_{ci} varies from 10MPa to 150MPa. The sensitivity lines for these cases are shown in Figure 4.19. In Figure 4.19, the slopes of the lines increase gradually as GSI increases, suggesting that FS becomes more sensitive to the change in σ_{ci} as GSI increases. In addition, these lines are almost straight, which indicates that $\partial FS/\partial \sigma_{ci}$ is not influenced much by the mean value of σ_{ci} itself. This is in good agreement with the weight provided in Table 4.9, where the contribution of σ_{ci} to $\partial FS/\partial \sigma_{ci}$ is small (GSI ≤ 70) or very small (GSI > 70) as such it can be ignored.

Table 4.12 Cases for verification of situations where FS is highly sensitive to σ_{ci}

Case	GSI	m_i	σ_{ci} (MPa)
1-7	30, 40, 50, 60, 70, 80, 90, 100	5	10 - 150

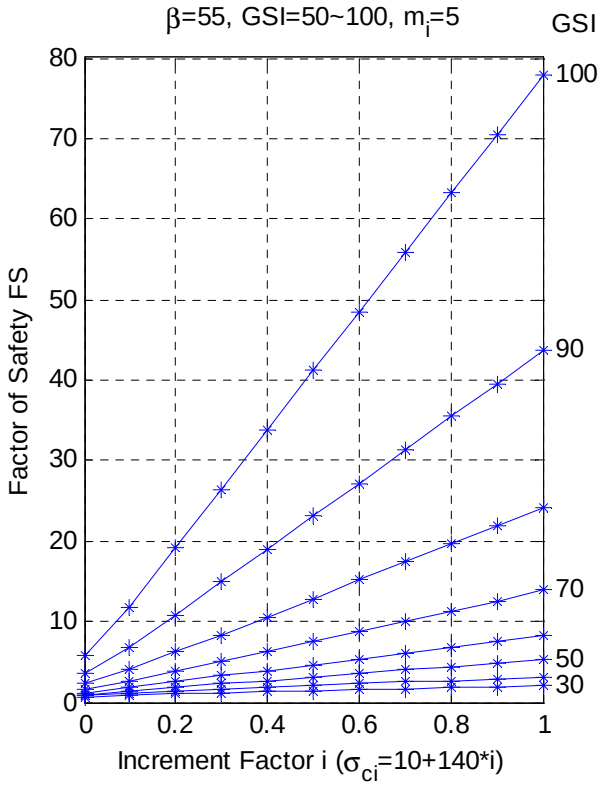

Figure 4.19 Verification of situations where FS is highly sensitive to the change in σ_{ci}

Based on the above discussions, it can be concluded the association between FS and σ_{ci} is always positive (i.e. FS always increases as σ_{ci} increases) and FS becomes sensitive to the change in σ_{ci} when GSI is large.

4.2.4 Conclusions

Conclusions regarding FS sensitivity with respect to each HB parameter are given here. These address two aspects: firstly, for any particular parameter, whether FS is sensitive to its change; and secondly, how is the contribution of this parameter to the derivatives of FS to other parameters.

GSI is the most critical parameter in both aspects. Firstly, FS is very sensitive to the change in GSI. This is reflected in Table 4.9 and the sensitivity graphs in Section 4.1.2. In Table 4.9, the coefficients for ∂FS/∂GSI are positive and large, which results in a large ∂FS/∂GSI and indicates high FS sensitivity; while in Figures 4.12 to 4.15, FS increases sharply as GSI increases. Secondly, GSI makes the largest contribution to ∂FS/∂GSI, ∂FS/∂m_i, and ∂FS/∂σ_{ci}. This is also reflected in Table 4.9, as the weight of contribution from GSI is generally large. Therefore, based on the discussions above and in Section 4.2.3, it can be concluded that when GSI is large, FS is expected to be highly sensitive to the change in GSI itself and that in σ_{ci}.

σ_{ci} is also a critical parameter. FS becomes sensitive to the change in σ_{ci} when GSI is large. On the other hand, σ_{ci} does not make as large contributions to ∂FS/∂m_i and ∂FS/∂σ_{ci} as does GSI. Thus σ_{ci} is only critical in this one aspect.

m_i is the least important parameter. Firstly, the only situation when FS is sensitive to the change in m_i is when GSI and σ_{ci} are both large. However, in such a situation, the FS is already very large (because of the large GSI and σ_{ci}) and its high sensitivity to m_i is of less importance. Secondly, m_i makes the least contribution to ∂FS/∂GSI, ∂FS/∂m_i, and ∂FS/∂σ_{ci}. Thus m_i is the least important in both aspects.

Based on the above conclusions, a typical situation where FS is highly sensitive would be when GSI is large. In this situation, FS is sensitive to the changes in both GSI and σ_{ci}.

A case study is presented below to demonstrate this point.

4.2.5 Case Study

FS are calculated (by *Slide6.0*) for the slope in Figure 4.1 with β = 55 and H = 100m based on three different combinations of HB parameters, as given in Table 4.13. These combinations of HB parameters are specifically designed to produce the same FS (to the second decimal place). The GSI values from Case 1 to Case 3 are in a descending order. Based on the conclusions in Section 4.2.4, Case 1 should be the most sensitive case and Case 3 should be the least.

To verify the sensitivity of FS, all HB parameters in Table 4.13 are decreased by 10%, as shown in Table 4.14. FS are re-calculated for the decreased parameters, as given in Table 4.14. The percentage decreases of FS for the three cases are also calculated.

Table 4.13 Three cases with the same FS but different combinations of HB parameters (for verification of FS sensitivity)

Case	GSI	m_i	σ_{ci} (MPa)	FS	Predicted sensitivity
1	69	13	10	1.63	High
2	38	13	50	1.63	Medium
3	23	13	132	1.63	Low

Table 4.14 Demonstration of the effect of reducing all HB parameters by 10% on FS for the cases in Table 4.13

Case	GSI	m_i	σ_{ci} (MPa)	FS	FS decrease
1	62.1	11.7	9	1.33	18.4%
2	34.2	11.7	45	1.42	12.9%
3	20.7	11.7	118.8	1.44	11.7%

The decreases of FS for the three cases are in good agreement with the sensitivity descriptions. Specifically, Case 1 is the most sensitive case and the decrease of FS for Case

1 is much larger than those of Case 2 and Case 3. The decrease of FS for Case 2 is also larger than that of Case 3, but not as significant as that in Case 1. This is because in Cases 2 and 3, GSI are generally small and hence the sensitivity change is also small.

4.3 Summary

The objectives of this chapter were to investigate the sensitivity of FS to the changes in HB parameters (FS sensitivity) and examine whether such sensitivity is affected by slope geometry. Qualitative sensitivity graphs and a quantitative equation fitting analysis have been used to achieve the research objectives.

Key conclusions of this chapter are as follows:

1. A general pattern of FS sensitivity exists and it can be studied independent of slope geometry.

2. The sensitivity of FS to the change in any particular HB parameter depends on the value of that parameter itself (the range within which it is changing) and on the values of other HB parameters.

3. Slope cases with the same FS values but different combinations of HB parameters can have different FS sensitivity.

4. GSI is the most critical parameter for FS sensitivity. FS always increases with increasing GSI. When GSI is large, FS becomes sensitive to the change in GSI itself and that in σ_{ci}. σ_{ci} is also a critical parameter with respect to FS sensitivity. FS always increases with increasing σ_{ci}. FS becomes sensitive to the change in σ_{ci} when GSI is large. m_i is the least critical parameter for FS sensitivity.

5. A typical situation where FS is highly sensitive would be when GSI is large. In this situation, FS is sensitive to the changes in both GSI and σ_{ci}.

Chapter 5

PROBABILISTIC ANALYSIS

5.1 Introduction

This chapter deals with the four remaining research objectives of this thesis: to investigate the influence of changes in the variability of HB parameters (quantified by the COV) on PF (Section 5.2.1); to evaluate the relative contribution of the variability of each HB parameter (quantified by the COV) to PF (Sections 5.2.2 and 5.2.3); to investigate the influence of the spatial variability of HB parameters (quantified by the scale of fluctuation θ) on the PF (Section 5.3); and to explore the relationship between FS sensitivity and PF (Sections 5.2.1 and 5.2.3).

To achieve these research objectives, a series of parametric studies were carried out under the framework of simplified probabilistic analyses and spatial probabilistic analyses. For the simplified probabilistic analysis, HB parameters are modelled as random variables and their spatial variability is not considered; for the spatial probability analysis, spatial variability of m_i and σ_{ci} is considered and these two parameters are modelled as random fields. Both analyses were based on a slope with the geometry shown in Figure 5.1

In Chapter 4, it has been demonstrated that slope cases with different combinations of HB parameters can have the same FS but different sensitivity. The study in this chapter extends this conclusion. Specifically, three cases with different combinations of HB parameters but the same FS are designed, as shown in Table 5.1. These cases are similar to those studied in Section 4.2.5 and thus similar sensitivity concepts can be applied. All studies in this

chapter are based on these cases. GSI, m_i, and σ_{ci} are assumed to follow truncated normal distributions (discussed in Section 3.3.2.1), and the truncations are given in Table 5.2.

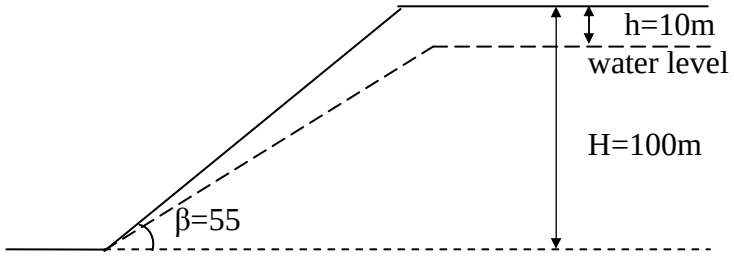

Figure 5.1 Slope geometry for the probabilistic analysis

Table 5.1 Three sets of HB parameters for the probabilistic analysis

Case	GSI	m_i	σ_{ci} (MPa)	FS	FS sensitivity
1	69	13	10	1.64	High
2	38	13	50	1.64	Medium
3	23	13	133	1.64	Low

Table 5.2 Truncations of HB parameters for the probabilistic analysis

Parameter	GSI	m_i	σ_{ci} (MPa)
Truncation	[1 100]	[5 40]	[1 200]

The output of a Monte Carlo simulation (MCS) based probabilistic analysis includes PF and statistical properties as well as the distribution of FS. The convergence of PF in the MCS is examined here by plotting the number of iterations N against the PF value (Section 3.3.2.2). One example of such a convergence plot is shown in Figure 5.2, where PF gradually stabilises as N increases. The header of Figure 5.2 shows the case ID and the COV for GSI, m_i, and σ_{ci}, based on which the probabilistic analysis is carried out. If the value of PF is too small to stabilise within the computation time frame, it is then estimated by the method given by Fenton and Griffiths (2008) (as introduced in Section 3.3.2.3). After PF is calculated or estimated, the distribution and statistical properties of FS,

including the mean, standard deviation, and the COV, can also be obtained. An example of the output from a MCS is shown in Figure 5.3, where SD-FS refers to the standard deviation of FS and N is the number of iterations.

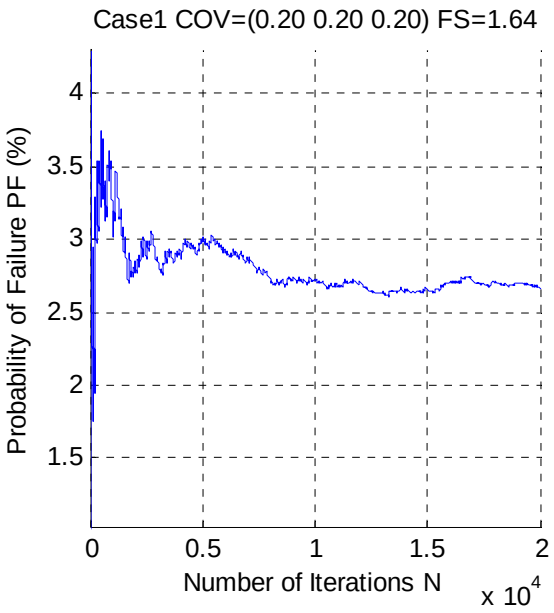

Figure 5.2 Example of the convergence of PF in a Monte Carlo simulation

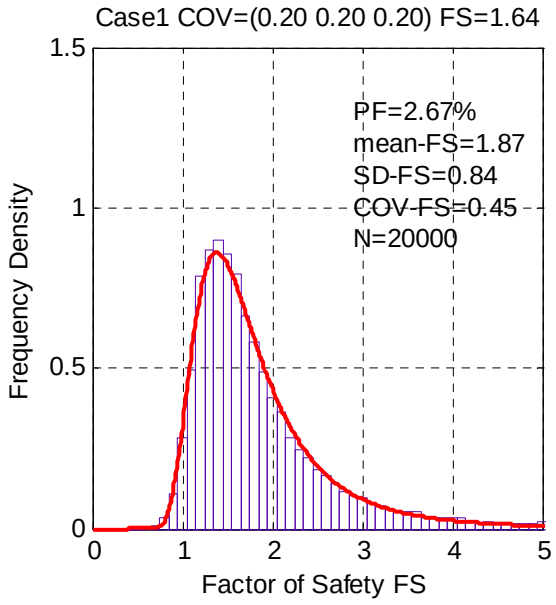

Figure 5.3 Example of the output from a Monte Carlo simulation

5.2 Simplified Probabilistic Analysis

The second, third, and fifth research objectives of this thesis are studied in this section. Two parametric studies and a case study based on simplified probabilistic analyses are carried out.

5.2.1 Parametric Study I

The first parametric study addresses the second and fifth research objectives, i.e. to investigate the influence of changes in the variability of HB parameters (quantified by the COV) on PF and to explore the relationship between FS sensitivity and PF. In this

parametric study, a series of simplified probabilistic analyses are carried out, where all three HB parameters are modelled as random variables and their COV are assumed to be equal and vary uniformly from 0.1 to 1.

The results from the parametric study are shown in Table 5.3 and plotted in Figure 5.4. In Table 5.3, the highlighted boxes indicate that the corresponding PF are obtained from estimations instead of from direct simulations. In Figure 5.4, each line shows the variation of PF for one case with changes in the COV of HB parameters.

Table 5.3 PF values from Parametric study I: three cases (Table 5.1) with the same FS but different FS sensitivity; HB parameters are modelled as random variables together and their COV are assumed to be equal and vary uniformly from 0.1 to 1

COV / PF (%)	0.1	0.2	0.3	0.4	0.5	0.6	0.7	0.8	0.9	1
Case 1	1.39E-03	2.7	10.6	18.8	25.0	29.5	33.0	35.5	37.4	38.9
Case 2	1.74E-06	0.41	4.6	11.8	19.4	25.5	30.6	34.7	37.9	40.3
Case 3	1.84E-09	0.22	3.5	10.2	17.7	23.9	29.4	33.8	37.4	40.4

Figure 5.4 shows that the PF for each case increases gradually as the COV increases, which conforms with expectation. On the other hand, even though the three cases have the same FS and identical COV for HB parameters, their PF are different. In most circumstances (COV $\leq$ 0.8), the PF for Case 1 is the largest and the PF for Case 3 is the smallest. These differences are significant when the COV is small ($\leq$ 0.6). As the COV increases, the differences between PF for the three cases become less and less and almost diminish eventually.

The above phenomenon is caused by the different FS sensitivity for the three cases. Based on the conclusions from Chapter 4, Case 1 is expected to be the most sensitive case and

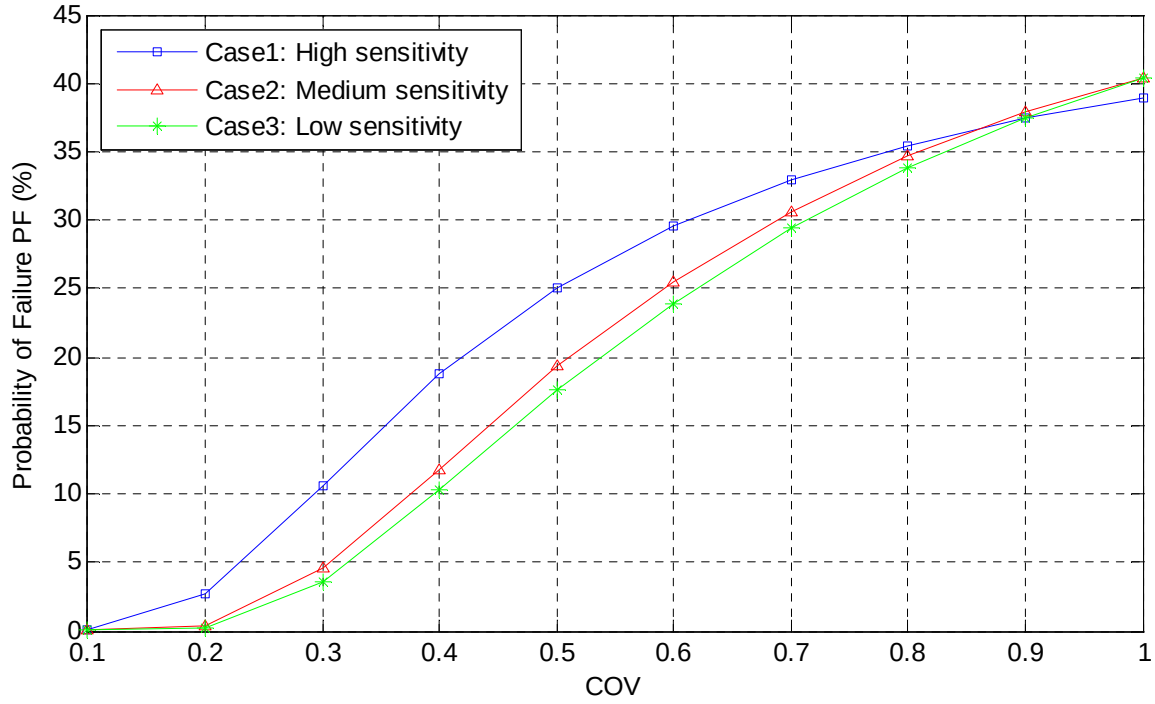

Figure 5.4 PF values from Parametric study I: three cases (Table 5.1) with the same FS but different FS sensitivity; HB parameters are modelled as random variables together and their COV are assumed to be equal and vary uniformly from 0.1 to 1

Case 3 is the least. When the COV is small, the random variations of GSI, m_i, and σ_{ci} are largely close to their mean values, which are the regions within which the effect of FS sensitivity is significant. Case 1 has the largest PF since its corresponding FS are most sensitive to the changes in HB parameters. However, as the COV increases, HB parameters of all the three cases begin to vary within their entire truncated ranges (Table 5.2) and finally become almost evenly spread out. In these circumstances, the effect of FS sensitivity diminishes and thus the PF for the three cases become very close to each other.

The statistical properties of FS from some of the probabilistic analyses in parametric study I are obtained to demonstrate the above points. Figures 5.5(a), 5.6(a), and 5.7(a) show the statistical properties and distributions of FS for Cases 1 to 3, with the COV of HB parameters equal to 0.2, and Figures 5.5(b), 5.6(b), and 5.7(b) show the statistical

properties and distributions of FS for the three cases, with the COV of HB parameters equal to 1.0.

As shown in Figures 5.5(a), 5.6(a), and 5.7(a), the variability of the calculated FS becomes smaller and smaller from Case 1 to Case 2 and to Case 3 (as the distributions of FS become narrower), causing the PF to decrease. On the other hand, the distributions of FS in Figures 5.5(b), 5.6(b), and 5.7(b) are similar to each other, indicating similar variability of FS and thus similar PF. These observations are in good agreement with discussions in the previous paragraph: when the COV of HB parameters equal to 0.2, the variations of HB parameters are small and close to their mean values and the effect of FS sensitivity is significant; in contrast, when the COV of HB parameters equal to 1.0, the variations of HB parameters are so great that their values for all three cases are similarly spread out (almost evenly) within their ranges and thus the effect of FS sensitivity diminishes.

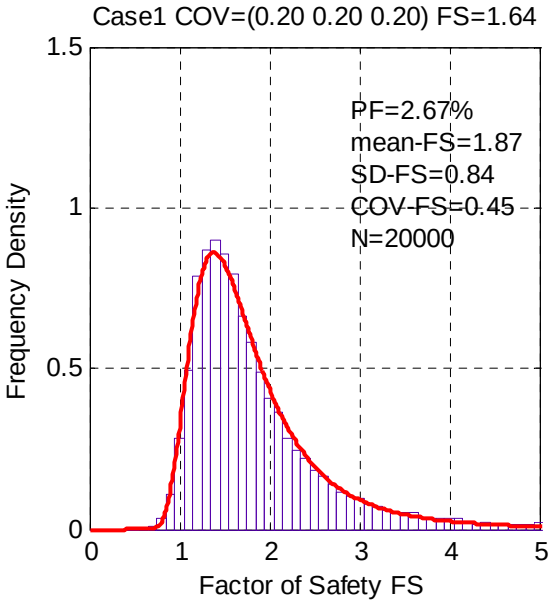

Figure 5.5 (a) Statistical properties of FS for Case 1 with the COV of HB parameters = 0.2

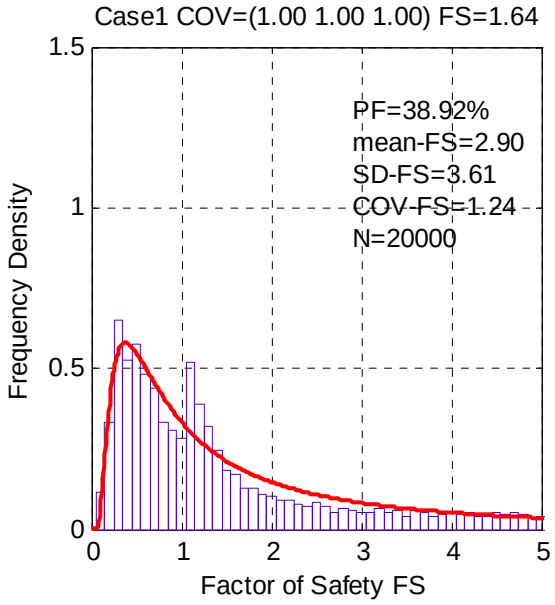

Figure 5.5 (b) Statistical properties of FS for Case 1 with the COV of HB parameters =1

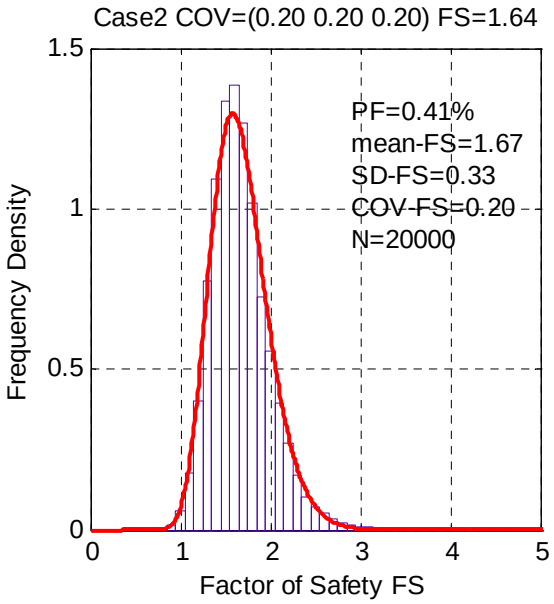

Figure 5.6 (a) Statistical properties of FS for Case 2 with the COV of HB parameters = 0.2

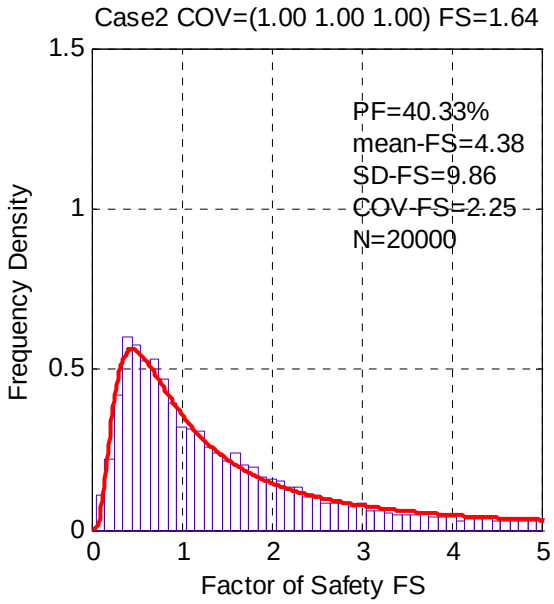

Figure 5.6 (b) Statistical properties of FS for Case 2 with the COV of HB parameters = 1

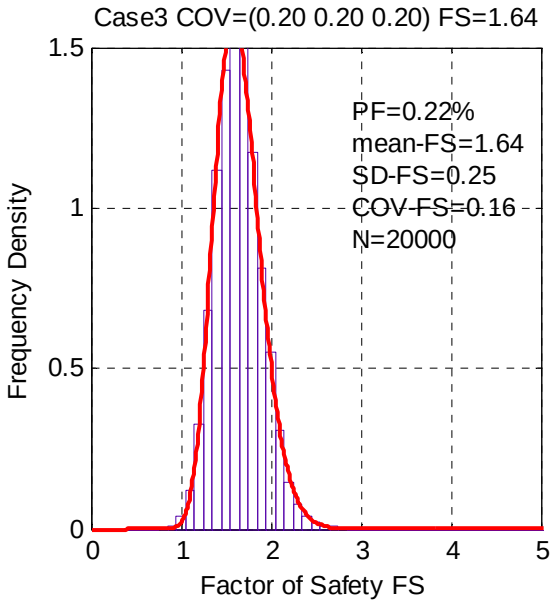

Figure 5.7 (a) Statistical properties of FS for Case 3 with the COV of HB parameters = 0.2

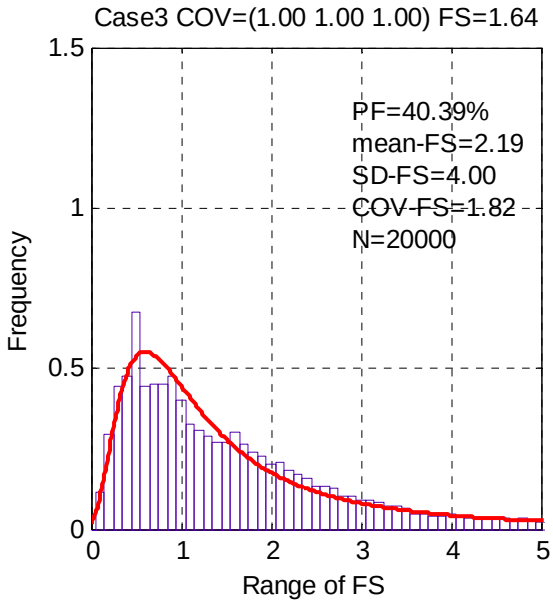

Figure 5.7 (b) Statistical properties of FS for Case 3 with the COV of HB parameters = 1

Based on the above results and discussions, key conclusions of this section are:

1. The probability of failure (PF) of a highly fractured rock slope increases as the coefficient of variation (COV) of the input HB parameters increase.

2. Even if their FS and variability of the input (quantified by the COV) are identical, cases with different combinations of HB parameters have different PF.

3. For cases whose FS are highly sensitive to the changes in HB parameters, their PF are also large, indicating higher risks. Therefore, probabilistic analysis is capable of detecting the effect of FS sensitivity on slope stability.

5.2.2 Parametric Study II

The second parametric study addresses the third research objective, i.e. to evaluate the relative contribution of the variability of each HB parameter (quantified by the COV) to PF. This parametric study is also based on the three cases given in Table 5.1 but HB parameters are now modelled as individual random variables. The COV again varies uniformly from 0.1 to 1 and HB parameters are still assumed to follow truncated normal distributions.

Since HB parameters are modelled as random variables separately, PF can simply be calculated from probability theory instead of from MCS. For Case 1 for example, the critical value of GSI (termed as Critical GSI) that makes FS equal to 1 is 39. Therefore, the PF of Case 1 when only GSI is modelled as a random variable (termed as PF-GSI) just equals to the Probability [GSI < Critical GSI, m_i = 13, σ_{ci} = 10MPa]. Similarly, PF-m_i = Probability [GSI = 69, m_i < Critical m_i, σ_{ci} = 10MPa], and PF-σ_{ci} = Probability [GSI = 69, m_i = 13, σ_{ci} < Critical σ_{ci}].

The critical values of GSI, m_i, and σ_{ci} that make FS equal to 1 for each slope case are listed in Table 5.4. In Table 5.4, N/A for m_i denotes that whatever value m_i takes, the FS of the slope is always larger than 1. Thus PF-m_i = 0 and the contribution of m_i variability to PF is considered to be very small.

PF-GSI and PF-σ_{ci} are given in Table 5.5 and plotted in Figures 5.8, 5.9, and 5.10.

Table 5.4 Critical value of each HB parameter that makes the FS equal to 1 for slope cases given in Table 5.1

Case	Critical GSI	Critical m_i	Critical σ_{ci} (MPa)
1	39	N/A	2.77
2	15.2	N/A	10.99
3	8	N/A	26.50

Table 5.5 PF values from parametric study II: three cases (Table 5.1) with the same FS but different FS sensitivity; HB parameters are modelled as random variables individually and the COV varies uniformly from 0.1 to 1

Case	PF (%)	COV						
		0.1	0.2	0.3	0.4	0.6	0.8	1
1	PF-GSI	6.87E-04	1.5	7.4	13.9	23.4	29.3	33.2
	PF-m_i	0	0	0	0	0	0	0
	PF-σ_{ci}	2.41E-11	1.50E-02	0.80	3.5	11.4	18.3	23.5
2	PF-GSI	9.87E-08	0.13	2.3	6.7	15.9	22.7	27.4
	PF-m_i	0	0	0	0	0	0	0
	PF-σ_{ci}	3.05E-13	4.79E-03	0.47	2.6	9.7	16.5	21.8
3	PF-GSI	3.47E-09	5.55E-02	1.5	5.2	13.9	20.7	25.7
	PF-m_i	0	0	0	0	0	0	0
	PF-σ_{ci}	5.85E-14	3.12E-03	0.38	2.3	9.1	15.8	21.2

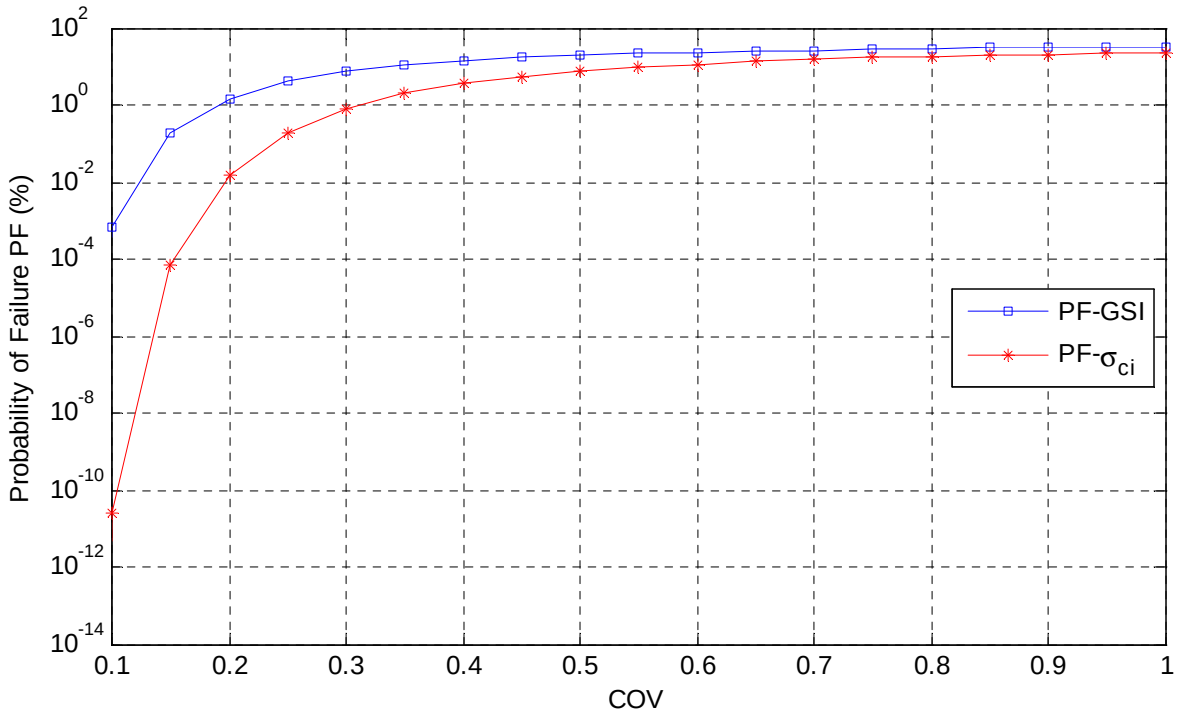

Figure 5.8 PF values from Case 1 of parametric study II: three cases (Table 5.1) with the same FS but different FS sensitivity; HB parameters are modelled as random variables individually and the COV varies uniformly from 0.1 to 1

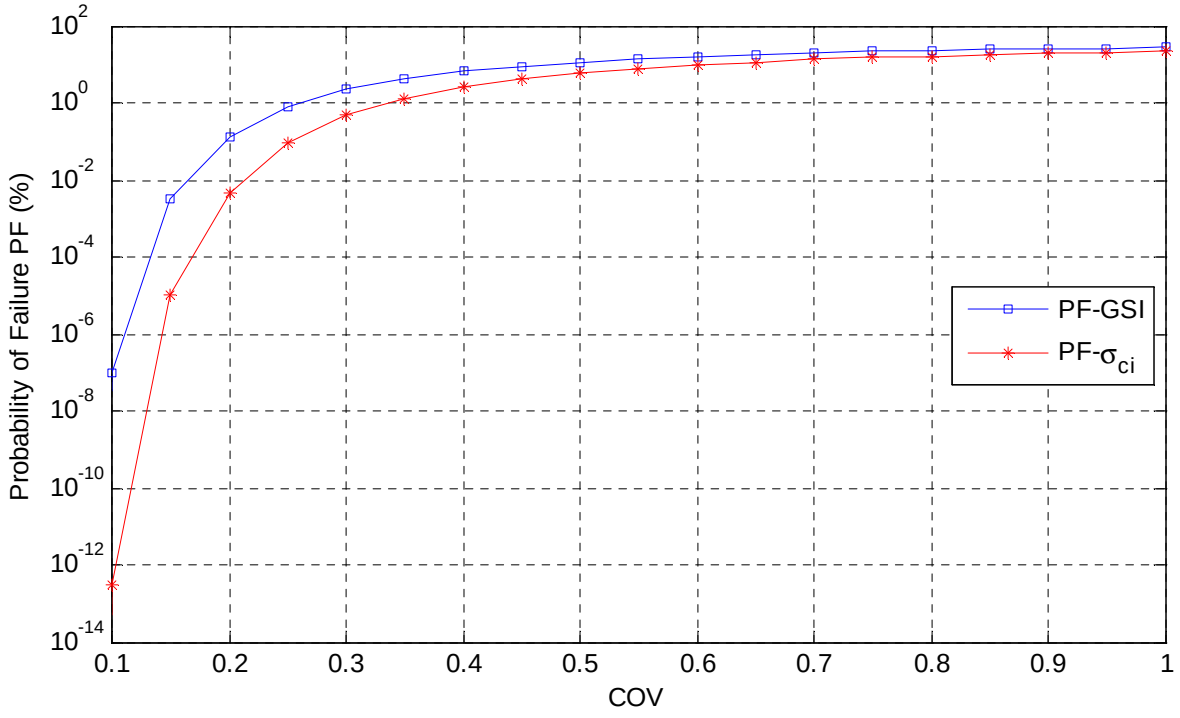

Figure 5.9 PF values from Case 2 of parametric study II: three cases (Table 5.1) with the same FS but different FS sensitivity; HB parameters are modelled as random variables individually and the COV varies uniformly from 0.1 to 1

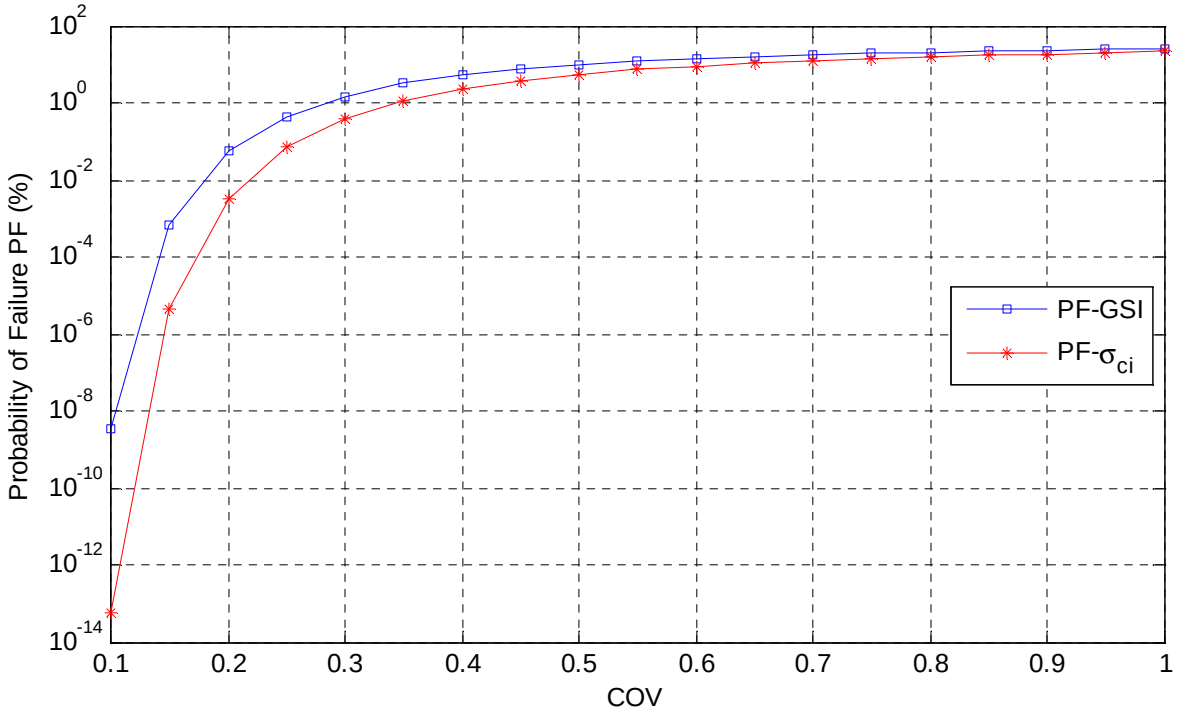

Figure 5.10 PF values from Case 3 of parametric study II: three cases (Table 5.1) with the same FS but different FS sensitivity; HB parameters are modelled as random variables individually and the COV varies uniformly from 0.1 to 1

Comparing the data in Table 5.5, we observe that for a given value of COV, the PF for when only GSI is modelled as a random variable (PF-GSI) lies in the order Case 1 > Case 2 > Case 3, and similarly for PF-σ_{ci}. This again verifies the conclusion from the previous section, i.e. a slope of high FS sensitivity gives a high PF.

In addition, comparison of PF-GSI and PF-σ_{ci} in Figures 5.8, 5.9, and 5.10 shows that for all three cases, given a specific value of COV, PF-GSI > PF-σ_{ci}. This suggests that when the COV of GSI and σ_{ci} are identical, the variability of GSI makes a larger contribution to PF than that of σ_{ci}. However, Section 3.3.2.1 shows that σ_{ci} generally has larger variability (COV) than GSI in practice, with the upper limit COV of GSI and σ_{ci} equal to 0.15 and 0.4 respectively. If these values are adopted, Figures 5.8, 5.9, and 5.10 show that PF-σ_{ci} > PF-

GSI for all three cases. This suggests that in engineering practice, the high variability of σ_{ci} will make a larger actual contribution to PF than that of GSI.

Based on these discussions, the following conclusions are drawn:

1. When the COV of GSI, m_i, and σ_{ci} are identical, the comparison of contributions to PF can be expressed as: GSI (variability) > σ_{ci} (variability) >> m_i (variability).

2. When the COV of GSI, m_i, and σ_{ci} are equal to the upper limit values observed in practice (0.15, 0.2, and 0.4 respectively), the comparison of contributions to PF can be expressed as: σ_{ci} (variability) > GSI (variability) >> m_i (variability).

5.2.3 Case Study

To be consistent with engineering practice, this section is devoted to simplified probabilistic analyses with the COV of HB parameters set to their upper limit values observed in practice (summarised in Section 3.3.2.1). The study is again based on the three slope cases given in Table 5.1.

The upper limit COV of the HB parameters and the corresponding PF calculated by MCS based on these COV are given in Table 5.6. The statistical properties and distributions of FS are shown in Figures 5.11, 5.12, and 5.13.

Table 5.6 Upper-limit COV values of HB parameters and resulting PF values from the case study of the simplified probabilistic analysis

Case	FS sensitivity	COV - GSI	COV - m_i	COV - σ_{ci}	PF (%)
1	High	0.15	0.2	0.4	5.5
2	Medium				3.2
3	Low				2.8

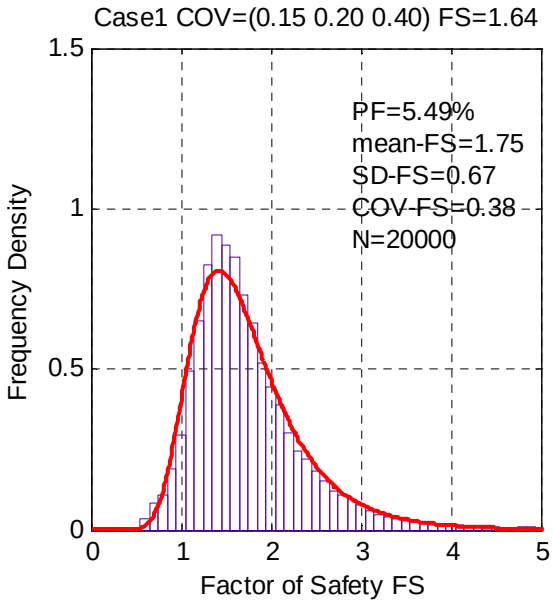

Figure 5.11 Statistical properties of FS for Case 1 with the COV of HB parameters set to upper limit values in engineering practice

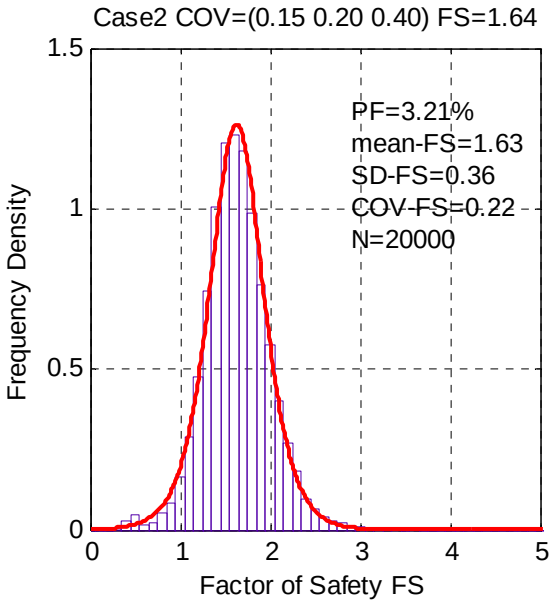

Figure 5.12 Statistical properties of FS for Case 2 with the COV of HB parameters set to upper limit values in engineering practice

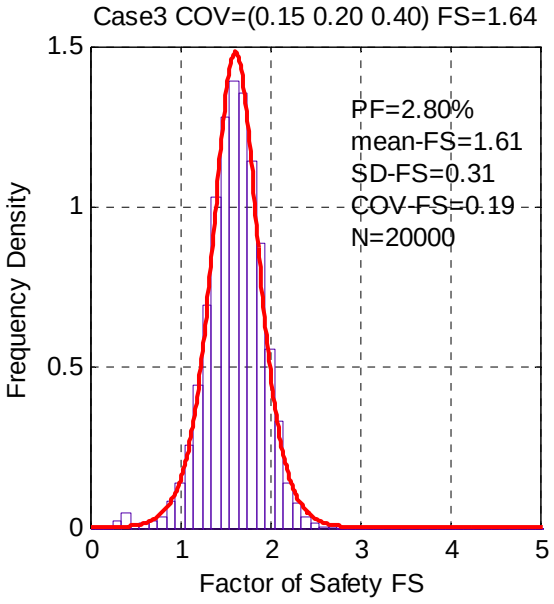

Figure 5.13 Statistical properties of FS for Case 3 with the COV of HB parameters set to upper limit values in engineering practice

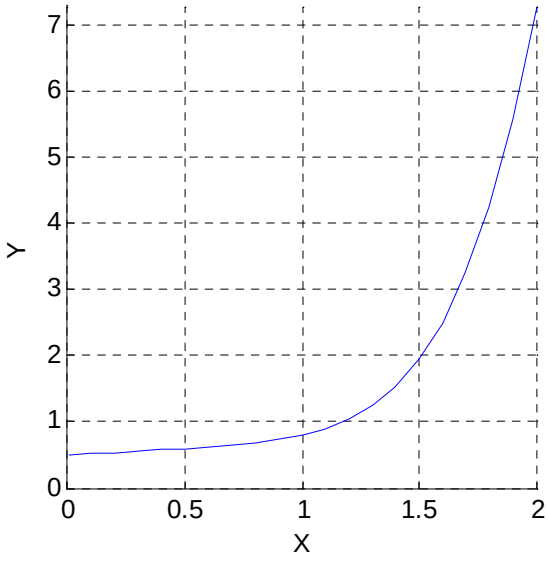

Figure 5.14 Example of a function plot demonstrating the concept of sensitivity of *y* to *x*

Table 5.6 shows that the PF of Case 1 is the largest among the three, which is in good agreement with its degree of sensitivity. However, Figure 5.11 shows that the mean value of FS obtained from the MCS for Case 1 equals to 1.75 and is much larger than 1.64 (which is the FS calculated based on the mean values of HB parameters). This suggests that the FS of Case 1 tends to be overestimated in practice, although its actual risk is higher (since the PF of Case 1 is the highest). On the other hand, the mean values of FS obtained from the MCS for other two cases are close to 1.64.

The above phenomenon can be explained by Figure 5.14, in which y (corresponds to FS) is a chosen function of x (corresponds to HB parameters). Figure 5.14 shows that for this function, y is not sensitive to x when x is varying between 0 and 1. This is similar to the conditions for Cases 2 and 3. On the other hand, y becomes sensitive to x when x is varying between 1 and 2. This is similar to the condition for Case 1. For $0 < x_1 < x_2 < 1$, where x_1 and x_2 are two arbitrary values of x, the value of $[f(x_1)+f(x_2)]/2$ would be close to that of $f[(x_1+x_2)/2]$, as the curve in Figure 5.14 between 0 and 1 is almost straight. However, for $1 < x_1 < x_2 < 2$, the value of $[f(x_1)+f(x_2)]/2$ would be larger than that of $f[(x_1+x_2)/2]$, as the curve in Figure 5.14 between 1 and 2 is concave. Therefore, for Case 1, where FS is most sensitive to changes in HB parameters, the mean of FS (obtained from the MCS) is larger than the mean FS (obtained from the deterministic analysis).

In addition to the output from the MCS, the Spearman correlation coefficients r_s between GSI, m_i, σ_{ci}, and FS for each case are also computed. The Spearman correlation coefficient measures the monotonic correlation between variables and has been used in several studies as an indicator of contribution of the variability of an input variable to the output (El-Ramly et al. 2002; Fisher and Eberhardt 2012).

Table 5.7 shows the calculated r_s for all three slope cases. Meanwhile, GSI, m_i, and σ_{ci} (20,000 random values) in Case 1 are plotted against the corresponding FS in Figures 5.15, 5.16, and 5.17.

Table 5.7 Spearman correlation coefficients r_s between GSI, m_i, σ_{ci}, and FS in the case study of the simplified probabilistic analysis

Spearman correlation coefficient r_s	Case 1	Case 2	Case 3
FS & GSI	0.73	0.57	0.53
FS & m_i	0.067	0.15	0.19
FS & σ_{ci}	0.61	0.76	0.78

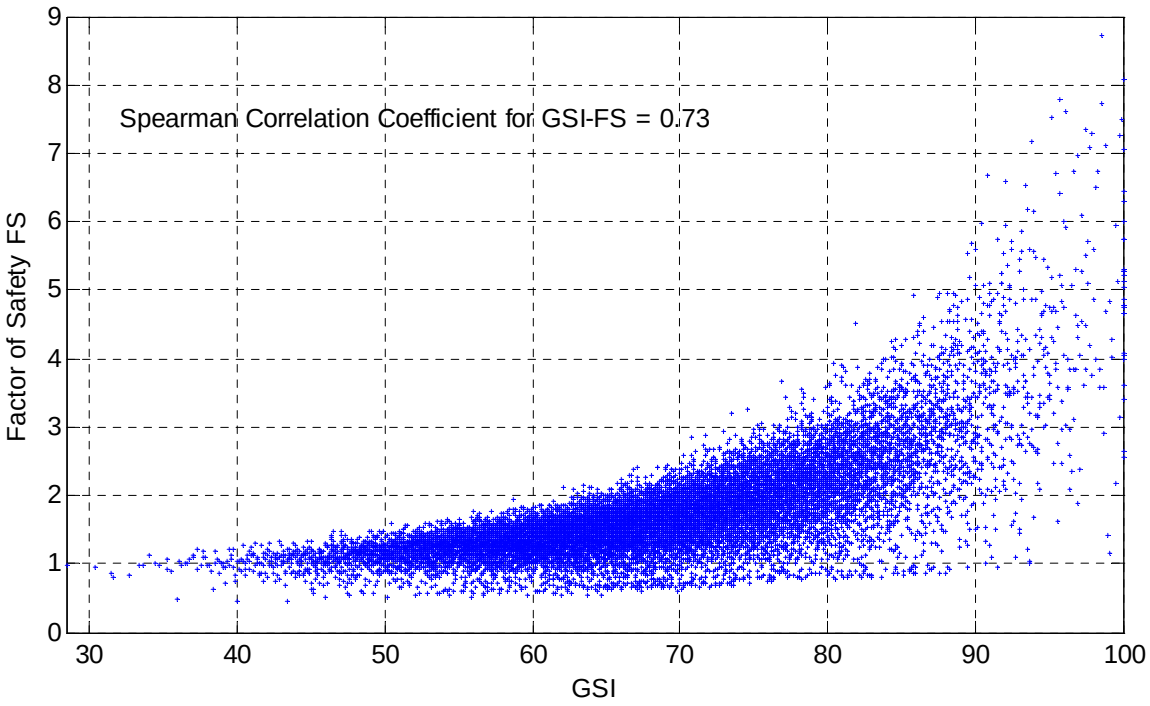

Figure 5.15 Spearman correlation coefficient r_s between GSI and FS from Case 1 in the case study of the simplified probabilistic analysis

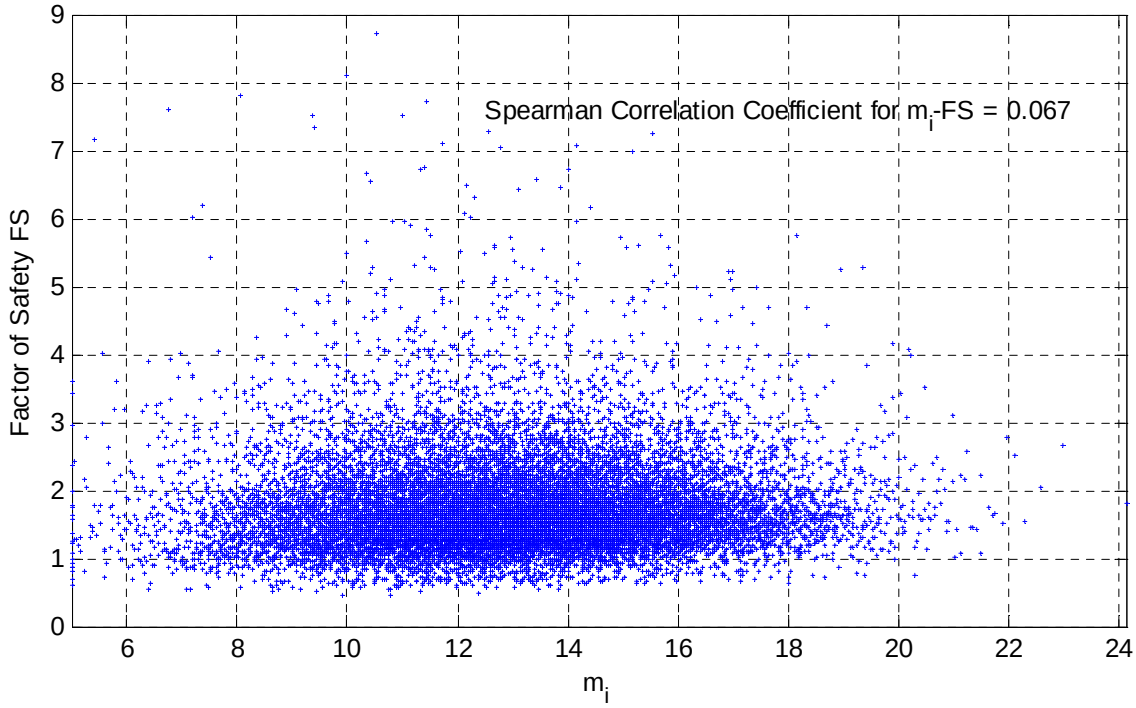

Figure 5.16 Spearman correlation coefficient r_s between m_i and FS from Case 1 in the case study of the simplified probabilistic analysis

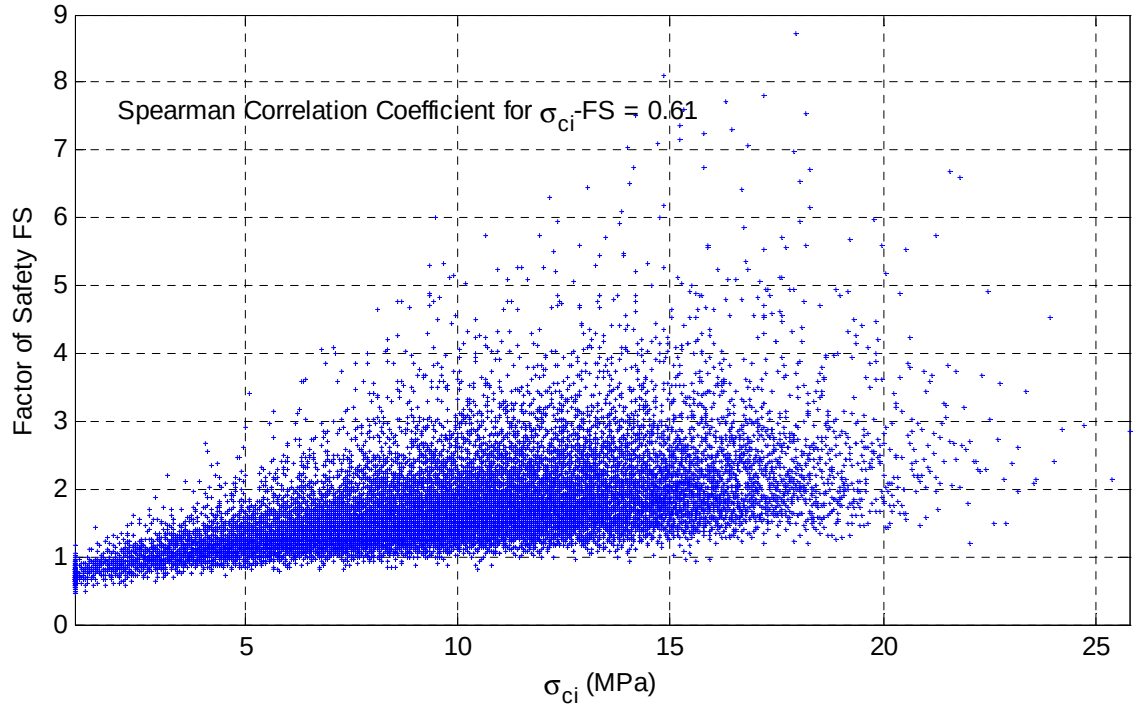

Figure 5.17 Spearman Correlation Coefficient r_s between FS and σ_{ci} from Case 1 in the case study of the simplified probabilistic analysis

Table 5.7 shows that for all three cases, the r_s between FS & GSI and FS & σ_{ci} are much larger than those between FS & m_i, which suggests that the variability of GSI and σ_{ci} has much larger contributions to PF than that of m_i. This is consistent with the conclusion from Section 5.2.2. For Cases 2 and 3, the r_s between FS & σ_{ci} is larger than that between FS & GSI, which suggests that for these two cases, the variability of σ_{ci} has a larger contribution to PF than that of GSI. This is also consistent with the conclusion from Section 5.2.2. On the other hand, for Case 1, the r_s between FS & GSI is slightly larger than the r_s between FS & σ_{ci}, suggesting that for Case 1, the variability of GSI has a slightly larger contribution to PF than that of σ_{ci}. This contradicts the conclusion from Section 5.2.2 (where it has been demonstrated that for all three cases, the PF corresponding to GSI with COV = 0.15 are smaller than the PF corresponding to σ_{ci} with COV = 0.4, which suggests that the variability of GSI makes a smaller contribution to PF than that of σ_{ci}). Since in Section 5.2.2, the contributions are measured directly by modelling HB parameter as individual random variables and then comparing the corresponding PF values whereas r_s is a indirect measurement, the contradiction suggests that r_s may not always be a reliable predictor for contribution of the variability of an input variable to the output and this is a topic that needs additional study.

In this section, probabilistic analyses have been carried out from a practical engineering perspective. Following conclusions are drawn:

1. For practical engineering cases, a slope of higher FS sensitivity gives a higher PF.

2. For a slope of high FS sensitivity (e.g. Case 1), its FS tends to be overestimated, suggesting a safer slope, but its actual risk (PF) is higher.

3. The Spearman correlation coefficients r_s between GSI, m_i, σ_{ci}, and FS show that the comparison of contributions of the variability of HB parameters to PF can be expressed as follows: for Case 1 (the most sensitive case), GSI (variability) > σ_{ci} (variability) >> m_i (variability); for Case 2 (the medium sensitive case), σ_{ci} (variability) > GSI (variability) >> m_i (variability); and for Case 3 (the least sensitive case), σ_{ci} (variability) > GSI (variability) >> m_i (variability). This partly contradicts the conclusion from the previous section. Since the measurement in the previous section is considered to be more reliable, the contradiction suggests that the Spearman correlation coefficient may not always be a reliable predictor for the contribution of the variability of an input variable to the output.

5.3 Spatial Probabilistic Analysis (Parametric Study III)

This section deals with the fourth research objective, i.e. to investigate the influence of the spatial variability of HB parameters (quantified by the scale of fluctuation θ) on PF. A parametric study is carried out, where the scale of fluctuation of HB parameters changes from a small value to infinity. The slope geometry in Figure 5.1 and the three cases shown in Table 5.1 are again used as the basis for the parametric study.

As discussed in Section 3.3.2.1, only m_i and σ_{ci} are regarded as spatial variables and modelled by random fields. The Markov model is adopted for the random field generation. The mean values of the random fields are those given in Table 5.1 and the COV of m_i and σ_{ci} are set to their upper-limit values, i.e. 0.2 and 0.4 respectively. The truncations in Table 5.2 are again imposed. On the other hand, GSI is modelled as a random variable for the entire rock mass. The mean values of GSI are those given in Table 5.1 and the COV of GSI is set to its upper limit value, i.e. 0.15.

In practice, the random field is generated along the slip surface and each slice is a unit of the random field. As discussed in Section 3.3.2.1, the number of slices for the LEM model in the spatial probabilistic analysis is set to 100 so that spatial averaging does not need to be applied. An example of a random field realisation for σ_{ci} is shown in Figure 5.18 (with mean = 133MPa, COV = 0.4, and θ = 50m).

The specific lengths for θ in the parametric study are given in Table 5.8. The relationships between these lengths and the slope height are also displayed. Except for the first and last cases, i.e. θ = 1m and θ → infinity, θ gradually increases by factors of 2.

The results from parametric study III are shown in Table 5.9 and plotted in Figure 5.19.

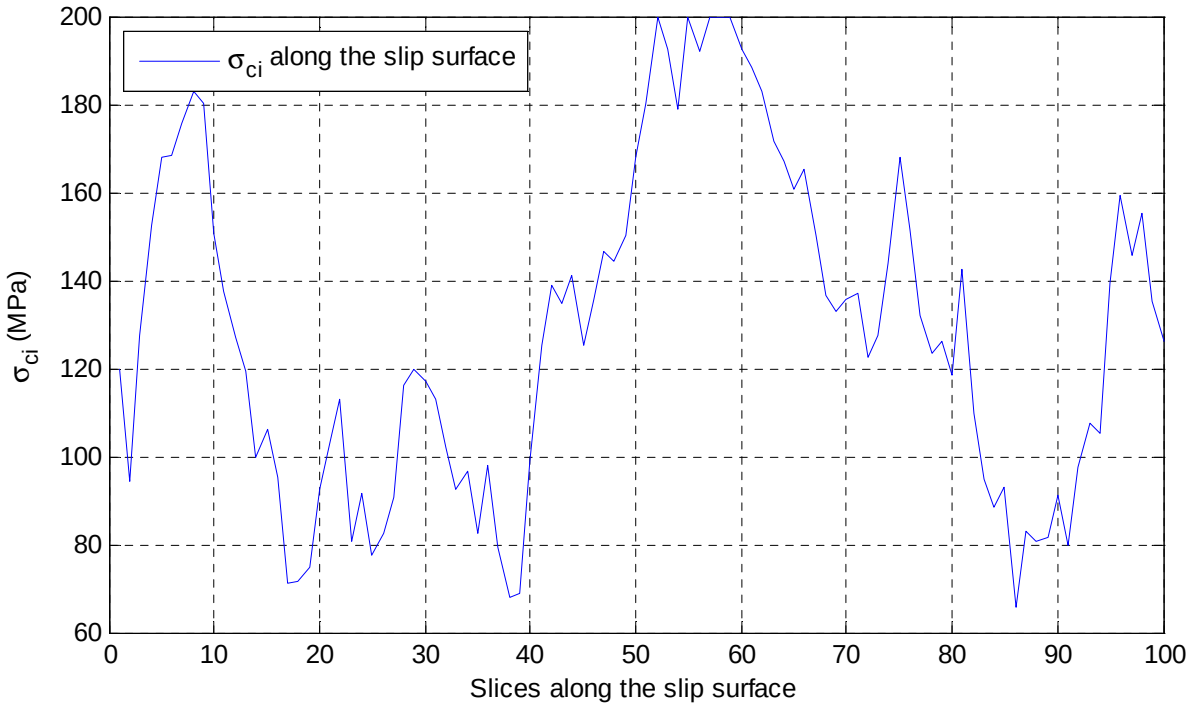

Figure 5.18 Example of a random field realisation for σ_{ci} along the slip surface (mean = 133MPa, COV = 0.4, and θ = 50m)

Table 5.8 Variation of the scale of fluctuation θ (only applicable to m_i and σ_{ci}) in parametric study III and their relationships with the slope height H

θ	1m	10m	20m	50m	100m	200m	500m	1000m	∞
θ-H	0.01H	0.1H	0.2H	0.5H	H	2H	5H	10H	∞

Table 5.9 PF values from parametric study III (based on spatial probabilistic analyses): m_i and σ_{ci} are modelled as random fields and GSI is modelled as a random variable; the scale of fluctuation θ of m_i and σ_{ci} varies from 1m to infinity

θ / PF (%)	1m	10m	20m	50m	100m	200m	500m	1000m	∞
Case 1	0.43	0.72	1.1	2.3	3.4	4.4	5.1	5.3	5.5
Case 2	1.26E-02	0.062	0.26	1.2	2.2	2.8	3.1	3.2	3.2
Case 3	2.99E-04	0.040	0.27	1.3	2.2	2.6	2.7	2.8	2.8

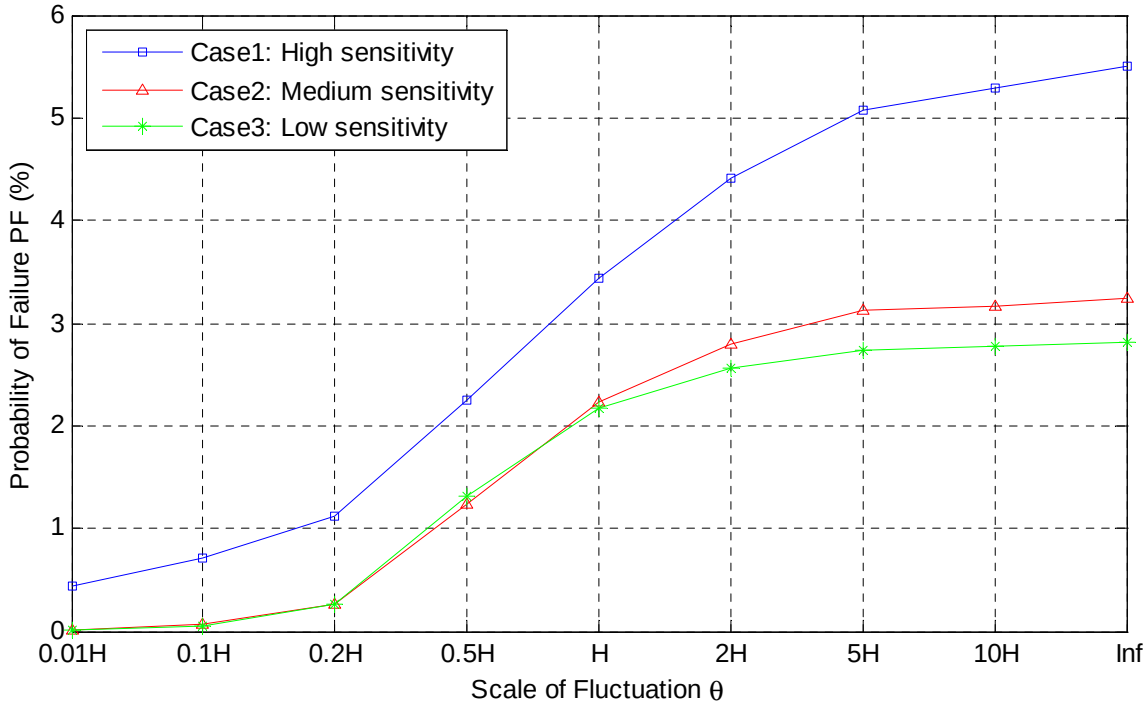

Figure 5.19 PF values from parametric study III (based on spatial probabilistic analyses): m_i and σ_{ci} are modelled as random fields and GSI is modelled as a random variable; the scale of fluctuation θ of m_i and σ_{ci} varies from 1m to infinity

The results (shown in Table 5.9 and Figure 5.19) are discussed below.

Firstly, Figure 5.19 shows that for all three cases, PF values increase as θ increases, which is consistent with the literature (El-Ramly et al. 2002; Griffiths et al. 2009; Cho 2010). In addition, when θ tends to infinity, theoretically, the spatial probabilistic analysis should become identical to the simplified probabilistic analysis. For the current study, when θ tends to infinity, the PF for Cases 1 to 3 become 5.5, 3.2, and 2.8 respectively, which are the same as the PF from the simplified probabilistic analyses (Table 5.6). Therefore, the results from the current study are consistent with theory.

Secondly, Figure 5.19 shows that for all three cases, PF is most sensitive to the change in θ between 1m and 500m.

Lastly, Figure 5.19 shows that for a particular length of θ, the PF for Case 1 is always the largest and the PF for Case 3 is generally the smallest (with a few exceptions). This suggests that the relative sensitivity of FS for the three cases is not affected by the spatial variability of HB parameters. On the other hand, the absolute differences of PF between the three cases increase as θ increases, suggesting that larger θ makes the effect of FS sensitivity on slope stability (measured by PF) more significant.

Based on the above discussions, following key conclusions can be made:

1. For a slope with FS > 1, the PF increases as the scale of fluctuation θ (of m_i and σ_{ci}) increases. When θ tends to infinity, PF from the spatial probabilistic analyses become identical to those from the simplified probabilistic analyses.

2. PF is most sensitive to the change in θ within the range of 0 – 500m.

3. In most circumstances, for any specific value of θ, PF of the three cases of different FS sensitivity can be expressed as: PF-Case 1 > PF-Case 2 > PF-Case 3. However, the absolute differences of PF between the three cases increase as θ increases, suggesting that larger θ makes the effect of FS sensitivity on slope stability (measured by PF) more significant.

5.4 Summary

The studies in this chapter were based on three slope cases with the same FS but different sensitivity (following the primary conclusion of Chapter 4). Key conclusions of this chapter are presented below:

1. FS sensitivity has a significant impact on slope stability and probabilistic analysis is capable of evaluating such impact. For cases with different combinations of HB parameters, even if their FS and the variability of input (quantified by the COV) are identical, their PF can be different. A highly sensitive slope case gives a high PF and indicates high risk.

2. PF of a slope increases as the COV of input HB parameters increase.

3. When the COV of GSI, m_i, and σ_{ci} are identical, the order of contributions to PF can be expressed as: GSI (variability) > σ_{ci} (variability) >> m_i (variability).

4. When the COV of GSI, m_i, and σ_{ci} are set to the upper limit values found in engineering practice (0.15, 0.2, and 0.4 respectively), the order of contributions to PF can be expressed as: σ_{ci} (variability) > GSI (variability) >> m_i (variability). This part is examined by two separate approaches in Sections 5.2.2 and 5.2.3,

where slightly contradictory conclusions were found, for which detailed discussions were given in Section 5.2.3.

5. For a slope with FS > 1, the PF increases as the scale of fluctuation θ (of m_i and σ_{ci}) increases. When θ tends to infinity, PF from the spatial probabilistic analyses become identical to those from the simplified probabilistic analyses.

6. PF is most sensitive to the change in θ (of m_i and σ_{ci}) within the range of 0 – 500m.

7. Larger θ makes the effect of FS sensitivity on slope stability more significant, i.e. the differences of PF between slopes of different FS sensitivity increase as θ increases.

Chapter 6

SUMMARY AND CONCLUSIONS

6.1 Summary

In this study, the Hoek-Brown (HB) strength criterion has been used to investigate the circular failure of highly fractured rock slopes. The overall focus has been on the relationship between the HB input (GSI, m_i, σ_{ci}, and their variability) and the output, Factor of Safety (FS) and Probability of Failure (PF). Both deterministic analyses and probabilistic analyses were carried out. A group of sensitivity analyses and parametric studies were designed and implemented. The final outcomes of this study provide the following knowledge: sensitive conditions (with regard to FS) of highly fractured rock slopes are identified, the relationship between FS sensitivity and PF is defined, and the effectiveness of probabilistic analysis is better understood.

In Chapter 2, relevant literature was reviewed with the aims of providing background knowledge and identifying specific research gaps for the study. The circular failure of highly fractured rock slopes was identified as a critical failure mode but little research effort has been devoted to it. The HB strength criterion was then discussed in detail and verified as an effective tool for fractured rock slope stability analysis. Input parameters for the HB strength criterion, including GSI, m_i, and σ_{ci}, were discussed; it was observed that the variability of GSI is generally low (the COV of GSI is between 0.15 and 0.35), the variability of m_i is medium (the COV of m_i is between 0.039 and 0.25), and the variability of σ_{ci} is generally high (the COV of σ_{ci} is between 0.1 and 0.4). Methods for deriving

equivalent Mohr-Coulomb (MC) parameters from HB parameters were also studied; three approximate solutions were compared, as summarised in Section 2.3.3. The Limit Equilibrium Method (LEM), particularly the method of slices was discussed. It was shown that Bishop's method of slices is appealing for Monte Carlo simulation (MCS) based probabilistic analysis because of its simplicity and accuracy. Algorithms for the Ordinary method of slices and Bishop's simplified method of slices were presented. Subsequently, Probabilistic Slope Stability Analysis (PSSA) was discussed. It was shown that PSSA is a critical development that supplements the deterministic analysis, and has become a primary research area in slope stability analysis (Table 2.9). Six major research directions of PSSA were then summarised (Table 2.10). It was shown that for highly fractured rock slopes, where the HB strength criterion can be employed, relatively little research has been carried out for one of the important research directions, namely the relationship between the input (HB parameters and their variability), and the output (FS and PF).

In Chapter 3, the methodology for determining this relationship was proposed. The study where FS was used as the slope stability measure has been named the deterministic analysis (Chapter 4) and the study where PF was used as the slope stability measure has been named the probabilistic analysis (Chapter 5). For the deterministic analysis, a sensitivity graph analysis and an equation fitting analysis were developed (Section 3.2). Bishop's simplified method of slices in *Slide6.0* (Rocscience 2011) was adopted as the LEM model for the deterministic analysis. The probabilistic analysis was based on MCS. A series of parametric studies were designed, including simplified probabilistic analyses where the spatial variability of HB parameters was not considered and spatial probabilistic analyses where it was considered. It was determined that truncated normal distributions are suitable for HB parameters (i.e. GSI, m_i and σ_{ci}). For the simplified probabilistic analysis,

HB parameters were modelled as random variables first together and then separately. For the spatial probabilistic analysis, it was decided that m_i and σ_{ci} would be modelled as spatial variables by random fields, while GSI would be modelled as an independent random variable for the entire rock mass. It was also decided that the Latin Hypercubic sampling technique was to be applied to MCS when applicable. Since *Slide6.0* is not able to incorporate spatial variability, a LEM model based on Bishop's method of slices was developed in *Matlab* for the probabilistic analysis (Figure 3.4). The validity of this model was examined by comparing its output with that from *Slide6.0*. For a number of specific cases, as shown in Table 3.3, the developed LEM model produced results with mostly less than 2% differences with those of *Slide6.0*. The validity of the random field generator adopted for the probabilistic analysis was also examined. It was demonstrated that the mean and covariance function of the generated random field are in good agreement with the theoretical values.

Chapter 4 addressed the sensitivity of FS to the changes in HB parameters (FS sensitivity) and whether such sensitivity is affected by slope geometry. The sensitivity graph analysis and the equation fitting analysis were applied to achieve the objectives. For the sensitivity graph analysis, the relationship between HB parameters and FS was plotted in a series of figures. For the equation fitting analysis, a large amount of data between HB parameters and FS were generated by *Slide6.0* and the data were fitted with a second order polynomial equation. FS sensitivity was then analysed by taking the derivatives of FS with respect to HB parameters based on the fitted equation (Section 4.2.2). The sequences of the study in this chapter are as follows: firstly, sensitivity graphs were employed to study whether FS sensitivity is affected by slope geometry and to provide some initial insights into the problem; secondly, the equation fitting analysis was applied to quantitatively analyse FS

sensitivity and a series of conclusions were obtained; next, sensitivity graphs were again used to provide a visual verification of the conclusions; and finally, a case study was undertaken to demonstrate the impact of FS sensitivity on slope stability. In summary, Chapter 4 leads to the following conclusions:

1. There is a general pattern of FS sensitivity exists, which can be studied independent of slope geometry.

2. The sensitivity of FS to the change in any particular HB parameter depends on the value of that parameter itself (the range within which it is changing) as well as on the values of other HB parameters.

3. Slope cases with the same geometry and the same FS values (but different combinations of HB parameters) have different FS sensitivity.

4. GSI is the most critical parameter for FS sensitivity. FS always increases with increasing GSI. When GSI is large, FS becomes sensitive to the change in GSI itself and that in σ_{ci}.

5. σ_{ci} is also a critical parameter for FS sensitivity. FS always increases with increasing σ_{ci}. FS becomes sensitive to the change in σ_{ci} when GSI is large.

6. m_i is the least critical parameter for FS sensitivity.

Chapter 5 was devoted to the remaining four research objectives, i.e. to investigate the influence of changes in the variability of HB parameters (quantified by the COV) on PF; to evaluate the relative contribution of the variability of each HB parameter (quantified by the COV) to PF; to investigate the influence of the spatial variability of HB parameters (quantified by the scale of fluctuation θ) on PF; and to explore the relationship between FS

sensitivity and PF. As it was demonstrated in Chapter 4 that slope cases with different combinations of HB parameters can have the same FS but different FS sensitivity, Chapter 5 was based on this conclusion. The sequences of the study in this chapter are as follows. Firstly, a parametric study was carried out to investigate the influence of changes in the variability of HB parameters on PF and to define the relationship between FS sensitivity and PF. In this parametric study, all three HB parameters were modelled as random variables and their COV were assumed to be equal and vary uniformly from 0.1 to 1. Secondly, a parametric study was carried out to compare the contributions of the variability of HB parameters to PF. In this parametric study, HB parameters were modelled as random variables separately and the COV of each HB parameter again varied uniformly from 0.1 to 1. Afterwards, to be consistent with engineering practice, a section was devoted to a case study of simplified probabilistic analyses with the COV of HB parameters set to their upper limit values observed in practice (Section 3.3.2.1). The Spearman correlation coefficients r_s between GSI, m_i, σ_{ci}, and FS were also computed as another approach to evaluate the relative contributions of the variability of HB parameters to PF. Lastly, a final parametric study was carried out to investigate the influence of the spatial variability of HB parameters on PF. In this parametric study, the scale of fluctuation θ of the corresponding HB parameters (m_i and σ_{ci}) varied from a small value to infinity. In summary, Chapter 5 leads to the following observations:

1. FS sensitivity has a significant impact on slope stability and probabilistic analysis is capable of evaluating such impact. For slope cases with different combinations of input HB parameters, even if their FS and the COV of input are identical, their PF can be quite different. A slope of high FS sensitivity has a high PF value, indicating a high risk.

2. PF of a slope increases as the COV of input HB parameters increase.

3. When the COV of GSI, m_i, and σ_{ci} are identical, the comparison of contributions to PF can be expressed as: GSI (variability) > σ_{ci} (variability) >> m_i (variability).

4. When the COV of GSI, m_i, and σ_{ci} are set to the upper limit values observed in engineering practice (0.15, 0.2, and 0.4 respectively), relative contributions to PF can be expressed as: σ_{ci} (variability) > GSI (variability) >> m_i (variability). The contributions were examined by two approaches in Sections 5.2.2 and 5.2.3 respectively, where slightly contradictory conclusions were found and it was inferred that the Spearman correlation coefficient may not always be a reliable predictor of the contribution of an input variable to the output.

5. For a slope with FS > 1, the PF increases as the scale of fluctuation θ (of m_i and σ_{ci}) increases. When θ tends to infinity, PF from the spatial probabilistic analyses become identical to those from the simplified probabilistic analyses.

6. PF is most sensitive to the change in the scale of fluctuation θ (of m_i and σ_{ci}) within the range of 0 – 500m.

7. Larger θ makes the effect of FS sensitivity on slope stability more significant, i.e. the differences of PF between slopes of different FS sensitivity increase as θ increases.

6.2 Recommendations for Further Research

In Chapter 4, a large amount of data between HB parameters and FS were fitted with a polynomial equation for the purpose of sensitivity analysis. The polynomial equation was

adopted since it is relatively straightforward to differentiate and allows a ready identification of self and mutual influences. The validation showed that the fitted equation can reproduce the relationship between HB parameters and FS with moderate accuracy, and that it is able to characterise the overall trends. It is possible that with a more advanced technique, such as artificial neural network, the relationship between HB parameters and FS could be more accurately represented by a function and this would provide a useful tool for the efficient assessment of rock slope stability.

In Chapter 5, both a parametric study and the Spearman correlation coefficient were applied to study the contributions of the variability of HB parameters to PF. The outcomes from these two methods did not support each other completely. The contradiction suggests that the Spearman correlation coefficient may not always be a reliable measurement of the contribution of an input variable to the output and this is a topic that is worth additional investigation.

In Chapter 5, m_i and σ_{ci} were modelled as spatial variables by random fields in the spatial probabilistic analysis. The scale of fluctuation θ of m_i and σ_{ci} was assumed to vary from very small to infinity in a parametric study. It was demonstrated that the spatial variability of HB parameters has significant influences on slope stability, and it would be worthwhile to investigate the actual spatial variability of m_i and σ_{ci} by random field theory or geostatistics.

Lastly, since this study has focused on rock slope stability, the output has been restricted to FS and PF. On the other hand, since the HB strength criterion is formulated to estimate the strength parameters of a rock mass, including Young's modulus E, cohesion, and angle of friction, the methodology of the current study can also be applied to investigate relationship between HB parameters and these strength parameters.

6.3 Conclusions

The following conclusions are derived from the present study.

1. For a highly fractured rock slope, the sensitivity of FS to the changes in input HB parameters (FS sensitivity) cannot be revealed by deterministic analyses unless sensitivity analyses are applied. Slope cases with the same geometry and the same FS (but different combinations of HB parameters) have different FS sensitivity. GSI is the most critical parameter in this respect. With increasing GSI, the stability (measured by FS) of a slope becomes more sensitive to the change in GSI itself and that in σ_{ci}.

2. FS sensitivity has a significant impact on slope stability and probabilistic analysis is capable of evaluating such impact. For slope cases with different combinations of input HB parameters, even if their FS and the variability of input (quantified by the COV) are identical, their PF can be quite different. A slope of high FS sensitivity has a high PF value, indicating a high risk.

3. It was found that when the variability of GSI, m_i, and σ_{ci} is identical, the order of contributions to PF can be expressed as GSI (variability) > σ_{ci} (variability) >> m_i (variability); however, when the variability of GSI, m_i, and σ_{ci} is set to their upper-limit values observed in practice, the order of contributions to PF becomes σ_{ci} (variability) > GSI (variability) >> m_i (variability).

4. Spatial variability of HB parameters (for m_i and σ_{ci}) has significant influences on slope stability (measured by PF). It was shown that for a slope with FS > 1, the PF of this slope increases as the scale of fluctuation θ of m_i and σ_{ci} increases and it is most sensitive to the change in θ within the range of 0 – 500m. When θ tends to

infinity, PF from the spatial probabilistic analyses become identical to those from the simplified probabilistic analyses. In addition, larger θ makes the effect of FS sensitivity on slope stability more significant, i.e. the differences of PF between cases of different FS sensitivity increase as θ increases.

REFERENCES

Babu, G., and Mukesh, M. 2004. Effect of soil variability on reliability of soil slopes. Geotechnique, 54(5): 335-337.

Baecher, G., and Christian, J. 2003. Reliability and statistics in geotechnical engineering. John Wiley & Sons, Inc.

Baker, R. 1980. Determination of the critical slip surface in slope stability computations. International Journal for Numerical and Analytical Methods in Geomechanics, 4(4): 333-359.

Balmer, G. 1952. A general analytical solution for Mohr's envelope. Am. Soc. Test. Mat, 52: 1260-1271.

Bishop, A. 1955. The use of the slip circle in the stability analysis of slopes. Géotechnique 5: 7-17.

Boutrup, E., and Lovell, C. 1980. Searching techniques in slope stability analysis. Engineering Geology, 16(1–2): 51-61.

Cai, M. 2011. Rock mass characterization and rock property variability considerations for tunnel and cavern design. Rock Mechanics and Rock Engineering, 44(4): 379-399.

Cai, M., Kaiser, P., Tasaka, Y., and Minami, M. 2007. Determination of residual strength parameters of jointed rock masses using the GSI system. International Journal of Rock Mechanics and Mining Sciences, 44(2): 247-265.

Cai, M., Kaiser, P., Uno, H., Tasaka, Y., and Minami, M. 2004. Estimation of rock mass deformation modulus and strength of jointed hard rock masses using the GSI system. International Journal of Rock Mechanics and Mining Sciences, 41(1): 3-19.

Carranza-Torres, C. Some comments on the application of the Hoek-Brown failure criterion for intact rock and rock masses to the solution of tunnel and slope problems. *In* MIR 2004–X Conference on Rock and Engineering Mechanics, Torino, Italy2004, pp. 285-326.

Chen, Z. Recent developments in slope stability analysis. *In* 8th ISRM Congress, Tokyo, Japan1995.

Chen, Z. 2004. A generalized solution for tetrahedral rock wedge stability analysis. International Journal of Rock Mechanics and Mining Sciences, 41(4): 613-628.

Cho, S. 2007. Effects of spatial variability of soil properties on slope stability. Engineering Geology, 92(3-4): 97-109.

Cho, S. 2010. Probabilistic assessment of slope stability that considers the spatial variability of soil properties. Journal of Geotechnical and Geoenvironmental Engineering, 136(7): 975-984.

Chowdhury, R., and Xu, D. 1992. Reliability index for slope stability assessment—two methods compared. Reliability Engineering and System Safety, 37(2): 99-108.

Chowdhury, R., and Xu, D. 1995. Geotechnical system reliability of slopes. Reliability Engineering and System Safety, 47(3): 141-151.

Christian, J. 2004. Geotechnical engineering reliability: How well do we know what we are doing? Journal of Geotechnical and Geoenvironmental Engineering, 130(10): 985-1003.

Christian, J., and Baecher, G. 1999. Point-estimate method as numerical quadrature. Journal of Geotechnical and Geoenvironmental Engineering, 125(9): 779.

Christian, J., Ladd, C., and Baecher, G. 1994. Reliability applied to slope stability analysis. Journal of Geotechnical Engineering, 120(12): 2180-2207.

Constantine, P. 2010. Random field simulation. http://www.mathworks.com.

Davis, M. 1987. Production of conditional simulations via the LU triangular decomposition of the covariance matrix. Mathematical Geology, 19(2): 91-98.

Dowd, P. 2006. Introduction to geostatistics. The University of Adelaide, Adelaide, Australia, p. 210.

Dowd, P., Xu, C., Mardia, K., and Fowell, R. 2007. A comparison of methods for the stochastic simulation of rock fractures. Mathematical Geology, 39(7): 697-714.

Duncan, J. 2000. Factors of safety and reliability in geotechnical engineering. Journal of Geotechnical and Geoenvironmental Engineering, 126(4): 307-316.

Duncan, J., and Wright, S. 2005. Soil strength and slope stability. John Wiley & Sons, Inc.

Duzgun, H., and Bhasin, R. 2009. Probabilistic stability evaluation of Oppstadhornet rock slope, Norway. Rock Mechanics and Rock Engineering, 42(5): 729-749.

Duzgun, H., Yucemen, M., and Karpuz, C. 2003. A methodology for reliability-based design of rock slopes. Rock Mechanics and Rock Engineering, 36(2): 95-120.

El-Ramly, H., Morgenstern, N., and Cruden, D. 2002. Probabilistic slope stability analysis for practice. Canadian Geotechnical Journal, 39(3): 665-683.

El-Ramly, H., Morgenstern, N., and Cruden, D. 2003. Probabilistic stability analysis of a tailings dyke on presheared clay-shale. Canadian Geotechnical Journal, 40(1): 192-208.

El-Ramly, H., Morgenstern, N., and Cruden, D. 2005. Probabilistic assessment of stability of a cut slope in residual soil. Géotechnique, 55(1): 77-84.

El-Ramly, H., Morgenstern, N., and Cruden, D. 2006. Lodalen slide: a probabilistic assessment. Canadian Geotechnical Journal, 43(9): 956-968.

Fenton, G., and Griffiths, D. 2008. Risk assessment in geotechnical engineering. John Wiley & Sons, Inc.

Fisher, B., and Eberhardt, E. 2012. Assessment of parameter uncertainty associated with dip slope stability analyses as a means to improve site investigations. Journal of Geotechnical and Geoenvironmental Engineering, 138(2): 166-173.

Fredlund, D., and Krahn, J. 1977. Comparison of slope stability methods of analysis. Canadian Geotechnical Journal, 14(3): 429-439.

Frohlich, O. The factor of safety with respect to sliding of a mass of soil along the arc of a logarithmic spiral. *In* 3rd International Conference on Soil Mechanics and Foundation Engineering, Switzerland1953, pp. 230-233.

Fu, W., Liao, Y., and He, P. Reliability assessment of Hoek-Brown rock mass stability. *In* 43rd U.S. Rock Mechanics Symposium and 4th U.S.-Canada Rock Mechanics Symposium, Asheville2009.

Grenon, M., and Hadjigeorgiou, J. 2008. A design methodology for rock slopes susceptible to wedge failure using fracture system modelling. Engineering Geology, 96(1-2): 78-93.

Griffiths, D., and Fenton, G. 2004. Probabilistic slope stability analysis by finite elements. Journal of Geotechnical and Geoenvironmental Engineering, 130(5): 507-518.

Griffiths, D., Huang, J., and Fenton, G. 2009. Influence of spatial variability on slope reliability using 2-D random fields. Journal of Geotechnical and Geoenvironmental Engineering, 135(10): 1367-1378.

Hasofer, A., and Lind, N. 1974. Exact and invariant second-moment code format. Journal of the Engineering Mechanics Division, 100(1): 111-121.

Hassan, A., and Wolff, T. 1999. Search algorithm for minimum reliability index of earth slopes. Journal of Geotechnical and Geoenvironmental Engineering, 125(4): 301-308.

Hoek, E. 1983. Strength of jointed rock masses. Géotechnique, 33(3): 187-222.

Hoek, E. 1998. Reliability of Hoek-Brown estimates of rock mass properties and their impact on design. International Journal of Rock Mechanics and Mining Sciences, 35(1): 63-68.

Hoek, E. 2007. Practical rock engineering. http://www.rocscience.com.

Hoek, E. Fundamentals of slope design. *In* Slope Stability 2009, Santiago, Chile2009.

Hoek, E., and Brown, E. 1980. Underground excavations in rock. Institution of Mining and Metallurgy, London.

Hoek, E., and Brown, E. 1997. Practical estimates of rock mass strength. International Journal of Rock Mechanics and Mining Sciences, 34(8): 1165-1186.

Hoek, E., and Marinos, P. 2007. A brief history of the development of the Hoek-Brown failure criterion. Soils and Rocks, 30(2): 85-92.

Hoek, E., Kaiser, P., and Bawden, W. 1995. Support of underground excavations in hard rock. Balkema, Rotterdam.

Hoek, E., Carranza-Torres, C., and Corkum, B. Hoek-Brown failure criterion-2002 edition. *In* 5th North American Rock Mechanics Symposium and 17th Tunneling Association of Canada Conference: NARMS-TAC2002, pp. 267-271.

Hong, H., and Roh, G. 2008. Reliability evaluation of earth slopes. Journal of Geotechnical and Geoenvironmental Engineering, 134(12): 1700-1705.

Hormazabal, E., Rovira, F., Walker, M., and Carranza-Torres, C. 2009. Analysis and design of slopes for Rajo Sur, an open pit mine next to the subsidence crater of El Teniente mine in Chile, http://www.srk.co.za.

Hsu, S., and Nelson, P. 2006. Material spatial variability and slope stability for weak rock masses. Journal of Geotechnical and Geoenvironmental Engineering, 132(2): 183-193.

Hudson, J., and Harrison, J. 2000. Engineering rock mechanics. Pergamon.

Idris, M., Saiang, D., and Nordlund, E. Numerical analyses of the effects of rock mass property variability on open stope stability. *In* 45th US Rock Mechanics/Geomechanics Symposium, San Francisco, California2011.

Jaksa, M. 1995. The influence of spatial variability on the geotechnical design properties of a stiff, overconsolidated clay. Ph.D. Thesis, The University of Adelaide, Adelaide, Australia.

Jaksa, M., Goldsworthy, J., Fenton, G., Kaggwa, W., Griffiths, D., Kuo, Y., and Poulos, H. 2005. Towards reliable and effective site investigations. Géotechnique, 55(2): 109-122.

Jing, L. 2003. A review of techniques, advances and outstanding issues in numerical modelling for rock mechanics and rock engineering. International Journal of Rock Mechanics and Mining Sciences, 40(3): 283-353.

Jing, L., and Hudson, J. 2002. Numerical methods in rock mechanics. International Journal of Rock Mechanics and Mining Sciences, 39(4): 409-427.

Journel, A., and Huijbregts, C. 1978. Mining geostatistics. Academic Press, London.

Kumar, P. 1998. Shear failure envelope of Hoek-Brown criterion for rockmass. Tunnelling and underground space technology, 13(4): 453-458.

Li, A., Merifield, R., and Lyamin, A. 2008. Stability charts for rock slopes based on the Hoek-Brown failure criterion. International Journal of Rock Mechanics and Mining Sciences, 45(5): 689-700.

Li, A., Merifield, R., and Lyamin, A. 2011. Effect of rock mass disturbance on the stability of rock slopes using the Hoek–Brown failure criterion. Computers and Geotechnics, 38(4): 546-558.

Li, K., and Lumb, P. 1987. Probabilistic design of slopes. Canadian Geotechnical Journal, 24(4): 520–535.

Low, B. Practical probabilistic slope stability analysis. *In* 12th Panamerican Conference on Soil Mechanics and Geotechnical Engineering and 39th U.S. Rock Mechanics Symposium, M.I.T., Cambridge, Massachusetts2003, pp. 2777–2784.

Low, B. 2007. Reliability analysis of rock slopes involving correlated nonnormals. International Journal of Rock Mechanics and Mining Sciences, 44(6): 922-935.

Low, B. 2008. Efficient probabilistic algorithm illustrated for a rock slope. Rock Mechanics and Rock Engineering, 41(5): 715-734.

Low, B., and Einstein, H. Simplified reliability analysis for wedge mechanisms in rock slopes. *In* Sixth International Symposium on Landslides, New Zealand1992, pp. 499-507.

Low, B., and Tang, W. 1997a. Probabilistic slope analysis using Janbu's generalized procedure of slices. Computers and Geotechnics, 21(2): 121-142.

Low, B., and Tang, W. 1997b. Efficient reliability evaluation using spreadsheet. Journal of Engineering Mechanics, 123(7): 749-752.

Lü, Q., and Low, B. 2011. Probabilistic analysis of underground rock excavations using response surface method and SORM. Computers and Geotechnics, 38(8): 1008-1021.

Mao, N., Al-Bittar, T., and Soubra, A. 2012. Probabilistic analysis and design of strip foundations resting on rocks obeying Hoek–Brown failure criterion. International Journal of Rock Mechanics and Mining Sciences, 49(0): 45-58.

Marinos, P., and Hoek, E. GSI: a geologically friendly tool for rock mass strength estimation. *In* GeoEng2000: An International Conference on Geotechnical & Geological Engineering, Melbourne, Australia2000, pp. 1422-1442.

Marinos, V., Marinos, P., and Hoek, E. 2005. The geological strength index: applications and limitations. Bulletin of Engineering Geology and the Environment, 64(1): 55-65.

Mostyn, G., and Douglas, K. Shear strength of intact rock and rock masses. *In* GeoEng2000: An International Conference on Geotechnical & Geological Engineering, Melbourne, Australia2000, pp. 1389-1421.

Pantelidis, L. 2009. Rock slope stability assessment through rock mass classification systems. International Journal of Rock Mechanics and Mining Sciences, 46(2): 315-325.

Park, H., and West, T. 2001. Development of a probabilistic approach for rock wedge failure. Engineering Geology, 59(3-4): 233-251.

Park, H., West, T., and Woo, I. 2005. Probabilistic analysis of rock slope stability and random properties of discontinuity parameters, Interstate Highway 40, Western North Carolina, USA. Engineering Geology, 79: 230-250.

Park, H., Um, J., Woo, I., and Kim, J. 2011. The evaluation of the probability of rock wedge failure using the point estimate method. Environmental Earth Sciences: 1-9.

Phoon, K., and Kulhawy, F. 1999. Characterization of geotechnical variability. Canadian Geotechnical Journal, 36(4): 612-624.

Priest, S. 2005. Determination of shear strength and three-dimensional yield strength for the Hoek-Brown criterion. Rock Mechanics and Rock Engineering, 38(4): 299-327.

Priest, S., and Brown, E. 1983. Probabilistic stability analysis of variable rock slopes. Trans. Instn. Min. Metall 92: A1-A12.

Read, J., and Stacey, P. 2009. Guidelines for open pit slope design. CSIRO.

Richards, L., and Read, S. A comparison of methods for determining m_i, the Hoek-Brown parameter for intact rock material. *In* 45th U.S. Rock Mechanics/Geomechanics Symposium, San Francisco, California2011.

Rocscience 2011. Slide6.0. http://www.rocscience.com.

Rosenblueth, E. 1975. Point estimates for probability moments. Proceedings of the National Academy of Sciences, 72(10): 3812-3814.

Rosenblueth, E. 1981. Two point estimates in probabilities. Applied Mathematical Modelling, 5(5): 329-335.

Ruffolo, R., and Shakoor, A. 2009. Variability of unconfined compressive strength in relation to number of test samples. Engineering Geology, 108(1-2): 16-23.

Sari, M., Karpuz, C., and Ayday, C. 2010. Estimating rock mass properties using Monte Carlo simulation: Ankara andesites. Computers & Geosciences, 36(7): 959-969.

Shen, J., Karakus, M., and Xu, C. 2012. Direct expressions for linearization of shear strength envelopes given by the Generalized Hoek–Brown criterion using genetic programming. Computers and Geotechnics, 44: 139-146.

Sjöberg, J. 1997. Estimating rock mass strength using the Hoek–Brown failure criterion and rock mass classification—a review and application to the Aznalcollar open pit, Division of Rock Mechanics, Department of Civil and Mining Engineering, Lulea University of Technology.

Sonmez, H., and Ulusay, R. 1999. Modifications to the geological strength index (GSI) and their applicability to stability of slopes. International Journal of Rock Mechanics and Mining Sciences, 36(6): 743-760.

Suchomel, R., and Mašín, D. 2010. Comparison of different probabilistic methods for predicting stability of a slope in spatially variable c-φ soil. Computers and Geotechnics, 37(1-2): 132-140.

Turnbull, W., and Hvorslev, M. 1967. Special problems in slope stability. Journal of Soil Mechanics & Foundations Div.

Vanmarcke, E. 1983. Random fields: analysis and synthesis. The MIT Press.

Wang, J., Tan, W., Feng, S., and Zhou, R. 2000. Reliability analysis of an open pit coal mine slope. International Journal of Rock Mechanics and Mining Sciences, 37(4): 715-721.

Wang, Y., Cao, Z., and Au, S. 2010. Efficient Monte Carlo Simulation of parameter sensitivity in probabilistic slope stability analysis. Computers and Geotechnics, 37(7-8): 1015-1022.

Wang, Y., Cao, Z., and Au, S. 2011. Practical reliability analysis of slope stability by advanced Monte Carlo simulations in a spreadsheet. Canadian Geotechnical Journal, 48: 162-172.

Webster, R., and Oliver, M. 2007. Geostatistics for environmental scientists. John Wiley & Sons, Inc.

Whitman, R. 1984. Evaluating calculated risk in geotechnical engineering. Journal of Geotechnical Engineering, 110(2): 143-188.

Wright, S., Kulhawy, F., and Duncan, J. 1973. Accuracy of equilibrium slope stability analysis. Journal of the Soil Mechanics and Foundations Division, 99(10): 783-791.

Wyllie, D., and Mah, C. 2004. Rock slope engineering: civil and mining. Taylor & Francis.

Xu, C., and Dowd, P. 2005. Geostatistics for Windows – the complete mineral resource evaluation package for the mining industry.

Xu, C., and Dowd, P. 2010. A new computer code for discrete fracture network modelling. Computers & Geosciences, 36(3): 292-301.

APPENDIX A

MATLAB CODES OF MODELS DEVELOPED FOR THE PROBABILISTIC ANALYSIS

A.1 Introduction

The probabilistic analysis (Chapter 5) has been carried out based on models developed in *Matlab*. In this appendix, codes of the LEM model (for the probabilistic analysis), the simplified probabilistic analysis model, and the spatial probabilistic analysis model are provided.

Nine *Matlab* codes are given in total, including *QMslope_geometry*, *QMslope_bishop*, *QMslope_HBprobabilistic*, *QMslope_HBspatial*, *QMslope_FSdistribution*, *cphi_bray*, *cphi_kumar*, *cphi_hoek2002*, and *cphi_shen*. Specifications of these codes, including their functions, input, and output, are firstly specified in Tables A.1, A.2, and A.3. Afterwards, the codes are provided in Section A.2.

Table A.1 Codes of models developed for the probabilistic analysis: functions

Code	Function
QMslope_geometry	computing the geometry of slices and the forces acting on them for the limit equilibrium analysis
QMslope_bishop	implementing limit equilibrium analysis for a slope based on Bishop's method of slices (output from *QMslope_geometry* is used in this code)
QMslope_HBprobabilistic	implementing simplified probabilistic analysis for a slope (*QMslope_bishop* is called in this code)
QMslope_HBspatial	implementing spatial probabilistic analysis for a slope (*QMslope_bishop* and the *Constantine random field generator* are called in this code)
QMslope_FSdistribution	plotting the distribution and statistical properties of FS; plotting the convergence of PF (output from either *QMslope_HBprobabilistic* or *QMslope_FSdistribution* is used in this code)
cphi_bray *cphi_kumar* *cphi_hoek2002* *cphi_shen*	converting HB parameters to equivalent MC parameters by Bray's, Kumar's, Hoek's or Shen's solution

Table A.2 Codes of models developed for the probabilistic analysis: input specifications

Code	Input	Specifications
QMslope_geometry	phi_face/H_slope	slope face angle/slope height
	nrslice	number of slices
	X/Y/R/ LX/LY/RX/RY	centre and right and left boundaries of the slip surface (found by *Slide6.0*)
	plot_geometry	specify whether to plot the slope geometry (Y or N)
QMslope_bishop	geometry	the *geometry* output from *QMslope_geometry*
	force	the *force* output from *QMslope_geometry*
	cohesion/friction	cohesion and angle of friction of the material

Table A.2 *Continued*

Code	Input	Specifications
QMslope_HBprobabilistic	phi_face/H_slope	slope face angle/slope height
	nrslice	number of slices
	slipcircle	centre and right and left boundaries of the slip surface (found by *Slide6.0*)
	HB_mean	mean values of HB parameters (GSI, m_i and σ_{ci})
	HB_COV	COV of HB parameters
	HB_truncation	truncations of HB parameters
	D	disturbance factor
	N	number of iterations
QMslope_HBspatial	phi_face/H_slope	slope face angle/slope height
	nrslice	number of slices
	slipcircle	centre and right and left boundaries of the slip surface (found by *Slide6.0*)
	HB_mean	mean values of HB parameters (GSI, m_i, σ_{ci})
	HB_COV	COV of HB parameters
	SOF	scale of fluctuation θ
	HB_truncation	truncations of HB parameters
	D	disturbance factor
	N	number of iterations
QMslope_FSdistribution	phi_face/H_slope	slope face angle/slope height
	GSI/mi/UCS	HB parameters
	cov_GSI/cov_mi/ cov_UCS	COV of HB parameters
	distribution	best fit distribution for FS
	POF	specify whether the PF is obtained from simulation or estimation
	type	specify whether it is a simplified probabilistic analysis or a spatial probabilistic analysis
	CL	scale of fluctuation θ
cphi_bray *cphi_kumar* *cphi_hoek2002* *cphi_shen*	GSI/mi/sigci/D	HB parameters
	sign	effective normal stress

Table A.3 Codes of models developed for the probabilistic analysis: output specifications

Code	Output	Specifications
QMslope_geometry	geometry	specific geometry of slices
	force	forces acting on slices
QMslope_bishop	FS	Factor of Safety
QMslope_HBprobabilistic	PF_final	Probability of Failure
	xxx.mat	a file that contains all output from the Monte Carlo simulation
QMslope_HBspatial	PF_final	Probability of Failure
	xxx.mat	a file that contains all output from the Monte Carlo simulation
QMslope_FSdistribution	xxx.fig	a figure that presents the distribution and statistical properties of FS
	xxx.fig	a figure that plots the convergence of PF
cphi_bray *cphi_kumar* *cphi_hoek2002* *cphi_shen*	c_i	cohesion
	phi_i	angle of friction
	chpi_method	name of the conversion method

A.2 Codes

A.2.1 QMslope_geometry

```
% ---------------------------------------------------------------------
function [geometry,force] =
QMslope_geometry(phi_face,H_slope,nrslice,X,Y,R,LX,LY,RX,RY,plot_geometry)

% this file is universal
% it calculates the geometry and basic forces for a given slope

% hand input part
% ---------------------------------------------------------------------
% ---------------------------------------------------------------------
% coordinate and radius of the slip circle (hand input)
center=[X,Y];

% left and right boundary of the slip circle (hand input)
P1_slip=[LX, LY]; P2_slip=[RX, RY];

% parameters for material
```

```
r_rock=27;  % KN
r_water=9.81;  % KN
% ------------------------------------------------------------------------
% ------------------------------------------------------------------------

% automatic calculation part
% ------------------------------------------------------------------------
% ------------------------------------------------------------------------

% generate slope, slip surface, water table boundary info.
% ------------------------------------------------------------------------
% boundary coordinates for the slope (H/automatic -- as long as
P1,P2,P5,P6 fixed)
P1_slope=[0 -60]; P2_slope=[300 -60]; P3_slope=[300 H_slope];
P4_slope=[100+H_slope/tand(phi_face) H_slope]; P5_slope=[100 0];
P6_slope=[0 0];

% boundary coordinates for the water (H/automatic -- as long as relative
distance between water table and slope fixed)
P1_water=P5_slope; P2_water=[P4_slope(1)+10 P4_slope(2)-10];
P3_water=[P3_slope(1) P3_slope(2)-10];
phi_water=atand((P2_water(2)-P1_water(2))/(P2_water(1)-P1_water(1)));
H_water=P2_water(2)-P1_water(2);

%dip of the water surface, degrees (automatic)
phi_water=atand((P2_water(2)-P1_water(2))/(P2_water(1)-P1_water(1)));

% Slice width, m; number of slices between toe and crest (automatic)
deta_x=(P2_slip(1)-P1_slip(1))/nrslice;
nrslices_tc=round((P4_slope(1)-P5_slope(1 ))/deta_x);

%info. for slide (for check)
P_center=[X,Y,R]; P_slip=[P1_slip;P2_slip];
P_slope=[P1_slope;P2_slope;P3_slope;P4_slope;P5_slope;P6_slope];
P_water=[P1_water;P2_water;P3_water]; nrslice; deta_x;
% ------------------------------------------------------------------------

% X coordinates for slices
% ------------------------------------------------------------------------
i=1:nrslice; % the serial number for each slice
xl_slices=zeros(nrslice,1); xr_slices=zeros(nrslice,1);
x_slices=zeros(nrslice,1); % pre-allocating memory
xl_slices(i)=P1_slip(1)+(i-1)*deta_x;  xr_slices(i)=
P1_slip(1)+i*deta_x; %X Coordinate of the left and right of the slices
x_slices(i)=(xl_slices(i)+xr_slices(i))/2; %X Coordinate of the slice
% ------------------------------------------------------------------------

%Y coordinates of slices and base angles for slices
% ------------------------------------------------------------------------
y2l_slices= - sqrt(R^2-(xl_slices - X).^2) + Y; y2r_slices= - sqrt(R^2-
(xr_slices - X).^2) + Y; %bottom coordinates of the left and right of the
slices

y1l_slices=(xl_slices-P5_slope(1)).*tand(phi_face);
y1l_slices(y1l_slices>H_slope)=H_slope; %top coordinates of the left of
slices
y1r_slices=(xr_slices-P5_slope(1)).*tand(phi_face);
y1r_slices(y1r_slices>H_slope)=H_slope; %top coordinates of the right of
slices
```

```
y1_slices=(y1l_slices+y1r_slices)/2; %top coordinates of the middle of
the slices
y2_slices=(y2l_slices+y2r_slices)/2; %bottom coordinates of the middle of
slices
h_slice=y1_slices-y2_slices;  %height of slices

phi_base=atand((y2r_slices-y2l_slices)/deta_x); %base angle of each
slices
% ------------------------------------------------------------------------

% in this step, the height of water table are calculated
% ------------------------------------------------------------------------
y1l_water=(xl_slices-P5_slope(1)).*tand(phi_water);
y1l_water(y1l_water>H_water)=H_water; %top coordinates of the left of
water
y1r_water=(xr_slices-P5_slope(1)).*tand(phi_water);
y1r_water(y1r_water>H_water)=H_water; %top coordinates of the right of
water

y1_water=(y1l_water+y1r_water)/2; %top coordinates of the middle of water
y2_water=y2_slices; %bottom coordinates of the water
h_water=y1_water-y2_water; h_water(h_water<0)=0; %height of water table
% ------------------------------------------------------------------------

% calculate effective normal stress by Fellenius solution
% ------------------------------------------------------------------------
w_slice=r_rock.*h_slice.*deta_x;
u_water=r_water.*h_water;

sig_f=(w_slice/deta_x-u_water).*(cosd(phi_base)).^2; %input effective
normal stress
sig_f(sig_f<0)=0;
% ------------------------------------------------------------------------

% write output information "geometry" and "forces"
% ------------------------------------------------------------------------
geometry.nrslice=nrslice;
geometry.detax=deta_x;
geometry.phibase=phi_base;
geometry.hslice=h_slice;
geometry.hwater=h_water;

force.wslice=w_slice;
force.uwater=u_water;
force.sign=sig_f;
% ------------------------------------------------------------------------

% plot slope, slip surface, water table boundary and slices
% ------------------------------------------------------------------------
if plot_geometry=='y'

    % generate points for the slip surface (automatic)
    fun1_slip=linspace(P1_slip(1),P2_slip(1),50); fun2_slip=-sqrt(R^2-
(fun1_slip-X).^2)+Y;
    figure,hold on, grid on
    % plot the slope geometry
    plot([P1_slope(1),P2_slope(1)],[P1_slope(2),P2_slope(2)]),
plot([P2_slope(1),P3_slope(1)],[P2_slope(2),P3_slope(2)]),plot([P3_slope(
```

```
1),P4_slope(1)],[P3_slope(2),P4_slope(2)]),plot([P4_slope(1),P5_slope(1)]
,[P4_slope(2),P5_slope(2)]),
plot([P5_slope(1),P6_slope(1)],[P5_slope(2),P6_slope(2)])
    % plot the water table

plot([P1_water(1),P2_water(1)],[P1_water(2),P2_water(2)]),plot([P2_water(
1),P3_water(1)],[P2_water(2),P3_water(2)])
    % plot the slip surface
    plot([X,P1_slip(1)],[Y,P1_slip(2)]),
plot([X,P2_slip(1)],[Y,P2_slip(2)]), plot(fun1_slip,fun2_slip)

    % plot the slices
    for i=1:nrslice

plot([xl_slices(i),xl_slices(i)],[y1l_slices(i),y2l_slices(i)],'r')
    end

    title_name=sprintf('Slope Geometry: \\beta=%.0f, H=%.0f',
phi_face,H_slope);  % in sprintf, \\ to creat \
    title(title_name), axis equal

elseif plot_geometry == 'n'
else
    error('Please specify whether slope geometry shall be plotted')
end
% --------------------------------------------------------------------
```

A.2.2 QMslope_bishop

```
% --------------------------------------------------------------------
function FS=QMslope_bishop(geometry,force,cohesion,friction)

deta_x=geometry.detax;
phi_base=geometry.phibase;

w_slice=force.wslice;
u_water=force.uwater;


% first input FS
% --------------------------------------------------------------------
FS_input=1;
% --------------------------------------------------------------------

% interative process for calculating FS
% --------------------------------------------------------------------
% --------------------------------------------------------------------
FS_output=sum((cohesion.*deta_x+(w_slice-
u_water.*deta_x).*tand(friction))./(cosd(phi_base)+sind(phi_base).*tand(f
riction)/FS_input))./sum(w_slice.*sind(phi_base));

while abs(FS_input-FS_output)>0.001
FS_input=FS_output;
```

```
FS_output=sum((cohesion.*deta_x+(w_slice-
u_water.*deta_x).*tand(friction))./(cosd(phi_base)+sind(phi_base).*tand(f
riction)/FS_input))./sum(w_slice.*sind(phi_base));

end
% --------------------------------------------------------------------
% --------------------------------------------------------------------

FS=FS_output;
% --------------------------------------------------------------------
```

A.2.3 QMslope_HBprobabilistic

```
% --------------------------------------------------------------------
function [PF_final] = QMslope_HBprobabilistic(phi_face, H_slope, nrslice,
slipcircle, HB_mean, D, HB_COV, HB_truncation, N)

% HB_mean: 1*3 matrix
% HB_COV: 1*3 matrix
% HB_truncation: 3*2 matrix
% the input for UCS should be kpa

% slip circle
% --------------------------------------------------------------------
X = slipcircle(1);
Y = slipcircle(2);
R = slipcircle(3);
LX = slipcircle(4);
LY = slipcircle(5);
RX = slipcircle(6);
RY = slipcircle(7);
% --------------------------------------------------------------------

% obtain the mean value of HB parameters
% --------------------------------------------------------------------
mean_GSI = HB_mean(1);
mean_mi = HB_mean(2);
mean_UCS = HB_mean(3);
mu = HB_mean;
% --------------------------------------------------------------------

% geometry and deterministic FS
% --------------------------------------------------------------------
[geometry,force]=QMslope_geometry(phi_face,H_slope,nrslice,X,Y,R,LX,LY,RX
,RY,'n');
[cohesion_dm,friction_dm]=cphi_kumar(mean_GSI,mean_mi,mean_UCS,D,force.si
gn);

FS_dm=QMslope_bishop(geometry,force,cohesion_dm,friction_dm)
% --------------------------------------------------------------------

% obtain the COV and SD of HB parameters
% --------------------------------------------------------------------
COV_GSI = HB_COV(1);
COV_mi = HB_COV(2);
COV_UCS = HB_COV(3);
```

```
SD_GSI = COV_GSI* mean_GSI;
SD_mi = COV_mi* mean_mi;
SD_UCS = COV_UCS* mean_UCS;

var = [SD_GSI^2 0 0;
       0 SD_mi^2 0;
       0 0 SD_UCS^2];
% -------------------------------------------------------------------------

% obtain the truncation of HB parameters
% -------------------------------------------------------------------------
Truncation_GSI = HB_truncation(1,:);
Truncation_mi = HB_truncation(2,:);
Truncation_UCS = HB_truncation(3,:);
% -------------------------------------------------------------------------

% generating HB random numbers
% -------------------------------------------------------------------------
random_sample=lhsnorm(mu,var,N);

GSI=random_sample(:,1);
mi=random_sample(:,2);
UCS=random_sample(:,3);
% -------------------------------------------------------------------------

% truncating HB random numbers
% -------------------------------------------------------------------------
GSI(GSI<Truncation_GSI(1))=Truncation_GSI(1);
GSI(GSI>Truncation_GSI(2))=Truncation_GSI(2);

mi(mi<Truncation_mi(1))=Truncation_mi(1);
mi(mi>Truncation_mi(2))=Truncation_mi(2);

UCS(UCS<Truncation_UCS(1))=Truncation_UCS(1);
UCS(UCS>Truncation_UCS(2))=Truncation_UCS(2);
% -------------------------------------------------------------------------

% probabilistic analysis
% -------------------------------------------------------------------------
rand('twister',5489);randn('state',0);

FS=repmat(1000,N,1);
PF=repmat(1000,N,1);

cohesion=repmat(-1,nrslice, N);
friction=repmat(-1,nrslice, N);

for i=1:N

[cohesion(:,i),friction(:,i)]=cphi_kumar(GSI(i),mi(i),UCS(i),D,force.sign
);

    FS(i)=QMslope_bishop(geometry,force,cohesion(:,i),friction(:,i));
```

```
If
i==N/10||i==2*N/10||i==3*N/10||i==4*N/10||i==5*N/10||i==6*N/10||i==7*N/10
||i==8*N/10||i==9*N/10||i==10*N/10;
        process=i/N*100;
        disp(sprintf('%0.f%% completed',process))
    else
    end

    PF(i)=length(FS(FS<1))/i*100;
end

PF_final=PF(N);

f_name=sprintf('QMslope_HBprobabilistic_%.0f_%.0f_%.0f_%.0f_%.0f_%.0f_%.0
f_%.0f',phi_face,H_slope,mean_GSI,mean_mi,mean_UCS,COV_GSI*100,COV_mi*100
,COV_UCS*100)

save(f_name,'phi_face','H_slope','nrslice','slipcircle','HB_mean','HB_COV
','HB_truncation','N','FS_dm','geometry','force','cohesion_dm','friction_
dm','GSI','mi','UCS','cohesion','friction','FS','PF')
% --------------------------------------------------------------------
```

A.2.4 QMslope_HBspatial

```
% --------------------------------------------------------------------
function [PF_final] = QMslope_HBspatial(phi_face, H_slope, nrslice,
slipcircle, HB_mean, D, HB_COV, SOF, HB_truncation, N)

% HB_mean: 1*3 matrix
% HB_COV: 1*3 matrix
% HB_truncation: 3*2 matrix
% the input for UCS should be kpa

% slip circle
% --------------------------------------------------------------------
X = slipcircle(1);
Y = slipcircle(2);
R = slipcircle(3);
LX = slipcircle(4);
LY = slipcircle(5);
RX = slipcircle(6);
RY = slipcircle(7);
% --------------------------------------------------------------------

% obtain the mean value of HB parameters
% --------------------------------------------------------------------
mean_GSI = HB_mean(1);
mean_mi = HB_mean(2);
mean_UCS = HB_mean(3);
mu = HB_mean;
% --------------------------------------------------------------------

% geometry and deterministic FS
% --------------------------------------------------------------------
[geometry,force]=QMslope_geometry(phi_face,H_slope,nrslice,X,Y,R,LX,LY,RX
,RY,'n');
```

```
[cohesion_dm,friction_dm]=cphi_kumar(mean_GSI,mean_mi,mean_UCS,D,force.si
gn);

FS_dm=QMslope_bishop(geometry,force,cohesion_dm,friction_dm)
% -------------------------------------------------------------------------

% obtain the COV and SD of HB parameters
% -------------------------------------------------------------------------
COV_GSI = HB_COV(1);
COV_mi = HB_COV(2);
COV_UCS = HB_COV(3);

SD_GSI = COV_GSI* mean_GSI;
SD_mi = COV_mi* mean_mi;
SD_UCS = COV_UCS* mean_UCS;
% -------------------------------------------------------------------------

% obtain the truncation of HB parameters
% -------------------------------------------------------------------------
Truncation_GSI = HB_truncation(1,:);
Truncation_mi = HB_truncation(2,:);
Truncation_UCS = HB_truncation(3,:);
% -------------------------------------------------------------------------

% generating HB random numbers
% -------------------------------------------------------------------------
% GSI (no spatial correlation considered)

GSI = (lhsnorm(mean_GSI,SD_GSI^2,N))';
GSI = repmat(GSI,geometry.nrslice,1);

% generate mesh for mi and UCS
mesh=linspace(geometry.detax/2, geometry.detax/2+(geometry.nrslice-
1)*geometry.detax, nrslice)';
% mesh needs to be a coloumb vector

cv_mi=@(x1,x2) gp_markov_cov(x1,x2,SOF,SD_mi);
cv_UCS=@(x1,x2) gp_markov_cov(x1,x2,SOF,SD_UCS);

mi=randomfield(cv_mi,mesh,'nsamples',N)+mean_mi;
UCS=randomfield(cv_UCS,mesh,'nsamples',N)+mean_UCS;
% -------------------------------------------------------------------------

% truncating HB random numbers
% -------------------------------------------------------------------------
GSI(GSI<Truncation_GSI(1))=Truncation_GSI(1);
GSI(GSI>Truncation_GSI(2))=Truncation_GSI(2);

mi(mi<Truncation_mi(1))=Truncation_mi(1);
mi(mi>Truncation_mi(2))=Truncation_mi(2);

UCS(UCS<Truncation_UCS(1))=Truncation_UCS(1);
UCS(UCS>Truncation_UCS(2))=Truncation_UCS(2);
% -------------------------------------------------------------------------

% probabilistic analysis
% -------------------------------------------------------------------------
```

```
rand('twister',5489);randn('state',0);

FS=repmat(1000,N,1);
PF=repmat(1000,N,1);

cohesion=repmat(-1,nrslice, N);
friction=repmat(-1,nrslice, N);

for i=1:N


[cohesion(:,i),friction(:,i)]=cphi_kumar(GSI(:,i),mi(:,i),UCS(:,i),D,forc
e.sign);

    FS(i)=QMslope_bishop(geometry,force,cohesion(:,i),friction(:,i));

    if
i==N/10||i==2*N/10||i==3*N/10||i==4*N/10||i==5*N/10||i==6*N/10||i==7*N/10
||i==8*N/10||i==9*N/10||i==10*N/10;
        process=i/N*100;
        disp(sprintf('%0.f%% completed',process))
    else
    end

    PF(i)=length(FS(FS<1))/i*100;
end

PF_final=PF(N);

f_name=sprintf('QMslope_HBspatial_%.0f_%.0f_%.0f_%.0f_%.0f_%.0f_%.0f_%.0f
_%.0f',phi_face,H_slope,mean_GSI,mean_mi,mean_UCS,COV_GSI*100,COV_mi*100,
COV_UCS*100,SOF)

save(f_name,'phi_face','H_slope','nrslice','slipcircle','HB_mean','HB_COV
','HB_truncation','SOF','N','FS_dm','geometry','force','cohesion_dm','fri
ction_dm','GSI','mi','UCS','cohesion','friction','FS','PF')
% --------------------------------------------------------------------
```

A.2.5 QMslope_FSdistribution

```
% --------------------------------------------------------------------
function
[mean_FS,SD_FS,fitting]=QMslope_FSdistribution(phi_face,H_slope,GSI,mi,UC
S,cov_GSI,cov_mi,cov_UCS,distribution,POF,type,CL)

% this code plot the distribution of FS
% distribution can be gev, inversegaussian, lognormal,
nakagami,tlocationscale, birnbaumsaunders, logistic, weibull, loglogistic
% POF can be 's'for simulated or 'e' for estimated or 'b' for both
% type can be 'threevari' or 'spatial'
% CL=10,20,50,100,200,500,1000,100000000
% --------------------------------------------------------------------

% round values
% this part round the input values *
```

```
% ------------------------------------------------------------------------
GSI=round(GSI); mi=(mi); UCS=round(UCS);
% ------------------------------------------------------------------------


% type and load file name *
% ------------------------------------------------------------------------
switch type
    case('threevari')

fname=sprintf('QMslope_HBprobabilistic_%.0f_%.0f_%.0f_%.0f_%.0f_%.0f_%.0f
_%.0f.mat',phi_face,H_slope,GSI,mi,UCS,cov_GSI*100,cov_mi*100,cov_UCS*100
);
    case('spatial')

fname=sprintf('QMslope_HBspatial_%.0f_%.0f_%.0f_%.0f_%.0f_%.0f_%.0f_%.0f_
%.0f.mat',phi_face,H_slope,GSI,mi,UCS,cov_GSI*100,cov_mi*100,cov_UCS*100,
CL);
end

load(fname);
% ------------------------------------------------------------------------

% bin information for histgram *
% ------------------------------------------------------------------------
bin_width=0.1; % bin width

bin=0:bin_width:200; % this is the bin for hist
envelop_bin=0:0.01:200; % this is for plotting the red curve

[hist1,hist2]=hist(FS,bin);
% ------------------------------------------------------------------------

% fit into theoretical distribution
% ------------------------------------------------------------------------
% gev, inversegaussian, lognormal, nakagami, tlocationscale,
% birnbaumsaunders, logistic, weibull

switch distribution
    case ('gev')
        fitting=gevfit(FS, 0.05);
        envelop = gevpdf(envelop_bin,fitting(1), fitting(2), fitting(3));
        PF_E=cdf('gev',1,fitting(1), fitting(2), fitting(3))*100;
    case ('inversegaussian')
        fitting=mle(FS, 'dist','inversegaussian', 'alpha',0.05);
        envelop = pdf('inversegaussian',envelop_bin,fitting(1),
fitting(2));
        PF_E=cdf('inversegaussian',1,fitting(1), fitting(2))*100;
    case ('lognormal')
        fitting=mle(FS, 'dist','lognormal', 'alpha',0.05);
        envelop = pdf('lognormal',envelop_bin,fitting(1), fitting(2));
        PF_E=cdf('lognormal',1,fitting(1), fitting(2))*100;
    case ('nakagami')
        fitting=mle(FS, 'dist','nakagami', 'alpha',0.05);
        envelop = pdf('nakagami',envelop_bin,fitting(1), fitting(2));
        PF_E=cdf('nakagami',1,fitting(1), fitting(2))*100;
    case ('tlocationscale')
        fitting=mle(FS, 'dist','tlocationscale', 'alpha',0.05);
```

```
        envelop = pdf('tlocationscale',envelop_bin,fitting(1), fitting(2),
fitting(3));
        PF_E=cdf('tlocationscale',1,fitting(1), fitting(2),
fitting(3))*100;
    case ('birnbaumsaunders')
        fitting=mle(FS, 'dist','birnbaumsaunders', 'alpha',0.05);
        envelop = pdf('birnbaumsaunders',envelop_bin,fitting(1),
fitting(2));
        PF_E=cdf('birnbaumsaunders',1,fitting(1), fitting(2))*100;
    case ('logistic')
        fitting=mle(FS, 'dist','logistic', 'alpha',0.05);
        envelop = pdf('logistic',envelop_bin,fitting(1), fitting(2));
        PF_E=cdf('logistic',1,fitting(1), fitting(2))*100;
    case ('weibull')
        fitting=mle(FS, 'dist','weibull', 'alpha',0.05);
        envelop = pdf('weibull',envelop_bin,fitting(1), fitting(2));
        PF_E=cdf('weibull',1,fitting(1), fitting(2))*100;
    case ('loglogistic')
        fitting=mle(FS, 'dist','loglogistic', 'alpha',0.05);
        envelop = pdf('loglogistic',envelop_bin,fitting(1), fitting(2));
        PF_E=cdf('loglogistic',1,fitting(1), fitting(2))*100;
end
% ------------------------------------------------------------------------

% statistic information *
% ------------------------------------------------------------------------
mean_FS=mean(FS);
SD_FS=sqrt(var(FS));
COV_FS=SD_FS/mean_FS;
PF_S=PF(N);
% ------------------------------------------------------------------------

% following part is for adjusting picture size *
% ------------------------------------------------------------------------
hFig=figure;

set(hFig,'Units', 'centimeters');
OldUnits=get(0,'Units');% get unit
set(0,'Units','centimeters');% set unit to centimerters
ScreenSize=get(0,'screensize');% get original screen size
set(0,'Units',OldUnits);%
set(hFig,'Units', 'centimeters');%??????????? ??
FigWidth=8; % 17 / 6
FigHeight=8; %11 / 10.5
StartX=(ScreenSize(3)-FigWidth)/2;%????????X
StartY=(ScreenSize(4)-FigHeight)/2;%????????Y
set(hFig,'position',[ StartX StartY FigWidth FigHeight]); %,???????,?????
% ------------------------------------------------------------------------

% plot the histgram *
% ------------------------------------------------------------------------
hFig=bar(hist2,hist1/N/bin_width,'hist');

set(hFig,'FaceColor','none','EdgeColor',[0.333333 0 0.666667],...
       'LineStyle','-', 'LineWidth',1);

hold on, grid on
% ------------------------------------------------------------------------
```

```
% label, title and text  *
% ------------------------------------------------------------------------
xlabel('Factor of Safety FS'), ylabel('Frequency Density')

text1=sprintf('mean-FS=%.2f',mean_FS); %text for mean FS
text2=sprintf('SD-FS=%.2f',SD_FS);  %text for SD FS
text3=sprintf('COV-FS=%.2f',COV_FS); %text for COV FS
text4=sprintf('N=%.0f',N);  %text for N

if PF_S<0.1
text5=sprintf('PF=%.2e%%',PF_S); %text for simulated PF
else
text5=sprintf('PF=%.2f%%',PF_S); %text for simulated PF
end

if PF_E<0.1
text6=sprintf('PF-E=%.2e%%',PF_E); %text for estimated PF
else
text6=sprintf('PF-E=%.2f%%',PF_E); %text for estimated PF
end

text7=sprintf('CL=%.0f',CL); %text for CL

text(2.9,1.2,text1); text(2.9,1.1,text2); text(2.9,1.0,text3);
text(2.9,0.9,text4);


switch POF
    case ('e')
        text(2.9,1.3,text6); %text for estimated PF
    case ('b')
        text(2.9,1.4,text5); %text for simulated PF
        text(2.9,1.3,text6); %text for estimated PF
    case ('s')
        text(2.9,1.3,text5); %text for simulated PF
end

switch type
    case ('threevari')
        switch HB_mean(1)
        case(69)
            tname=sprintf('Case1 COV=(%.2f %.2f %.2f)
FS=1.64',cov_GSI,cov_mi,cov_UCS);
        case(38)
            tname=sprintf('Case2 COV=(%.2f %.2f %.2f)
FS=1.64',cov_GSI,cov_mi,cov_UCS);
        case(23)
            tname=sprintf('Case3 COV=(%.2f %.2f %.2f)
FS=1.64',cov_GSI,cov_mi,cov_UCS);
        end
    case ('spatial')
        switch HB_mean(1)
        case(69)
            tname=sprintf('Case1 COV=(%.2f %.2f %.2f)
FS=1.64',cov_GSI,cov_mi,cov_UCS);
        case(38)
            tname=sprintf('Case2 COV=(%.2f %.2f %.2f)
FS=1.64',cov_GSI,cov_mi,cov_UCS);
```

```
        case(23)
            tname=sprintf('Case3 COV=(%.2f %.2f %.2f)
FS=1.64',cov_GSI,cov_mi,cov_UCS);
        end

        text(2.9,0.9,text7);
end

title(tname)
% --------------------------------------------------------------------

% plot the distribution envelop *
% --------------------------------------------------------------------
plot(envelop_bin,envelop,'Color',[1 0 0],...
          'LineStyle','-', 'LineWidth',1.5,...
          'Marker','none', 'MarkerSize',6);
xlim([0 5]); ylim([0 1.5]);
% --------------------------------------------------------------------

% this part plot the convergence of PF
% --------------------------------------------------------------------
hFig=figure; hold on; plot(PF);grid on

if PF(N)~=0
ylim([PF(N)-sqrt(PF(N)), PF(N)+sqrt(PF(N))]);
else
end

xlabel('Number of Iterations N'); ylabel('Probability of Failure PF (%)');

title(tname)
% --------------------------------------------------------------------

% following part is for adjusting picture size *
% --------------------------------------------------------------------
set(hFig,'Units', 'centimeters');
OldUnits=get(0,'Units');% get unit
set(0,'Units','centimeters');% set unit to centimerters
ScreenSize=get(0,'screensize');% get original screen size
set(0,'Units',OldUnits);%
set(hFig,'Units', 'centimeters');%??????????? ??
FigWidth=8; % 17 / 6
FigHeight=8; %11 / 10.5
StartX=(ScreenSize(3)-FigWidth)/2;%????????X
StartY=(ScreenSize(4)-FigHeight)/2;%????????Y
set(hFig,'position',[ StartX StartY FigWidth FigHeight]); %,???????,?????
% --------------------------------------------------------------------
```

A.2.6 Codes for concerting HB parameters to MC parameters

A.2.6.1 cphi_bray

```
% --------------------------------------------------------------------
function [c_i,phi_i,cphi_method] = cphi_bray(GSI,mi,sigci,D,sign)
```

```
% Bray's analytical method for calculating instantaneous c and phi
% c and phi change with normal stress
% [c_i,phi_i,cphi_method] = cphi_bray(GSI,mi,sigci,D,sign);
% the input for UCS should be kpa
% Refer: Hoek & Marinos, 2007

% tested 20120716

% expand input parameters (GSI,mi,sigci)
% --------------------------------------------------------------------
nrslices=length(sign);

if length(GSI)==1
    GSI=repmat(GSI,nrslices,1);
elseif length(GSI)~=1 && length(GSI)~=nrslices
    error('error in GSI length')
end

if length(mi)==1
    mi=repmat(mi,nrslices,1);
elseif length(mi)~=1 && length(mi)~=nrslices
    error('error in mi length')
end

if length(sigci)==1
    sigci=repmat(sigci,nrslices,1);
elseif length(sigci)~=1 && length(sigci)~=nrslices
    error('error in sigci length')
end
% --------------------------------------------------------------------
mb=mi.*exp((GSI-100)./(28-14*D));
s=exp((GSI-100)./(9-3*D));
a=0.5+ 1/6*(exp(-GSI/15) -exp(-20/3));
sig_cm=sigci.*(mb+4*s-a.*(mb-8*s)).*(mb/4+s).^(a-1)./(2*(1+a).*(2+a));

para_h=1+16*(sign.*mb+s.*sigci)./(3*mb.^2.*sigci);
para_w=(90+atand(1./sqrt(para_h.^3-1)))/3;
phi_i=atand(1./sqrt(4.*para_h.*(cosd(para_w)).^2-1));
tau_f=mb.*sigci.*(cotd(phi_i)-cosd(phi_i))/8;
c_i=tau_f-sign.*(tand(phi_i));

cphi_method='Bray1983';
% --------------------------------------------------------------------
```

A.2.6.2 cphi_kumar

```
% --------------------------------------------------------------------
function [c_i,phi_i,cphi_method] = cphi_kumar(GSI,mi,sigci,D,sign)

% Kumar's numerical method for calculating instantaneous c and phi
% c and phi change with normal stress
% [c_i,phi_i,cphi_method] = cphi_kumar(GSI,mi,sigci,D,sign);
% the input for UCS should be kpa
% Refer: Jiayi Shen
% tested - correct 20120716
```

```
% expand input parameters (GSI,mi,sigci)
% -------------------------------------------------------------------------
nrslices=length(sign);

if length(GSI)==1
    GSI=repmat(GSI,nrslices,1);
elseif length(GSI)~=1 && length(GSI)~=nrslices
    error('error in GSI length')
end

if length(mi)==1
    mi=repmat(mi,nrslices,1);
elseif length(mi)~=1 && length(mi)~=nrslices
    error('error in mi length')
end

if length(sigci)==1
    sigci=repmat(sigci,nrslices,1);
elseif length(sigci)~=1 && length(sigci)~=nrslices
    error('error in sigci length')
end
% -------------------------------------------------------------------------

mb=mi.*exp((GSI-100)./(28-14*D));
s=exp((GSI-100)./(9-3*D));
a=0.5+ 1/6*(exp(-GSI/15) -exp(-20/3));

sign(sign<0)=0;

for i=1:nrslices;

    y(i)=fzero(@(sinphi)
(2/(mb(i)*a(i)))*(mb(i)*sign(i)/sigci(i)+s(i))^(1-a(i))-(1-
sinphi)/sinphi*(1+sinphi/a(i))^(1-a(i)),0.6);

    % already double checked, only 0.6 as initial value gives right ans

    % when GSI<8 and UCS=1000 // GSI=1 and UCS<2800 error occurs
    % only possible solution to solve this problem is by truncation

    phi_i(i)=asind(y(i)); %phi

tau(i)=0.5*sigci(i)*cosd(phi_i(i))*((mb(i)*sign(i)/sigci(i)+s(i))^a(i))/(
1+sind(phi_i(i))/a(i)).^a(i);
    c_i(i)=tau(i)-sign(i)*tand(phi_i(i));
end

c_i=c_i'; phi_i=phi_i';

cphi_method='Kumar1998';
% -------------------------------------------------------------------------
```

A.2.6.3 cphi_hoek2002

```
% -------------------------------------------------------------------------
function [c_i,phi_i,cphi_method] =
cphi_hoek2002(GSI,mi,sigci,D,r_rock,H_slope)

% Hoek 2002 analytical method for calculating instantaneous c and phi
% c and phi do not change with normal stress
% [c_i,phi_i,cphi_method] = cphi_hoek2002(GSI,mi,sigci,D,r_rock,H_slope);
% the input for UCS should be kpa
% Refer: Hoek & Marinos, 2007

% tested 20120716

mb=mi.*exp((GSI-100)./(28-14*D));
s=exp((GSI-100)./(9-3*D));
a=0.5+ 1/6*(exp(-GSI/15) -exp(-20/3));
sig_cm=sigci.*(mb+4*s-a.*(mb-8*s)).*(mb/4+s).^(a-1)./(2*(1+a).*(2+a));

sig_0=r_rock*H_slope;  % equal to rock*Hslope
sig_3max=0.72.*(sig_cm./sig_0).^(-0.91).*sig_cm;
sig_3n=sig_3max./sigci;
c_i=(sigci.*((1+2*a).*s+(1-a).*mb.*sig_3n).*(s+mb.*sig_3n).^(a-
1)./((1+a).*(2+a).*sqrt(1+(6*a.*mb.*(s+mb.*sig_3n).^(a-
1))./((1+a).*(2+a))));
phi_i= asind((6*a.*mb.*(s+mb.*sig_3n).^(a-
1))./(2*(1+a).*(2+a)+6*a.*mb.*(s+mb.*sig_3n).^(a-1)));

cphi_method='Hoek2002';
% -------------------------------------------------------------------------
```

A.2.6.4 cphi_shen

```
% -------------------------------------------------------------------------
function [c,phi,cphi_method] = cphi_shen(GSI,mi,sigci,D,sign)

% Shen's analytical method for calculating instantaneous c and phi
% c and phi change with normal stress
% [c,phi,cphi_method] = cphi_shen(GSI,mi,sigci,D,sign);
% the input for UCS and sign should be kpa
% Refer: Shen 2012

% tested - correct 20120716

% expand input parameters (GSI,mi,sigci)
% -------------------------------------------------------------------------
nrslices=length(sign);

if length(GSI)==1
    GSI=repmat(GSI,nrslices,1);
elseif length(GSI)~=1 && length(GSI)~=nrslices
    error('error in GSI length')
end
```

```
if length(mi)==1
    mi=repmat(mi,nrslices,1);
elseif length(mi)~=1 && length(mi)~=nrslices
    error('error in mi length')
end

if length(sigci)==1
    sigci=repmat(sigci,nrslices,1);
elseif length(sigci)~=1 && length(sigci)~=nrslices
    error('error in sigci length')
end
% --------------------------------------------------------------------

mb=mi.*exp((GSI-100)./(28-14*D));
s=exp((GSI-100)./(9-3*D));
a=0.5+ 1/6*(exp(-GSI/15) -exp(-20/3));
sig_cm=sigci.*(mb+4*s-a.*(mb-8*s)).*(mb/4+s).^(a-1)./(2*(1+a).*(2+a));

sig3_sigci=a.*sign./sigci./(sqrt(a.*(1+sqrt(mb))-sign./sigci));
P=2+a.*mb.*(mb.*sig3_sigci+s).^(a-1);

phi=asind(1-2./P);
tau=sigci.*sqrt(P-1)./P.*(mb.*sign./sigci+s).^a./((P.*a+P-2)./a./P).^a;
c=tau-sign.*tand(phi);

cphi_method='Shen2012';
% --------------------------------------------------------------------
```

APPENDIX B

DATA FOR THE EQUATION FITTING

The full sets of data (168 in total) generated by *Slide6.0* for the equation fitting (discussed in Section 4.2.1) are provided in this appendix, as in Table B.1.

Table B.1 Full sets of data for the equation fitting

Data set	GSI	m_i	σ_{ci} (MPa)	FS
1	10	5	10	0.38
2	10	5	35	0.551
3	10	5	65	0.664
4	10	5	95	0.751
5	10	5	120	0.812
6	10	5	150	0.874
7	10	17	10	0.608
8	10	17	35	0.84
9	10	17	65	0.976
10	10	17	95	1.076
11	10	17	120	1.145
12	10	17	150	1.215
13	10	28	10	0.731
14	10	28	35	0.989
15	10	28	65	1.145
16	10	28	95	1.248
17	10	28	120	1.321
18	10	28	150	1.396
19	10	40	10	0.826
20	10	40	35	1.105
21	10	40	65	1.272
22	10	40	95	1.39
23	10	40	120	1.469
24	10	40	150	1.55

Data set	GSI	m_i	σ_{ci} (MPa)	FS
25	25	5	10	0.58
26	25	5	35	0.885
27	25	5	65	1.117
28	25	5	95	1.308
29	25	5	120	1.448
30	25	5	150	1.606
31	25	17	10	0.855
32	25	17	35	1.215
33	25	17	65	1.45
34	25	17	95	1.63
35	25	17	120	1.757
36	25	17	150	1.89
37	25	28	10	0.992
38	25	28	35	1.383
39	25	28	65	1.642
40	25	28	95	1.823
41	25	28	120	1.952
42	25	28	150	2.089
43	25	40	10	1.1
44	25	40	35	1.525
45	25	40	65	1.793
46	25	40	95	1.987
47	25	40	120	2.121
48	25	40	150	2.262
49	40	5	10	0.776
50	40	5	35	1.287
51	40	5	65	1.742
52	40	5	95	2.15
53	40	5	120	2.452
54	40	5	150	2.798
55	40	17	10	1.065
56	40	17	35	1.574
57	40	17	65	1.958
58	40	17	95	2.28
59	40	17	120	2.523
60	40	17	150	2.785
61	40	28	10	1.221

Data set	GSI	m_i	σ_{ci} (MPa)	FS
62	40	28	35	1.754
63	40	28	65	2.13
64	40	28	95	2.434
65	40	28	120	2.659
66	40	28	150	2.903
67	40	40	10	1.338
68	40	40	35	1.898
69	40	40	65	2.287
70	40	40	95	2.587
71	40	40	120	2.797
72	40	40	150	3.034
73	55	5	10	1.053
74	55	5	35	2.015
75	55	5	65	2.958
76	55	5	95	3.87
77	55	5	120	4.587
78	55	5	150	5.446
79	55	17	10	1.314
80	55	17	35	2.121
81	55	17	65	2.824
82	55	17	95	3.46
83	55	17	120	3.947
84	55	17	150	4.482
85	55	28	10	1.471
86	55	28	35	2.245
87	55	28	65	2.904
88	55	28	95	3.451
89	55	28	120	3.882
90	55	28	150	4.377
91	55	40	10	1.602
92	55	40	35	2.374
93	55	40	65	2.996
94	55	40	95	3.523
95	55	40	120	3.911
96	55	40	150	4.355
97	70	5	10	1.592
98	70	5	35	3.627

Data set	GSI	m_i	σ_{ci} (MPa)	FS
99	70	5	65	5.914
100	70	5	95	8.224
101	70	5	120	10.163
102	70	5	150	12.448
103	70	17	10	1.73
104	70	17	35	3.215
105	70	17	65	4.641
106	70	17	95	6.026
107	70	17	120	7.126
108	70	17	150	8.415
109	70	28	10	1.849
110	70	28	35	3.186
111	70	28	65	4.467
112	70	28	95	5.58
113	70	28	120	6.49
114	70	28	150	7.574
115	70	40	10	1.959
116	70	40	35	3.227
117	70	40	65	4.398
118	70	40	95	5.437
119	70	40	120	6.219
120	70	40	150	7.141
121	85	5	10	2.79
122	85	5	35	7.827
123	85	5	65	13.798
124	85	5	95	19.754
125	85	5	120	24.73
126	85	5	150	30.71
127	85	17	10	2.562
128	85	17	35	5.677
129	85	17	65	9.112
130	85	17	95	12.579
131	85	17	120	15.492
132	85	17	150	18.969
133	85	28	10	2.566
134	85	28	35	5.214
135	85	28	65	8.044

Data set	GSI	m_i	σ_{ci} (MPa)	FS
136	85	28	95	10.743
137	85	28	120	13.003
138	85	28	150	15.732
139	85	40	10	2.624
140	85	40	35	5.038
141	85	40	65	7.489
142	85	40	95	9.835
143	85	40	120	11.723
144	85	40	150	13.996
145	100	5	10	5.867
146	100	5	35	18.805
147	100	5	65	34.36
148	100	5	95	49.937
149	100	5	120	62.922
150	100	5	150	78.481
151	100	17	10	4.433
152	100	17	35	12.079
153	100	17	65	21.213
154	100	17	95	30.262
155	100	17	120	37.827
156	100	17	150	46.921
157	100	28	10	4.124
158	100	28	35	10.245
159	100	28	65	17.524
160	100	28	95	24.743
161	100	28	120	30.683
162	100	28	150	37.828
163	100	40	10	4.027
164	100	40	35	9.31
165	100	40	65	15.38
166	100	40	95	21.526
167	100	40	120	26.604
168	100	40	150	33.67